Detecting and Modeling Landfast Ice in the Alaskan Bering Sea

David Aaron Jensen

Dissertation submitted to the faculty of the Virginia Polytechnic Institute and State University in partial fulfillment of the requirements for the degree of

Doctor of Philosophy

In

Geospatial and Environmental Analysis

Lynn Resler, Chair

Andy Mahoney

Yang Shao

Jim Campbell

May 11th 2020

Blacksburg, Virginia

Keywords: Landfast; Sea Ice; Subarctic; Bering Sea

Detecting and Modeling Landfast Ice in the Alaskan Bering Sea
David Jensen

SCIENTIFIC ABSTRACT

Seasonal sea ice – ice which freezes in late fall and melts completely the following summer – is a central feature in the ecology, geomorphology, and climatology of the Bering Sea. In this region's coastal zones, sea ice becomes locked into a stationary position against the coastlines to become landfast ice, which influences bioegophysical processes in the region, as well as exchanges of energy and matter among land, ocean, and atmosphere. It provides a platform for human mobility and subsistence activities, habitat for certain marine mammals, regulates terregenous nutrient cycling into ocean environments, and modulates the effect of erosive wind/wave action against coastlines. However, a thorough understanding of how this stationary ice, known as landfast ice, affects biogeophysical processes in the Bering Sea is limited by a lack of data on its areal coverage and seasonal duration.

This dissertation establishes a baseline set of observations of landfast ice conditions in the Bering Sea through the creation and analysis of continuous spatial datasets. Chapter 1 focuses on the landfast ice annual cycle in the Eastern Bering Sea, which spans from the western tip of the Seward Peninsula to the southernmost point on the Yukon-Kuskokwim River Deltas. Chapter 1 results in the creation of landfast ice spatial data in these areas ranging from 1996 – 2008. Results show the spatial distribution and seasonal duration of landfast ice vary regionally within our study area, does not generally reach water depths associated with stabilization of the landfast ice cover in other regions of the Arctic, and is shortening in seasonal duration by approximately 9 days. Chapter 2 focuses on the landfast ice annual cycle on St. Lawrence Island, an Alaska Island located in the northern Bering Sea. Chapter 2 results in the creation of landfast ice spatial data in these areas ranging from 1996 – 2019. Results show the spatial distribution of landfast ice to vary regionally on the island, based on the coastlines orientation towards prevailing winds that transport pack ice through the Bering Strait. We also observed a sharp decline in landfast ice cover from 2017-2019, which coincides with record-breaking declines in sea ice coverage for the entire Bearing Sea. We also found coastal morphology and orientation have limited explanatory power when modeling landfast ice widths – the distance between the landfast ice edge and coastline – suggesting the consideration of meteorological variables is needed to improve models. Chapter 3 uses the landfast ice data from Chapter 2 to create an explanatory logistic regression model of landfast ice cover on St. Lawrence Island, using a combination of geographic and meteorological predictor variables. Using these variables, the model was able to predict the location of landfast ice cover with 80-90% accuracy, depending on the region of St. Lawrence Island. The model outputs resulted in very low commission error, with high omission error, which may be improved in future studies with the additional predictor variables.

Cumulatively, this dissertation is the most comprehensive analysis of landfast ice cover to date on Alaskan Bering Sea coastlines. Research findings advance scholarly understandings of coastal ice conditions in the Bering Sea, and the geographic as wellas meteorological factors that enable their presence.

Detecting and Modeling Landfast Ice in the Alaskan Bering Sea
David Jensen

GENERAL AUDIENCE ABSTRACT

Landfast sea ice – sea ice that becomes locked into a stationary position against the coastline – is a central feature in the ecology, geomorphology, and climatology of the Bering Sea. However, a thorough understanding of how this stationary ice, known as landfast ice, affects human/environmental processes (e.g. climate regulation, sediment mixing in marine environments, wildlife habitat/behavior, human transportation) in the Bering Sea is limited by a lack of data on its areal coverage and seasonal duration. This dissertation establishes a baseline set of observations of landfast ice conditions in the Bering Sea through the creation and analysis of continuous spatial datasets. Cumulatively, this dissertation is the most comprehensive analysis of landfast ice cover to date on Alaskan Bering Sea coastlines. First, this dissertation creates and analyzes the landfast ice annual cycle from 1996 – 2008 on the Eastern Bering Sea. Second, this dissertation creates a similar dataset from 1996 – 2019 on St. Lawrence Island, finding significant declines in landfast ice coverage that match broader sea ice trends in the northern Bering Sea. Third, this dissertation uses the landfast ice data on St. Lawerence Island to create a model explaining outcomes in the location of landfast ice cover under certain geographic and meteorological conditions.

Acknowledgements

I would like to thank the following individuals who have contributed to this research. I would not have been able to see this endeavor through without them.

I would first like to acknowledge my advisor, Dr. Lynn M. Resler. I could not have completed this dissertation without her unwavering support, patience, and willingness to explore a new topic. Dr. Resler's encouragement pushed me out of my comfort zone, giving me the opportunity to teach classes, attend conferences across the country, and pursue field opportunities where I saw the topic of my research up close in Utqiagvik. I am very fortunate for these experiences, and all that I have learned under her mentorship. I would also like to thank Dr. Andy Mahoney my external committee member from University of Alaska Fairbanks Geophysical Institute. Dr. Mahoney's contribution to my research is difficult to overstate, as he advanced the methods of landfast ice detection and analysis that made this dissertation possible, and helped to advance this research toward publication. I would finally like to thank my remaining two committee members: Dr. Yang Shao and Dr. Jim Campbell, for their advice and mentorship as well, through individual meetings as well as through classes they taught. I would also like to thank the institutions that helped me with my dissertation. Namely Virginia Tech's Department of Geography and University of Alaska Fairbanks Geophysical Institute and Alaska Satellite Facility, and Kawerak in Nome, Alaska. Finally, the Interdisciplinary Graduate Education Program (IGEP) in Remote Sensing was exceptionally helpful in getting me to this point, and I would like to thank Dr. Randy Wynne, the program's Co-Director, in particular.

I would like to acknowledge the contributions of my family, especially my father, Kevin Jensen. His encouragement and enthusiasm for science has inspired me at a young age, and sustained me through my dissertation. I also want to express my gratitude for my mother, Janet Jensen, my sister, Cassie Jensen, and my grandmother, Millie Jacks, who have all supported me in their own ways.

I would finally like to acknowledge the local businesses of Roanoke and Blacksburg. I estimate 70% of my dissertation was written in one coffee shop or another

around town. I would like to acknowledge Downshift, Sweet Donkey, RND Roasters, and Mill Mountain for keeping me caffeinated and working.

Table of Contents

Chapter 1. Statement of Purpose, Background

1.1 Statement of Purpose

Arctic and subarctic regions are experiencing major and rapid changes to its landscapes, oceans, and climate (Hinzman et al. 2005; IPCC 2013). These changes are strongly driven by the retreat of cryospheric features such as sea ice (Serreze et al. 2007). In the Arctic Ocean and adjacent subarctic seas, multi-year sea ice concentrations are declining, and seasonal sea ice features are present for shorter periods of time with diminished areal extent (Grebmeier et al. 2006; Stroeve et al. 2007; Wadhams and Davis 2000). Such changes carry implications for the net flow of energy into and out of the earth system by reducing planetary albedo and diminishing the polar heat sink through which energy is released into space (Qu et al. 2006; Serreze et al. 2000). Consequences of sea ice change also manifest at more regional scales, affecting regional ecologies, geomorphology, and human activities (Grebmeier et al. 2006; Oceana and Kawerak 2014; Radosavljevic et al. 2016).

Sea ice presence and influence on interacting processes has been particularly affected by climatic shifts. Summer minimum sea ice extent in the Arctic Ocean has declined by an average of 10% per decade since 1979 (Comiso et al. 2008; Goosse et al. 2009). Sea ice decline has paralleled change in the functions of interacting processes through marine mammal habitat reduction (Kawerak 2013; Oceana and Kawerak 2014; Ray et al. 2016), increasing tundra vegetation productivity (Bhatt et al. 2010; Post et al. 2013), and altering food webs structured by the predictable recurrence of sea ice conditions (Boetius et al. 2013; Grebmeier et al. 2006; Hunt et al. 2002). Changing sea ice conditions can also alter the geomorphology of coastlines by increasing exposure to erosive ocean and wind action

(USACE 2009). These changes can also occur in subarctic regions bordering the Arctic Ocean, such as the Bering Sea where food webs have shifted with changing seasonal ice conditions (Grebmeier et al. 2006).

Increased periods of ice-free conditions as a result of sea ice decline carry important implications for human activities in Arctic and Subarctic environments. Sea ice plays an integral role in subsistence activities by providing seasonal travel platforms and habitat for marine mammals (Kawerak 2013; Ray et al. 2016), and is generally viewed by Arctic indigenous peoples as an essential environmental feature for the continuity of cultural identity and practice (Oceana and Kawerak 2014). Diminishing sea ice cover creates economic incentives for increased human activities and presence in Arctic environments, which can create new challenges such as food insecurity for subsistence communities (Beaumier et al. 2010; Ford et al. 2010, 2011), disruptive or fatal interactions between wildlife and maritime vessels (Burek et al. 2008; Oceana and Kawerak 2014), and the increased risk of oil spills as maritime activity increases (Whiteman et al. 2013). Increasingly ice-free conditions also present new opportunities for human activities. Diminishing pack ice in the Northwest Passage and Northern Sea Route are creating increasingly reliable summertime shipping routes through the Arctic Ocean (Stephenson et al. 2013), and facilitating the extraction of hydrocarbons that were once inaccessible (Gautier et al. 2009).

The consequences associated with sea ice decline have incentivized increased attention in recent years to landfast ice (Howell et al. 2016; Mahoney et al. 2007, 2014; Yu 2014). Landfast ice forms in coastal zones and inner-shelf waters, where sea ice can freeze into a stationary position against the coastline. The annual cycle – the seasonal

process by which landfast ice forms in the winter, interacts with the surrounding environment, and melts in the spring – influences interactions between terrestrial, marine, and atmospheric processes (Eicken et al. 2005; Heil et al. 1996; Mahoney et al. 2007). Landfast ice mediates energy fluxes by suppressing erosive energy from wind and wave action (Goldenberg 2014; König and Holland 2010; Rawlings 2015), and reflecting incident solar radiation (Allison et al. 1993; Langelben 1971). Landfast ice also mediates the exchanges of matter between marine and terrestrial environments. For example, landfast ice freezes against river mouths and generally melts later than inland river ice and snow. River discharge floods the surface of landfast ice (an occurrence referred to as an *overflow event*) and is confined below the surface. These ice barriers regulate the mixing of sediments, including organic matter for marine food webs, into ocean environments (Dunton et al. 2006; McClelland et al. 2012). Overflow processes also introduce heat into these environments by lowering the surface albedo of landfast ice and sensible heat flux from the water flooding the ice (Dean et al. 1994; Weingartner et al. 2017).

Due to its mediating effect on coastal conditions, changes in the seasonal extent and duration of landfast ice have consequences for many critical processes on which terrestrial and marine environments depend. On Bering Sea coastlines in Western Alaska, landfast ice has been observed to change by forming later, melting earlier, and becoming increasingly unstable and harder to predict (Huntington et al. 2013; Kawerak 2013). These changes have influenced associated challenges in the Bering Sea; subsistence activity and seasonal travel are becoming more arduous (Huntington et al. 2013; Oceana and Kawerak 2014), viable habitat for migratory marine mammals is diminishing

(USFWS 2008), and accelerated coastal erosion threaten community infrastructure and livelihoods (Goldenberg 2014; Mahoney et al. 2007a; Rawlings 2015).

Research on the extent to which landfast ice change is altering interacting terrestrial and marine environments, and presents new challenges in coastal zones, is constrained by limited data and research. This is particularly true for our understanding of Bering Sea landfast ice, where the landfast ice annual cycle – and how it is influenced by the physical geography and climatology of the region – is generally understudied compared to the more comprehensively examined Chukchi and Beaufort Seas (Mahoney et al. 2014). This dissertation research provides a baseline set of Bering Sea landfast ice observations, and explores relationships between the landfast ice annual cycle and the physical geography and climatology of the region, by addressing three comprehensive research objectives.

- **Research Objective 1:** Establish a baseline set of observations of spatial and temporal landfast ice patterns on the Eastern Bering Sea and St. Lawrence Island coastlines using remote sensing and GIS modeling with a time series of Radarsat-1, ENVISAT, and Sentinel-1 imagery
- **Research Objective 2:** Identify relationships between landfast ice spatial distribution and the physical geography of the Bering Sea region
- **Research Objective 3:** Advance created datasets towards the creation of a spatial model exploring how geographic and meteorlogical conditions influence the spatial distribution of landfast ice cover.

Fulfillment of these three research objectives will contribute to a broader and more thorough understanding of the role of landfast ice in the earth system, and its relationships with the physical geography and climatology of the Bering Sea region, through the generation of new knowledge and datasets

1.2 Structure of Dissertation

This dissertation is organized into five chapters. The broad aim and objectives of this research are introduced in Chapter 1, as well as a review of literature pertinent to landfast sea ice, methods of remote sensing, and the physical geography of the Bering Sea. Chapter 2 provides a baseline set of observations on landfast ice cover in the Eastern Bering Sea from 1996–2008by using a time series of Radarsat-1 imagery to characterize the annual cycle and infer relationships with the region's physical geography. Chapter 3 provides a longer baseline set of observations of landfast ice cover on St. Lawrence Island from 1996–2019 by using a combination of SAR sensors to characterize the landfast ice annual cycle and infer relationships with the region's physical geography using a simple multivariate modeling approach. Chapter 4 uses the data created in Chapter 3 to develop a logistic regression model that further explores the relationships between landfast ice and geographic and meteorological conditions in the northern Bering Sea. Chapter 5 provides the final conclusions reached, and future avenues for research.

1.3 Background

1.3.1 Sea Ice and its relevance to global systems

Sea ice refers to ice that forms in seawater with the onset of freezing temperatures, where it maintains a strong presence in Arctic and Subarctic environments. The study of sea ice features and their spatial and temporal change is important for assessing how sea ice interacts with other processes and earth system components, especially in the context of ongoing environmental change. At a global scale, the effects are numerous. The continued presence of Arctic and Subarctic sea ice is integral to earth system processes at both local and global scales. For example, sea ice regulates heat exchanges and therefore has profound consequences for the global energy budget. Open ocean generally reflects 7% of incident solar radiation (Curry et al 1995; Perovich et al. 2002). By comparison, sea ice is highly reflective; bare sea ice reflects 65%, whereas snow-covered sea ice reflects 85% of incident radiation (Stroeve et al. 2012). Moreover, sea ice acts as a physical barrier limiting turbulent heat exchange between atmosphere and oceans (Barry and Preller 1993) meaning that the persistence of sea ice in Arctic and Subarctic environments enables these regions to reflect more heat into space than absorbed (the ice-albedo feedback). The Arctic, therefore, acts as a global "heat sink", where heat transported by ocean and atmospheric circulations from lower latitudes is released into space when reaching higher latitudes.

Sea ice is further integrated into *local* processes within Arctic and Subarctic environments, for example, by influencing Arctic tundra vegetation productivity (Bhatt et al. 2010; Post et al. 2013), marine food webs (Oceana and Kawerak 2014; Grebmeier et

al. 2006), and human behavior (Huntington et al. 2013; Kawerak 2013). This integration is true particularly in coastal zones, where landfast sea ice maintains a stationary position to mediate land, ocean, and atmospheric interactions.

1.3.2 Landfast Ice

The term *landfast ice* refers specifically to sea ice that is frozen into a stationary position against a coastline. This definition is based on numerous interpretations of sea ice morphology in the existing literature. John Weaver (1951, p. 780) describes landfast ice as "the young coastal ice which, in stationary sheets, builds seaward from the shore of landmasses, and goes through a yearly cycle of appearance, extension, disintegration, and disappearance in successive seasons. By being more or less attached to the shore… it does not move or drift." Similarly, the World Meteorological Organization (1970) describes landfast ice as "[remaining] fast along the coast, where it is attached to the shore, to an ice wall, to an ice front, over shoals, or between grounded icebergs". Mahoney et al. (2006) narrows this definition based on landfast ice properties observable through remote sensing methods by using two criteria: (1) The sea ice is contiguous with the coastline; (2) the sea ice exhibits no detectable motion for approximately 20 days. Because the chapters contained in this dissertation rely heavily on remote sensing methods, we follow the criteria and terminology in Mahoney et al. (2006)

Landfast ice is generally a seasonal coastal feature, with the exception of multiyear landfast ice observed in the Canadian Archipelago and the Russian Tymyr Peninsula (Reimnitz et al. 1995). The phenological events that comprise the seasonal duration of landfast ice is referred to as the *annual cycle*. Landfast ice annual cycles typically span

from early winter to late spring, and are characterized by the spatial and temporal variability in growth and retreat relative to a coastline (Mahoney et al. 2014).

The formation and growth of landfast ice at the onset of an annual cycle occurs when in-situ freezing of open water in sheltered regions assimilates with incoming pack ice to form grounding (anchored) pressure ridges (Mahoney et al. 2007). Anchored pressure ridges allow the sea ice to freeze into a stationary position against the coastline to become landfast ice. This stationary position is reinforced by *bottomfast ice* – the portion of landfast ice entirely frozen against the seabed (Figure 1.1). Landfast ice continues to grow until late spring, when rising air temperatures and downwelling radiative fluxes begin melting the ice cover (Persson et al. 2002), thereby weakening ice to the point that it breaks from the coastline to become drift ice, or melts entirely, ending the annual cycle.

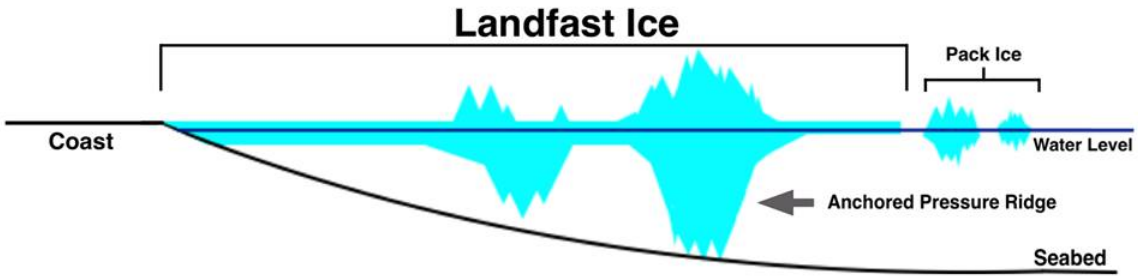

Figure 1.1: Landfast Ice Conceptual Model

Landfast ice annual cycles are important for its influence on other biogeophysical processes; this relevance is evident in the diversity of topics addressed by studies where landfast ice is a necessary consideration. For example, landfast ice features in literature pertaining to the migration and habitat of marine mammals such as walrus and seal (Kawerak 2013; Oceana and Kawerak 2014; Ray et al. 2016), where the timing and distribution of landfast ice influences the timing and location of migrations. Studies on coastal Alaskan subsistence activities have noted that landfast ice serves an important

role as a travel/hunting platform (Huntington et al. 2013; Ray et al. 2016; Robards et al. 2013). Landfast ice is also relevant to gas development by providing a stabilizing platform (Anders 1973; Eicken et al. 2009; Mahoney et al. 2006).

Landfast ice has further relevance to Arctic and Subarctic coastal processes. Coastal morphology and erosion, for example, are processes directly impacted by the capacity of landfast ice to absorb eroding wind and ocean energy (Lantuit and Pollard 2008). Landfast ice has also been shown to regulate freshwater dispersal in winter and spring months (Eicken et al. 2005; Nalimov 1995; Reimnitz 2000) as well as the transport of dissolved and particulate matter into oceans (Gordeev et al. 1996; Rachold et al 1996; Lobbes et al. 2000).

Changes in the landfast ice annual cycle have the potential to alter the dynamics of these interacting processes, noted above. For example, reduced seasonal durations can increase coastal exposure to storms and other erosive energy; reduced seasonal extent can interfere with wildlife migratory/foraging behavior and impede subsistence activities. Thus, studies that characterize the landfast ice annual cycle are widely cited by studies addressing land, ocean, and atmospheric processes in Arctic and Subarctic coastal zones. For example, Radosavljevic et al. (2016) considers landfast ice decline to influence coastal vulnerability when in assessing potential erosion and flood hazards in the Beaufort Sea. Pickart et al. (2011) investigates an autumn upwelling event on the Beaufort slope using oceanic and atmospheric data, of which landfast ice is a relevant feature. Williams and Carmack (2015) consider landfast ice phenology and morphology in their review of how sea ice retreat affects nutrient and water cycling between inner and outer shelves in the Arctic Ocean.

1.3.3 Remote Sensing in Landfast Ice Research

Remote sensing methods are necessary in the study of landfast ice processes that occur over broad spatial and temporal scales. Studies applying remote sensing methods generally rely on satellite imagery to account for large landfast ice spatial extents, as well as rapid changes in surface properties and position. In such studies, areas of landfast ice are commonly identified using methods that differentiate stationary and moving sea ice.

Fraser et al. (2009) detects landfast ice using cloud-free composites of MODIS visible and thermal-infrared imagery over East Antarctica. MODIS images acquired over ten consecutive days comprise the cloud-free composite images. Using this method, landfast ice is distinguishable by the absence of leads – linear cracks caused by divergent motion of ice bodies. The landfast ice adjacent to the East Antarctic coastline in these composites are manually digitized, using sea ice extent data from the Special Sensor Microwave Imager (SSM/I) as a reference. Fraser et al. (2012) applies this method to create the first continuous time series of landfast ice extent along the East Antarctic coast from March 2000 to December 2008. The use of visible and thermal infrared sensors to detect landfast ice in this study is complicated by cloud cover, polar nights, and difficulty distinguishing the thermal signatures of sea ice and ocean water with the onset of melt conditions.

Synthetic Aperture Radar (SAR) can overcome some of the limitations inherent in optical imagery. Mahoney et al. (2004) uses RADARSAT-1 imagery to advance a method for landfast ice detection in the Alaskan Arctic. This method entails using three consecutive RADARSAT-1 ScanSAR wide beam images obtained within a 20 day period to distinguish stationary and moving sea ice. To identify areas of landfast ice, the horizontal and vertical gradient fields are calculated for each image, which are then used

to calculate the net gradient difference among the three images. The calculation of gradient fields is necessary to account for differing incidence angles between sensor orbits that may result in different back scatter values unrelated to sea ice motion. Landfast ice is evident when the final output reveals linear regions of high net gradient difference that are contiguous with the coastline. These regions represent the landfast ice edge. Mahoney et al. (2007) applies this method to characterize monthly minimum, mean, and maximum landfast ice extents and their linkages to atmospheric circulation and bathymetry in the Beaufort Sea. Mahoney et al. (2014) extends the method from Mahoney et al. (2004), to characterize the annual cycle of landfast ice in the Beaufort and Chukchi Seas from 1996 to 2008.

Landfast ice has been identified using Interferometric Synthetic Aperture Radar (InSAR). Meyer et al. (2011) advances an InSAR approach with imagery from the Advanced Land Observing Satellite (ALOS). This was accomplished by pairing SAR images over the study area in order to generate interferograms where surface deformations between the acquisition of the two images can be determined. Generally, the time between the two images is informed by the repeat interval of the orbiting satellite. Therefore, this study defined landfast ice as sea ice that has remained stationary for 46 days–the repeat interval of the ALOS satellite. High coherence regions (areas of low surface deformation)that are contiguous to the coastline are classified as landfast ice; low coherence regions are classified as open water or moving pack ice. The accuracy of these results were determined using Mahoney et al.'s (2004) net gradient difference method over the same area.

1.3.4 Study Area: The Bering Sea

The geographic region of study in this dissertation is the Bering Sea, a marginal subarctic sea in the northern Pacific Ocean (*Figure 1.2*). The Bering Sea extends from the Alaska Peninsula and Aleutian Island chain in the south to the Bering Strait in the north, and is flanked by Siberia to the west, and Alaska to the east (IHO 1953). The seafloor consists of a shallow continental shelf that rapidly descends into the North Aleutians Basin in the southern Bristol Bay Region. The subduction of the Kula Plate under Alaska has resulted in the formation of numerous volcanic islands in the region (Delong et al. 1978). More recently, the subduction of the Pacific tectonic plate against the North American plate has resulted in a chain of 40 active volcanoes that comprise the Aleutian Islands (Harbert et al. 1986). The Bering Sea region is also notable for having one of the largest river deltas in the world: The Yukon-Kuskokwim (YK) Delta, which is the largest source of terrigenous sediment transport into the Bering Sea (Drake et al. 1980).

Sea ice is a seasonal feature in the Bering Sea, and occurs with the onset of freezing temperatures and the wind-driven transport of sea ice through the Bering Strait (Robards et al. 2013; Stabeno et al. 2007). Some of this sea ice is transported into coastal zones to become landfast ice. Seasonal ice cover is integral to human activities, wildlife behavior, and the marine ecology of the Bering Sea. Sea ice is an essential feature for the Inupiat, Yupik, and St. Lawrence Island Yupik communities on Alaskan coastline, as it provides a surface for travel (Robards et al. 2013), facilitates subsistence activities and resources (Kawerak 2013; Oceana and Kawerak 2014), and protects coastal infrastructure from storm surges (Lantuit & Pollard 2008; Vermaire et al. 2013). Sea ice also provides habitat

for migratory marine mammals. Landfast ice provides platforms for ringed seals to rest, give birth, and nurse young; walrus congregate on mobile pack ice and forage on benthic communities. The seasonal presence and absence of ice cover influences photosynthetic activity of phytoplankton, which form the foundation of benthic and pelagic communities that sustain migratory marine mammals and subsistence communities (Oceana and Kawerak 2014). As multiyear and first year sea ice retreats northward (Serreze and Strove 2015), sea ice cover in the Bering Sea has experienced the greatest reductions in sea ice extent since satellite observations began in 1972 (Eisner 2018; Stabeno et al. 2018). Declines in sea ice cover – including landfast ice cover – carry consequences for human activities (Oceana and Kawerak 2014; Robards et al. 2013), ecosystem function (Grebmeier et al. 2006; Mueter and Litzow 2008), and coastline protection (Lantuit & Pollard 2008; Vermaire et al. 2013) in the Bering Sea.

This dissertation focuses on landfast ice in the northern and eastern regions of the Bering Sea. St. Lawrence Island is the focus of the northern Bering Sea research; the sections of Alaskan coastline extending from the western tip of the Seward Peninsula to the Kuskokwim river delta is the focus of the eastern Bering Sea research (*Figure 1.2*). St. Lawrence Island is a volcanic island to the west of mainland Alaska, approximately 60 60° North. Two communities are located on the northern and northwest coasts of the Island: Savoogna (population: 705) and Gambell (population: 700), respectively (U.S. Census Bureau 2018). The communities are culturally St. Lawrence Island Yupik and host subsistence economies based on the migratory patterns of marine mammals. From late spring to early summer, St. Lawrence Island is encircled by a combination of landfast ice and high concentrations of pack ice. During winter, the northern coast is typically

bordered by several kilometers of landfast ice with little or no open water at its edge where it meets the drifting pack ice, which frequently attaches and separates from the coast (Oceana and Kawerak 2014). By contrast, landfast ice on the southern coast is much narrower and is typically bordered by polynyas – persistent areas of open water in sea ice conditions – and low-

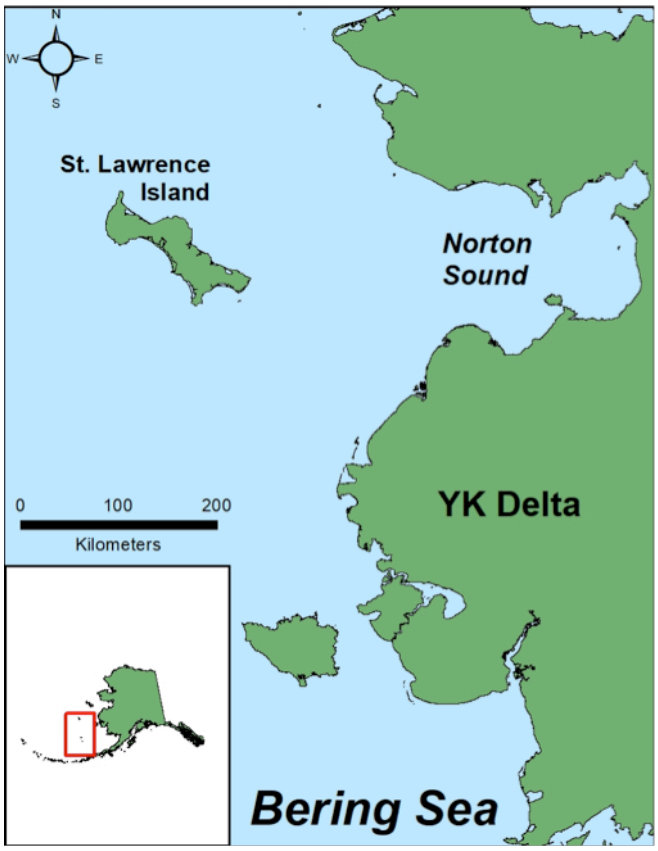

Figure 1.2: Study Area

concentration drift ice (Kapsch et al. 2010; Kawerak 2013). The eastern Bering Sea contains the Norton Sound and YK Delta. Bathymetry is relatively shallow, and contains a broad shelf less than 50 meters deep that can be attributed to large sediment deposits from the YK Delta (Drake et al. 1980). High concentrations of pack ice generally occur in the Norton Sound, and landfast ice typically borders the YK Delta (Barry et al. 1979; Kawerak 2013).

1.4 References

Anders, E. (1973). *U.S. Patent No. 3,749,162*. Washington, DC: U.S. Patent and Trademark Office.

Barry, R.G., Moritz, R.E., Rogers, J.C., 1979. The fast ice regimes of the Beaufort and Chukchi Sea coasts, Alaska. Cold Regions Science and Technology, 1 (2), 129–152.

Barry, R. G., Serreze, M. C., Maslanik, J. A., & Preller, R. H. (1993). The Arctic sea ice-climate system: Observations and modeling. *Reviews of Geophysics*, *31*(4), 397-422.

Barry, R. G. (1996). The parameterization of surface albedo for sea ice and its snow cover. *Progress in Physical Geography*, *20*(1), 63-79.

Beaumier, M. C., & Ford, J. D. (2010). Food insecurity among Inuit women exacerbated by socioeconomic stresses and climate change. *Canadian Journal of Public Health/Revue Canadienne de Sante'e Publique*, 196-201.

Bhatt, U. S., Walker, D. A., Raynolds, M. K., Comiso, J. C., Epstein, H. E., Jia, G., ... & Webber, P. J. (2010). Circumpolar Arctic tundra vegetation change is linked to sea ice decline. *Earth Interactions*, *14*(8), 1-20.

Boetius, A., Albrecht, S., Bakker, K., Bienhold, C., Felden, J., Fernández-Méndez, M., ... & Nicolaus, M. (2013). Export of algal biomass from the melting Arctic sea ice. *Science*, *339*(6126), 1430-1432.

Borgerson, S. G. (2008). Arctic meltdown: the economic and security implications of global warming. *Foreign affairs*, 63-77.

Burek, K. A., Gulland, F. M., & O'Hara, T. M. (2008). Effects of climate change on Arctic marine mammal health. *Ecological Applications*, *18*(sp2), S126-S134.

Comiso, J. C., Parkinson, C. L., Gersten, R., & Stock, L. (2008). Accelerated decline in the Arctic sea ice cover. *Geophysical research letters*, *35*(1).

Curry, J. A., Schramm, J. L., & Ebert, E. E. (1995). Sea ice-albedo climate feedback mechanism. *Journal of Climate*, *8*(2), 240-247.

Delong, S. E., Fox, P. J., & McDowell, F. W. (1978). Subduction of the Kula ridge at the Aleutian trench. *Geological Society of America Bulletin*, *89*(1), 83-95.

Drake, D. E., Cacchione, D. A., Muench, R. D., & Nelson, C. H. (1980). Sediment transport in Norton Sound, Alaska. *Marine Geology*, *36*(1-2), 97-126.

Eicken, H., Lovecraft, A. L., & Druckenmiller, M. L. (2009). Sea-ice system services: A framework to help identify and meet information needs relevant for Arctic observing networks. *Arctic*, 119-136.

Ford, J. D., Berrang-Ford, L., King, M., & Furgal, C. (2010). Vulnerability of Aboriginal health systems in Canada to climate change. *Global Environmental Change*, *20*(4), 668-680.

Ford, J. D., & Beaumier, M. (2011). Feeding the family during times of stress: experience and determinants of food insecurity in an Inuit community. *The Geographical Journal*, *177*(1), 44-61.

Fraser, A. D., Massom, R. A., & Michael, K. J. (2009). A method for compositing polar MODIS satellite images to remove cloud cover for landfast sea-ice detection. *IEEE Transactions on Geoscience and Remote Sensing*, *47*(9), 3272-3282.

Fraser, A. D., Massom, R. A., & Michael, K. J. (2010). Generation of high-resolution East Antarctic landfast sea-ice maps from cloud-free MODIS satellite composite imagery. *Remote Sensing of Environment*, *114*(12), 2888-2896.

Fraser, A. D., Massom, R. A., Michael, K. J., Galton-Fenzi, B. K., & Lieser, J. L. (2012). East Antarctic landfast sea ice distribution and variability, 2000–08. *Journal of Climate*, *25*(4), 1137-1156.

Gautier, D. L., Bird, K. J., Charpentier, R. R., Grantz, A., Houseknecht, D. W., Klett, T. R., ... & Sørensen, K. (2009). Assessment of undiscovered oil and gas in the Arctic. *Science*, *324*(5931), 1175-1179.

Goldenberg, S. (2014). America's first climate refugees. In *The Ocean* (p. 179).

Goosse, H., Arzel, O., Bitz, C. M., de Montety, A., & Vancoppenolle, M. (2009). Increased variability of the Arctic summer ice extent in a warmer climate. *Geophysical Research Letters*, *36*(23).

Gordeev, V. V., Martin, J. M., Sidorov, I. S., & Sidorova, M. V. (1996). A reassessment of the Eurasian river input of water, sediment,

Grebmeier, J. M., Overland, J. E., Moore, S. E., Farley, E. V., Carmack, E. C., Cooper, L. W., ... & McNutt, S. L. (2006). A major ecosystem shift in the northern Bering Sea. *Science*, *311*(5766), 1461-1464.

Harbert, W., Scholl, D. W., Vallier, T. L., Stevenson, A. J., & Mann, D. M. (1986). Major evolutionary phases of a forearc basin of the Aleutian terrace: Relation to North Pacific tectonic events and the formation of the Aleutian subduction complex. *Geology*, *14*(9), 757-761.

Hunt Jr, G. L., Stabeno, P., Walters, G., Sinclair, E., Brodeur, R. D., Napp, J. M., & Bond, N. A. (2002). Climate change and control of the southeastern Bering Sea pelagic ecosystem. *Deep Sea Research Part II: Topical Studies in Oceanography*, *49*(26), 5821-5853.

Huntington, H. P., Noongwook, G., Bond, N. A., Benter, B., Snyder, J. A., & Zhang, J. (2013). The influence of wind and ice on spring walrus hunting success on St. Lawrence Island, Alaska. *Deep Sea Research Part II: Topical Studies in Oceanography*, *94*, 312-322.

International Hydrographic Organization (1953) *Limits of Oceans and Seas, 3rd edition*.

IPCC, 2013: Climate Change 2013: The Physical Science Basis. Contribution of Working Group I to the Fifth Assessment Report of the Intergovernmental Panel on Climate Change [Stocker, T.F., D. Qin, G.-K. Plattner, M. Tignor, S.K. Allen, J. Boschung, A. Nauels, Y. Xia, V. Bex and P.M. Midgley (eds.)]. Cambridge University Press, Cambridge, United Kingdom and New York, NY, USA, 1535 pp, doi:10.1017/CBO9781107415324.

Kawerak, Inc. 2013. Seal and walrus harvest and habitat areas for nine Bering Strait Region communities. Nome, AK: Kawerak, Inc., Social Science Program

Lantuit, H., & Pollard, W. H. (2008). Fifty years of coastal erosion and retrogressive thaw slump activity on Herschel Island, southern Beaufort Sea, Yukon Territory, Canada. *Geomorphology*, *95*(1-2), 84-102.

Lobbes, J. M., Fitznar, H. P., & Kattner, G. (2000). Biogeochemical characteristics of dissolved and particulate organic matter in Russian rivers entering the Arctic Ocean. *Geochimica et Cosmochimica Acta*, *64*(17), 2973-2983.

Mahoney, A., Eicken, H., Graves, A., Shapiro, L., & Cotter, P. (2004, September). Landfast sea ice extent and variability in the Alaskan Arctic derived from SAR imagery. In *Geoscience and Remote Sensing Symposium, 2004. IGARSS'04. Proceedings. 2004 IEEE International* (Vol. 3, pp. 2146-2149). IEEE.

Mahoney, A., Eicken, H., Gaylord, A. G., & Shapiro, L. (2007). Alaska landfast sea ice: Links with bathymetry and atmospheric circulation. *Journal of Geophysical Research: Oceans*, *112*(C2).

Mahoney, A. R., Eicken, H., Gaylord, A. G., & Gens, R. (2014). Landfast sea ice extent in the Chukchi and Beaufort Seas: The annual cycle and decadal variability. *Cold Regions Science and Technology*, *103*, 41-56.

Meyer, F. J., Mahoney, A. R., Eicken, H., Denny, C. L., Druckenmiller, H. C., & Hendricks, S. (2011). Mapping arctic landfast ice extent using L-band synthetic aperture radar interferometry. *Remote sensing of environment*, *115*(12), 3029-3043.

Nalimov, Y. V. (1995). The ice-thermal regime at front deltas of rivers of the Laptev Sea. *Reports on Polar Research*, *176*, 55-61.

Oceana and Kawerak. 2014. Bering Strait Marine Life and Subsistence Use Data Synthesis. Oceana and Kawerak, Juneau, AK.

Perovich, D. K., Grenfell, T. C., Light, B., & Hobbs, P. V. (2002). Seasonal evolution of the albedo of multiyear Arctic sea ice. *Journal of Geophysical Research: Oceans*, *107*(C10), SHE-20.

Persson, P. O. G., Fairall, C. W., Andreas, E. L., Guest, P. S., & Perovich, D. K. (2002). Measurements near the Atmospheric Surface Flux Group tower at SHEBA: Near-surface conditions and surface energy budget. *Journal of Geophysical Research: Oceans*, *107*(C10), SHE-21.

Petrich, C., & Eicken, H. (2010). Growth, structure and properties of sea ice. *Sea ice*, *2*, 23-77.

Pickart, R. S., Spall, M. A., Moore, G. W., Weingartner, T. J., Woodgate, R. A., Aagaard, K., & Shimada, K. (2011). Upwelling in the Alaskan Beaufort Sea: Atmospheric forcing and local versus non-local response. *Progress in Oceanography*, *88*(1-4), 78-100.

Post, E., Bhatt, U. S., Bitz, C. M., Brodie, J. F., Fulton, T. L., Hebblewhite, M., ... & Walker, D. A. (2013). Ecological consequences of sea-ice decline. *Science*, *341*(6145), 519-524.

Rachold, V., Alabyan, A., Hubberten, H. W., Korotaev, V. N., & Zaitsev, A. A. (1996). Sediment transport to the Laptev Sea–hydrology and geochemistry of the Lena River. *Polar Research*, *15*(2), 183-196.

Radosavljevic, B., Lantuit, H., Pollard, W., Overduin, P., Couture, N., Sachs, T., ... & Fritz, M. (2016). Erosion and flooding—threats to coastal infrastructure in the Arctic: a case study from Herschel Island, Yukon Territory, Canada. *Estuaries and Coasts*, *39*(4), 900-915.

Rawlings, A. (2015). Erosion-induced community displacement in Newtok, Alaska and the need to modify FEMA and NEPA to establish a relocation framework for a warming world. *Seattle J. Envtl. L.*, *5*, i.

Ray, G. C., Hufford, G. L., Overland, J. E., Krupnik, I., McCormick-Ray, J., Frey, K., & Labunski, E. (2016). Decadal Bering Sea seascape change: consequences for Pacific walruses and indigenous hunters. Ecological Applications, 26(1), 24-41.

Reimnitz, E., Dethleff, D., & Nürnberg, D. (1994). Contrasts in Arctic shelf sea-ice regimes and some implications: Beaufort Sea versus Laptev Sea. *Marine Geology*, *119*(3-4), 215-225.

Reimnitz, E., Eicken, H., & Martin, T. (1995). Multiyear fast ice along the Taymyr Peninsula, Siberia. *Arctic*, 359-367.

Robards, M. D., Kitaysky, A. S., & Burns, J. J. (2013). Physical and sociocultural factors affecting walrus subsistence at three villages in the northern Bering Sea: 1952–2004. Polar Geography, 36(1-2), 65-85.

Serreze, M. C., Holland, M. M., & Stroeve, J. (2007). Perspectives on the Arctic's shrinking sea-ice cover. *science*, *315*(5818), 1533-1536.

Stephenson, S. R., Smith, L. C., & Agnew, J. A. (2011). Divergent long-term trajectories of human access to the Arctic. *Nature Climate Change*, *1*(3), 156.

Stephenson, S. R., Smith, L. C., Brigham, L. W., & Agnew, J. A. (2013). Projected 21st-century changes to Arctic marine access. *Climatic Change*, *118*(3-4), 885-899.

Stroeve, J., Holland, M. M., Meier, W., Scambos, T., & Serreze, M. (2007). Arctic sea ice decline: Faster than forecast. *Geophysical research letters*, *34*(9).

Stroeve, J. C., Serreze, M. C., Holland, M. M., Kay, J. E., Malanik, J., & Barrett, A. P. (2012). The Arctic's rapidly shrinking sea ice cover: a research synthesis. *Climatic Change*, *110*(3-4), 1005-1027.

USACE. 2009. Alaska Baseline Erosion Assessment: Study Findings and Technical Report. U.S. Army Corps of Engineers, Alaska District.

U.S. Fish and Wildlife Service, 2008. Endangered and threatened wildlife and plants; determination of threatened status for the polar bear (Ursus maritimus) throughout its range; Final rule. *Federal Register* 73 (95)

Vermaire, J. C., Pisaric, M. F., Thienpont, J. R., Courtney Mustaphi, C. J., Kokelj, S. V., & Smol, J. P. (2013). Arctic climate warming and sea ice declines lead to increased storm surge activity. *Geophysical Research Letters*, *40*(7), 1386-1390.

Wadhams, P., & Davis, N. R. (2000). Further evidence of ice thinning in the Arctic Ocean. *Geophysical Research Letters*, *27*(24), 3973-3975.

Weaver, J.C, 1951, The ice of sea in the North American Arctic, in Vilhjalmur Stefansson (ed.) Encyclopedia Arctica, Vol. 7 (12), The Stefansson Library, New York

Whiteman, G., Hope, C., & Wadhams, P. (2013). Climate science: Vast costs of Arctic change. *Nature*, *499*(7459), 401.

Williams, W. J., & Carmack, E. C. (2015). The 'interior'shelves of the Arctic Ocean: Physical oceanographic setting, climatology and effects of sea-ice retreat on cross-shelf exchange. *Progress in Oceanography*, *139*, 24-41.

World Meteorological Organization. (1970). *WMO Sea-ice Nomenclature: Terminology, Codes, Illustrated Glossary and Symbols*. Secretariat of the World Meteorological Organization.

Chapter 2. The Annual Cycle of Landfast Ice in the Eastern Bering Sea

2.1 Introduction

This chapter analyzes spatial and temporal patterns of landfast ice distribution in the Eastern Bering Sea using a time series of Radarsat-1 Synthetic Aperture Radar (SAR) imagery. The objectives of this study are to 1) collect landfast ice data to identify patterns in its spatial distribution along Eastern Bering Sea coastlines; 2) Identify the relationship between landfast ice spatial distribution and the physical geography of the Eastern Bering Sea region; 3) measure interannual variability of the landfast ice annual cycle. To achieve these objectives, we used net-gradient difference algorithms on the Radarsat-1 SAR imagery to identify regions of landfast ice, and quantified its spatial and temporal patterns in a GIS.

2.2 Publication

The manuscript related to this chapter was published in *Cold Regions Science and Technology*, and can be found in Appendix A.

Jensen, D., Mahoney, A., & Resler, L. (2020). The annual cycle of landfast ice in the eastern Bering Sea. *Cold Regions Science and Technology*, 103059.

Chapter 3. Interannual Declines of St. Lawrence Island Landfast Ice Cover

3.1 Introduction

This Chapter analyzes spatial and temporal patterns of landfast ice distribution on St. Lawrence Island using a time series of Radarsat-1, ENVISAT, and Sentinel-1 Synthetic Aperture Radar (SAR) imagery. The objectives of this study are to 1) Identify patterns in the spatial distribution and seasonal duration of St. Lawrence Island's landfast ice cover; 2) Observe how St. Lawrence Island and the northern Bering Sea's physical geography influence Objective 1 findings; and 3) characterize interannual change of Objective 1 findings from 1996 – 2019.

3.2 Manuscript

Appendix B contains the draft of the original manuscript to be submitted to *Physical Geography*.

Jensen, David A., Andy Mahoney, Lynn M. Resler. In Preparation. "Significant Interannual Declines of St. Lawrence Island Landfast Ice Cover." *Physical Geography.*

Chapter 4. Modeling Landfast Ice Cover on St. Lawrence Island, AK, USA

4.1 Introduction

This chapter advances a spatial logistic regression modeling approach toward the study of landfast ice cover on St. Lawrence Island. The objectives of this study are to determine geographic and meteorological correlates of landfast ice cover distribution using freely accessible data and methods that expedite the estimation of landfast ice cover.

4.2 Publication

The draft of this manuscript is in Appendix C. It is currently being revised for submission into Geocarto International

Jensen, David A., Lynn M. Resler, Yang Shao. In Preparation. "Modeling Landfast Ice Cover on St. Lawrence Island, AK, USA."

Chapter 5. Conclusions

The global retreat of cryospheric features provides impetus for observing and monitoring landfast ice conditions in Arctic and Subarctic environments. Such information will enable scientists and communities to anticipate and understand how change in landsfast ice cover may influence human and environmental processes. The research presented in this dissertation aimed to: 1) Establish a baseline analysis of spatial and temporal landfast ice patterns on Eastern Bering Sea coastlines and its relationship with the region's physical geography; 2) Use multiple SAR sensors to broaden the temporal scale of landfast ice observation over regions of interest in the Bering Sea; and 3) Use datasets from landfast ice observations toward the creation of a spatial model that explores the relationship between landfast ice cover and the Bering Sea's physical geography.

This dissertation research resulted in several findings that are useful to the observation and synthesis of landfast ice conditions in the Bering Sea. First, I established a baseline set of observations in the Eastern Bering Sea and St. Lawrence Island. The first set of observations focused on the Eastern Bering Sea from 1996–2008 using a time series of Radarsat-1 imagery. The second set of observations focused on St. Lawrence Island from 199 –2008 using a time series of Radarsat-1, ENVISAT, and Sentinel-1 imagery. The data created from these observations are the most comprehensive landfast ice spatial datasets to date in the Bering Sea region. Together these observations revealed a unique landfast ice regime distinct from the Beaufort and Chukchi Seas. The information from these observations can be used to examine relationships between landfast ice and the Bering Sea physical geography.

Second, this dissertation used the baseline set of observations to examine relationships between landfast ice cover and the Bering Sea's physical geography, such as bathymetry and coastal morphology. This research also assessed interannual variations in landfast ice spatial and temporal patterns. This research revealed landfast ice cover in the Bering Sea to exhibit changes consistent with broader variability in the region's sea ice cover, especially on St. Lawrence Island. Outcomes in landfast ice variability were influenced by the physical geography of the region. Findings from this research can be

used to anticipate future landfast ice changes elsewhere as the Arctic Isothermal Boundary retreats northward.

Third, this research advances a spatial modeling method to estimate the location of landfast ice cover under varying conditions in the physical environment and regional climate. Using landfast ice data we created over St. Lawrence Island, we determined geographic and meteorological correlates of landfast ice cover distribution. The method provides an alternative approach to generating landfast ice spatial data, which has been generally created using remote sensing methods that are labor-intensive and difficult to automate. By measuring the influence of physical and meteorological conditions, this modeling approach can expedite the estimation of landfast ice cover in a given area. Further, this modeling approach was accomplished with freely-accessible data, increasing its utility in other study regions.

Lastly, this study provides a basis for future Bering Sea research where landfast ice is a relevant consideration. This dissertation can inform research spanning across numerous disciplines. Landfast ice in the Bering Sea is a feature relevant to community livelihoods, ecosystem functions, coastal geomorphology, and the regulation of regional as well as global climate systems. The data and findings of this research will facilitate future research and discussion of challenges and opportunities facing the Bering Sea region.

Appendix: Publications related to this research

Appendix A. Jensen, Mahoney and Resler (2020). The Landfast Ice Annual Cycle in the Eastern Bering Sea

Cold Regions Science and Technology 174 (2020) 103059

Contents lists available at ScienceDirect

Cold Regions Science and Technology

journal homepage: www.elsevier.com/locate/coldregions

The annual cycle of landfast ice in the eastern Bering Sea

David Jensen[a,*], Andy Mahoney[b], Lynn Resler[a]

[a] Department of Geography, College of Natural Resources and Environment, Virginia Polytechnic Institute and State University, Blacksburg, VA, USA
[b] Geophysical Institute, University of Alaska Fairbanks, Fairbanks, Alaska

ARTICLE INFO

Keywords:
Landfast
Sea ice
Subarctic
Bering Sea

ABSTRACT

Seasonal sea ice – ice which freezes in late fall and melts completely the following summer – is a central feature in the ecology, geomorphology, and climatology of the eastern Bering Sea. In this region's coastal zones, sea ice becomes locked in a stationary position against coastlines and influences interactions among land, ocean, and atmospheric processes. A thorough understanding of how this stationary ice, known as landfast ice, affects unique biogeophysical processes in the eastern Bering Sea region is limited by a lack of data on its areal coverage and seasonal duration. Here, we present the most comprehensive landfast ice dataset created to date for the Alaska Bering Sea region, derived using satellite imagery dated 1996–2008. This study provides a baseline set of observations regarding the landfast ice regime by identifying patterns in spatial distribution and interannual change. Our results show that spatial distribution and interannual change vary by regional geography in the eastern Bering Sea. Landfast ice widths averaged approximately 4.2 km on Northern Section, 18.8 km on the Central Section coastlines, and 8.9 km on the Yukon-Kuskokwim Delta. Modal water depths at the landfast ice edge varied by the Northern Northern, Central, and Southern Section coastlines as well, with respective modal values of −13 m, −7 m, and − 8.5 m. We attribute these regional variations in width and water depth to differing conditions in near-shore bathymetry and coastal morphology. On an interannual basis, landfast ice formed 5 days later in the year, and broke up 4 days earlier on average in the eastern Bering Sea region from 1996 to 2008. Notably, ice-free conditions occurred 15 days later on the Central Section coastlines. The spatial distribution and interannual change of landfast ice is of importance to associated environmental changes in the eastern Bering Sea region, including accelerated coastal erosion, difficulties surrounding subsistence activities, diminishing wildlife habitat, and seasonal shifts in sediment transport into marine food webs from rivers.

1. Introduction

Seasonal and multiyear sea ice is declining in Arctic and Subarctic seas (Stroeve et al., 2007, 2008). These declines are geographically heterogeneous. For example, sea ice in the Beaufort and Chukchi seas have declined on an interannual basis, whereas sea ice coverage in the Bering Sea has exhibited increasing interannual variability that could not similarly be characterized as a decline (Frey et al., 2015). This declining trend is of particular importance for coastal zones and inner-shelf waters, where sea ice assumes a stationary position against coastlines and shallow seabeds, becoming landfast ice. Landfast ice, also termed *fast* or *shorefast* ice, refers to stationary sea ice that is frozen in place against a coastline (World Meteorological Organization, 1970). Landfast ice plays an important role in mediating exchanges and interactions among land, ocean, and the atmosphere (Lantuit and Pollard, 2008; Mahoney et al., 2014). Changes in the landfast ice annual cycle – the seasonal process by which landfast ice forms in the winter, interacts with the surrounding environment, and melts in the spring – carry wide-ranging implications for interacting human (Druckenmiller et al. 2009; Kawerak 2013; Oceana and Kawerak, 2014), ecological (Attard et al. 2018; Hamilton et al. 2017; Oceana and Kawerak, 2014), and geophysical processes (Antonova, 2011; Barnhart et al., 2014; Lantuit and Pollard, 2008). However, incomplete spatial datasets of landfast ice in recent decades limit how ongoing changes are understood and modeled in the Bering Sea region.

In Western Alaska, direct observations have been used to characterize change in landfast ice in areas for which there are limited comprehensive datasets (Kawerak 2013; Oceana and Kawerak, 2014). Observations from Western Alaskan communities in the Bering Sea describe landfast ice as forming later and becoming increasingly harder to predict with regards to spatial extent and seasonal onset (Huntington et al., 2013; Kawerak 2013). Such changes are accompanied by human and ecological challenges, such as the maintenance of subsistence activities and transportation (Huntington et al., 2013; Oceana and

* Corresponding author at: Department of Geography, Virginia Tech, 220 Stranger Street, Blacksburg, VA 24061, USA.
E-mail address: ajdavid6@vt.edu (D. Jensen).

https://doi.org/10.1016/j.coldregions.2020.103059
Received 16 July 2019; Received in revised form 10 January 2020; Accepted 25 March 2020
Available online 26 March 2020
0165-232X/

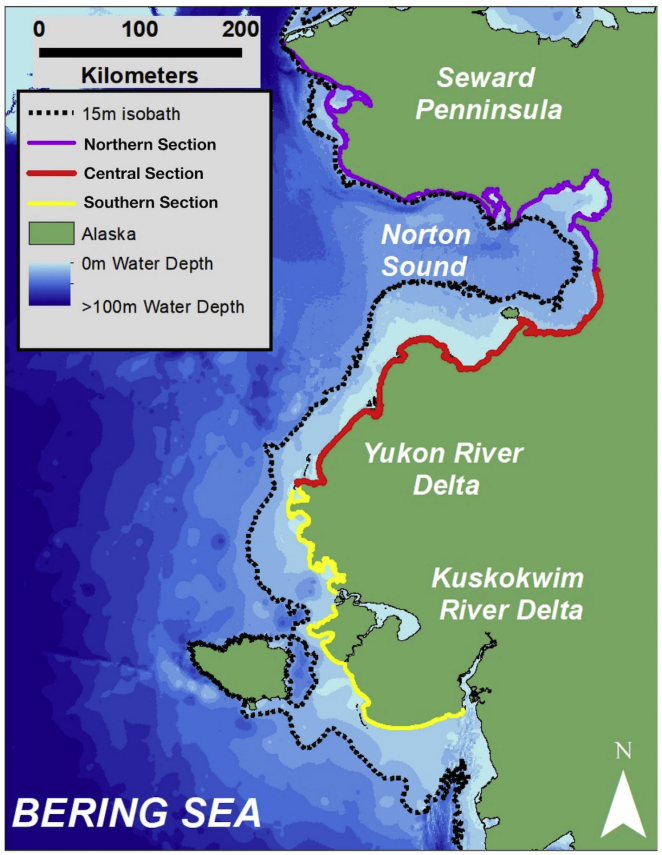

Fig. 1. Alaskan Coastlines on the Bering Sea. Also depicted are the three geographic regions of our study area: Northern Section, Central Section and Southern Section. The dashed line represents the 15 m isobath contour overlain with a Digital Elevation Model of the ocean floor.

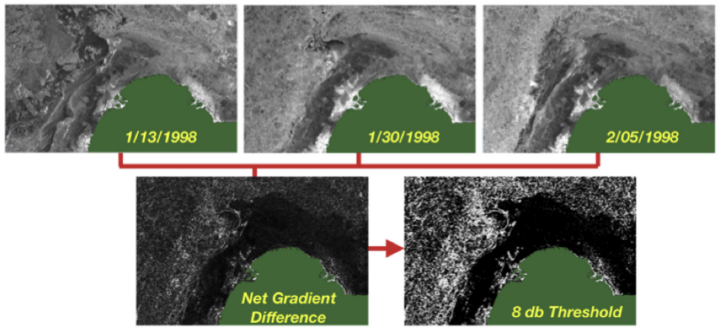

Fig. 2. Visualization of process output in the Norton Sound. Note the 8-dB threshold on pixel values increases the contrast between stationary and moving ice.

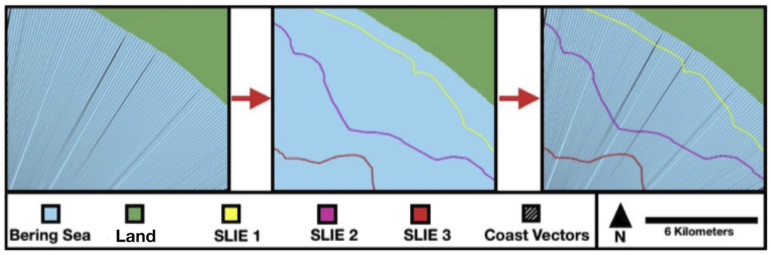

Fig. 3. Geospatial modeling steps to measure distance of the SLIE from the coast.

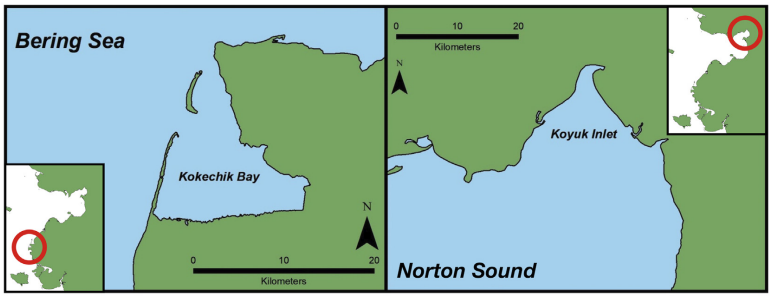

Fig. 4. Examples of sheltered regions identified in our study area. The Koyuk Inlet on the Northern Section is an example of a concave section of coast identified as a sheltered embayment. The Kokechik Bay on the Southern Section is an example of a coastal area behind barrier islands.

Kawerak, 2014), habitat reduction for migratory marine mammals (U.S. Fish and Wildlife Service, 2008), and accelerated coastal erosion (Lantuit and Pollard, 2008).

The accuracy of research on the Bering Sea's changing landfast ice annual cycle and understanding of problems associated with this change would be improved by comprehensive datasets with a spatial and temporal resolution that is capable of resolving the annual cycle on an interannual basis. Generally, comprehensive datasets are created by tracking the position of the seaward landfast ice edge (SLIE), the area where landfast ice transitions to open water or floating drift ice, using satellite imagery (Fraser et al. 2009, 2010, 2012; Mahoney et al. 2004, Mahoney et al., 2007a; Mahoney et al., 2014; Meyer et al. 2011). Although landfast ice in the Chukchi and Beaufort Sea has been studied in some detail (Mahoney et al., 2007a, 2014), no comparable datasets created by tracking the SLIE to characterize interannual change existed for the Bering Sea prior to this study. However, it should be noted that Bering Sea landfast ice is considered in Yu et al.' (2014) pan-Arctic analysis of interannual landfast ice variability using ice charts from the National Ice Center. Further, Stringer's (1978) assessment of nearshore ice conditions using satellite and aerial imagery included Bering Sea landfast ice from 1973 to 76.

The objectives of this study are to: 1) collect landfast ice data to identify patterns in its spatial distribution along the Alaskan Bering Sea coastlines; 2) identify the relationship between landfast ice spatial distribution and the physical geography of the Bering Sea region; and 3) measure interannual variability of the landfast ice annual cycle. To address these objectives, we use Radarsat-1 satellite imagery to identify landfast ice, and geospatial methods to assess spatial distribution and interannual variability.

2. Background

The Bering Sea (Fig. 1) is a marginal subarctic sea of the Pacific Ocean bordered on the north by the Bering Strait and the south by the Aleutian Island Chain. Sea ice is a seasonal phenomena in the northern Bering Sea, and typically appears during the fall and winter months when a combination of diminishing solar radiation and wind-driven transport of northern-latitude ice initiates the onset of freezing conditions (Robards et al., 2013; Stabeno et al., 2007). From mid-winter to mid-spring much of the Bering Sea region is ice covered. During this time period, landfast ice is episodically changing by gradually advancing from the coast in the late fall/early winter, and retreating in the late spring/early summer, as it does in the Chukchi and Beaufort Seas (Barry et al., 1979; Mahoney et al., 2014).

The seasonal properties of landfast and drift ice in the Bering Sea are changing on an interannual basis. In the Bering Sea, the areal extent and seasonal duration of sea ice conditions have exhibited a more complex interannual variability compared to the steady declines observed in the Chukchi and Beaufort Seas (Frey et al., 2015). However, it is notable that sea ice conditions in the Bering Sea have reached historic lows in recent years. From 2017 to 2018, sea ice extent declined to the lowest levels since satellite observations began in 1972 (Eisner 2018; Stabeno and Bell, 2019). Record lows in sea ice extent continued from 2018 to 2019 as well (Duffy-Anderson et al., 2019). Low sea ice coverage during recent years was strongly influenced by warmer southerly air circulations raising surface temperatures and inhibiting the transport of sea ice into the Eastern Bering Sea (Perovich et al., 2019). Some studies suggest that landfast ice has similarly changed with unpredictable seasonal durations and spatial extents (ACIA 2005; Oceana and Kawerak, 2014), furthering the need for comparably comprehensive landfast ice spatial datasets and studies in the Bering sea region.

Bathymetric and coastal features (e.g., lagoons, inlets, shoals)

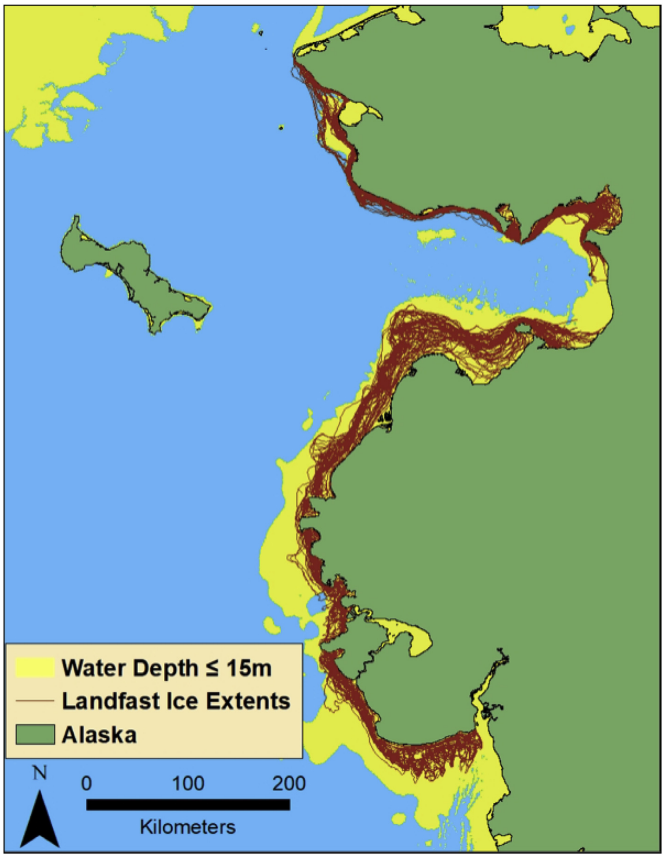

Fig. 5. All digitized SLIEs on Eastern Bering Sea coastlines from 1996 to 2008. The yellow region depicts areas where the water depth is less than or equal to 15 m. Note that a gap in Radarsat-1 coverage prevented the identification of SLIE occurrence in the southeast corner of the Norton Sound. (For interpretation of the references to colour in this figure legend, the reader is referred to the web version of this article.)

generally govern landfast ice properties in a given region. Bathymetry in the northern Bering Sea is relatively shallow (as can be seen in Fig. 1), and contains of a broad shallow shelf to the north less than 50 m deep. This shelf transitions to the North Aleutians Basin, a submarine depression, in the Bristol Bay region to the south. Bathymetry generally governs the maximum seaward extent of landfast ice in a given season by influencing how far from the coastline grounded pressure ridges may occur. Thus, regions with extensive shallow bathymetry enable greater maximum seaward extents compared to regions with steep bathymetric gradients (Mahoney et al., 2007). Furthermore, the relationship between landfast ice, bathymetry, and coastal morphology generally varies by geographic region, complicating attempts to broadly characterize landfast ice across regions (Mahoney et al., 2014). For this reason, studies characterizing the landfast ice annual cycle are typically applicable to a particular region of study, rather than polar regions as a whole (Barry et al., 1979; Divine et al., 2004; Mahoney et al., 2007a, 2014).

Landfast ice is important for its influence on many coastal processes. For example, it provides habitat for migratory marine mammals (Kawerak 2013; Oceana and Kawerak, 2014; Ray et al., 2016), protects coastlines by absorbing energy from ocean and wind action (Dumas et al., 2005; Forbes and Taylor, 1994), and provides seasonal platforms for communities to access subsistence resources (Oceana and Kawerak, 2014; Ray et al., 2016; Robards et al., 2013). Sea ice changes in the Bering Sea have paralleled changes in associated human and biogeophysical processes in recent decades. Subsistence hunters have observed increasingly unpredictable landfast ice conditions that reduce the seasonal window for safe and reliable access to subsistence resources (Kawerak 2013; Huntington et al., 2013; Robards et al. 2013). These challenges to subsistence activities have been compounded by an accompanying shift in wildlife behavior as a result of changing coastal ice conditions (Oceana and Kawerak, 2014; U.S. Fish and Wildlife Service, 2008). Furthermore, landfast ice protects coastal community infrastructure from storm surges (Vermaire et al., 2013). Changes in landfast ice cover can increase the vulnerability of coastlines to erosion (Lantuit and Pollard, 2008), and reductions of near-coastal ice have been observed to influence terrestrial ecology in Arctic and Subarctic environments (Bhatt et al., 2010; Post et al., 2013). A dataset

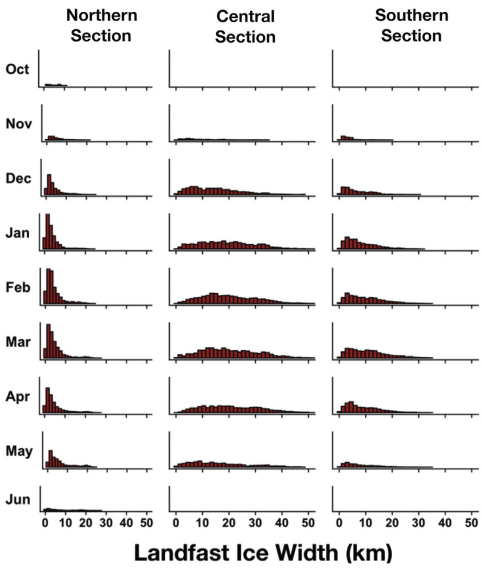

Fig. 6. Histograms of landfast ice width in the three geographic regions of the Eastern Bering Sea. Note that the Northern Section's width values are clustered between 0 and 30 km, while Central Section and Southern Section's width values extend to 60 km.

Table 1
Width Parameters in the Eastern Bering Sea.

	Northern section	Central section (S)	Southern section
Width mean	4 km	18.5 km	8.6 km
Width mode	2 km	14 km	3 km
Standard deviation	4.8 km	10.6	6.3
Upper decile	8.8 km	33.6	17.5
Skewness	2.17	0.49	1.03

characterizing the annual cycle of landfast ice and its interannual variability benefits the broader study of associated changes in human, ecological, and geophysical processes in the Bering Sea region.

3. Data and methods for landfast ice identification and analysis

3.1. Study area

We divided our study area into three areas of interest: the Northern, Central, and Southern Sections (as can be seen in Fig. 1). Geographically, these sections include the western tip of the Seward Peninsula, the Norton Sound, and the Yukon-Kuskokwim river deltas. The Norton Sound is a Bering Sea inlet to the south of the Seward Peninsula. Bathymetry in the Norton Sound is generally no deeper than 25 m. The YK Delta (located in the Central and Southern Sections) refers to the coastlines where the Yukon and Kuskokwim rivers drain into the Bering Sea to form one of the largest river deltas in the world. The YK delta is further notable as being the largest single source of sediment transport into the Bering Sea (Drake et al. 1980). Based on a previous study in the Chukchi and Beaufort Seas (e.g., Mahoney et al., 2014), we hypothesize that bathymetry and coastal morphology will influence the spatial and temporal properties of landfast ice in the Bering Sea.

3.2. Measuring landfast ice extent using synthetic aperture radar imagery

Following Mahoney et al. (2006), we used two criteria to define landfast ice in satellite imagery: 1) the sea ice is contiguous with the coastline, and 2) the sea ice exhibits no detectible motion for approximately 20 days. This definition relies on a means to identify whether sea ice has moved or remained stationary. The 20 day period allows us to exclude sea ice that is motionless, yet not held fast in a stationary position against the coastline. The criteria have been used successfully in characterizing the interannual variation of landfast ice properties (Lovvorn et al., 2018; Mahoney et al., 2007a, 2014).

A time series of synthetic aperture radar (SAR) satellite images comprises the primary dataset for this study. We used moderate resolution (100 m) Radarsat-1 ScanSAR wide beam data obtained from the Alaska Satellite Facility Vertex data gateway. Imagery selection was based on obtaining sufficient coverage to identify landfast ice within 20 day windows for our study area from 1996 to 2008. Our study period coincides with that of Mahoney et al. (2014) for the Chukchi and Beaufort Seas, and contributes to the characterization of the landfast ice annual cycle for all of Alaska from 1996 to 2008. Because Radarsat-1 stopped collecting imagery in the spring of 2008, we used ENVISAT ASAR WSM imagery from the European Space Agency's EO Data Gateway to supplement data gaps in the 2007–2008 annual cycle year. SAR is advantageous for observing sea ice in satellite imagery because sea ice can generally be identified by its higher backscatter coefficient compared to open water (Kwok et al., 1992). Furthermore, SAR image quality is not affected by weather events and prolonged polar nights, permitting year-round sea ice observation in polar environments. For these reasons, SAR is commonly used to observe landfast ice and characterize its annual cycle (Dammann et al., 2018; Mahoney et al. 2004, Mahoney et al., 2007a, Mahoney et al., 2014; Meyer et al. 2011).

We used SAR imagery to identify landfast ice areas based on the two-criteria definition described above. The stationary nature of landfast ice does not bestow it with any unique SAR backscatter characteristics that distinguish it from drifting pack ice. Therefore, landfast ice cannot generally be identified using a single satellite image. We overcame this limitation by applying a method advanced by Mahoney et al. (2004; 2006; 2007a 2014) to differentiate between stationary landfast ice and moving drift ice by visually examining the changing gradient fields of three consecutive SAR images acquired within a ~20-day period and a composite, "gradient difference" image created to highlight linear features that have remained unchanged. The technique is described in detail by Mahoney et al. (2004; 2006). Areas of low net-gradient difference in the output image represent regions that have minimally changed during the ~20-day period; areas of high net-gradient difference represent regions that have changed. The SLIE appears as a bright linear region of high net-gradient difference that is contiguous with the coastline (Fig. 2). We used the gradient difference image and consecutive SAR images to guide our identification of the SLIE. Identified SLIEs were then digitized into polyline shapefiles using ArcMap 10.6.1. This approach was advantageous over more common change-detection methods because it accounts for the fact that the backscatter values of landfast ice can change under circumstances unrelated to sea ice motion, such as when ice freezes or breaks up (Mahoney et al., 2014). Further, the calculation of gradient fields was necessary to account for differing incidence angles between sensor orbits resulting in different backscatter values of sea ice features that have not moved.

Polylines delineating the SLIE allowed us to examine the changing spatiotemporal variability of landfast ice positions over time. This is accomplished using techniques advanced by Mahoney et al. (2007a) by referencing digitized SLIEs with coastal vectors positioned at 200 m intervals along the coastline. In this study, we created 3204 vectors. Vectors are defined by creating a polyline parallel to the coast in a GIS, and finding the closest point on the coastline at 200-m intervals along this polyline. This process was repeated from the coastline to the

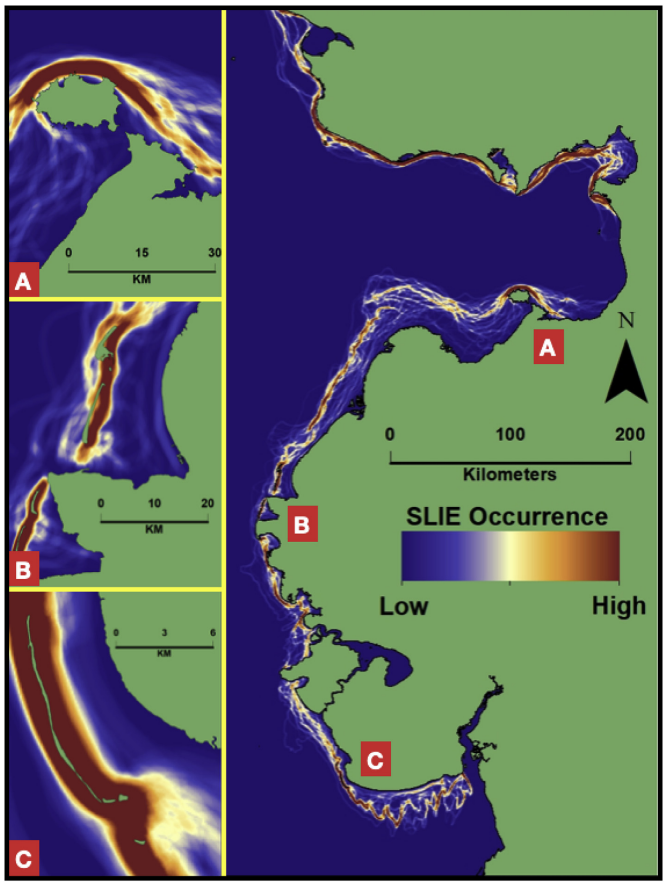

Fig. 7. Line density maps of all SLIEs in our study area. Density values are based on the occurrence of an SLIE within a 1 km buffer. Blue regions indicate low-density areas; red regions indicate high-density areas. High density areas suggest the existence of grounding features that enable the frequent recurrence of SLIEs. Note in regions A, B, and C, these grounding features are islands proximate to the coastline, that either provide shallow water depths for grounding pressure ridges, or protection from shearing forces (ie. wind/wave energy, collisions with drift ice). (For interpretation of the references to colour in this figure legend, the reader is referred to the web version of this article.)

polyline for gaps on the coast where points are more than 200 m apart, such as in concave sections. We simplified coastal topology by omitting small islands (e.g. barrier islands) from the coastal vector creation process. Identifying the points where SLIE polylines and coastal vectors intersect enabled us to measure landfast ice width (Fig. 3).

3.3. Ancillary datasets

For landfast ice anchored by grounded pressure ridges (i.e. not landlocked or anchored by icebergs), bathymetry influences the average location of the SLIE by governing where grounded pressure ridges may form. Pressure ridges form when the drifting ice floes converge, break and pile up vertically, resulting in ridges with "sails" above the waterline and keels below. These ridges may become grounded when the keel connects with the seabed in shallow water (Reimnitz et al. 1978; Kovacs, 1976; Mahoney et al. 2007b). The average location of the SLIE can be used as a proxy for understanding when landfast ice is stabilized by grounded pressure ridges. However, the relationship between bathymetry and the SLIE generally varies by region (e.g., Mahoney et al., 2014 and references therein). To observe the relationship between bathymetry and the SLIE in the Bering Sea, we used the Alaska region bathymetric digital elevation model (ARBDEM, Danielson et al. 2008) to record the water depth values at the SLIE. This dataset covers the Arctic and Pacific Oceans between 130 E to 120 W and 45 N to 75 N at 1-degree resolution. We reprojected the ARBDEM to NAD 1983 Alaska Albers, and resampled it to match the 100-m spatial resolution of the Radarsat-1 ScanSAR wide-beam imagery. To further explore how landfast ice position is influenced by coastal morphology, we obtained a shapefile of the State of Alaska from the Alaska State Geospatial Clearinghouse to visually identify sheltered embayments and lagoons. We consider embayments to be concave sections of the coast, whereas lagoons are sections of the coast behind barrier islands (Fig. 4).

3.4. Key events within the landfast ice annual cycle

We used the created data in combination with the ancillary data to identify four key landfast ice annual cycle events based on the observations of similar studies (Barry et al., 1979; Mahoney et al., 2007a, 2014). These included *First Ice*, *Stable Ice*, *Break Up* and *Ice Free*

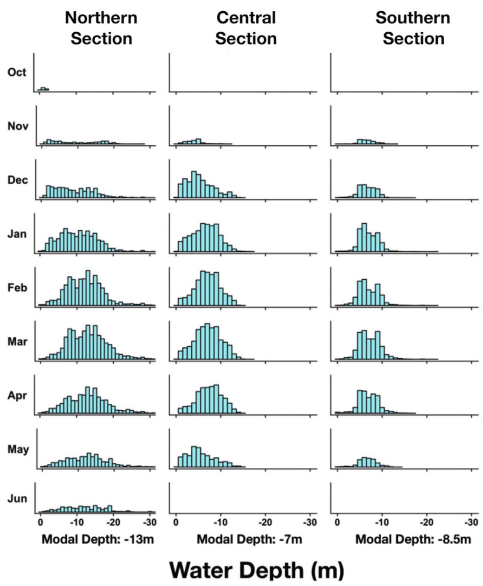

Fig. 8. Monthly histograms of water depth, by geographic region in our study area. It is important to note the how the modal values of water depth at the SLIE vary by geographic region. This is consistent with Mahoney et al.' (2014) suggestion that the relationship between landfast ice and bathymetry is can be unique to a given region of study.

coastlines:

First Ice is identifiable at the beginning of the landfast ice season when the SLIE is greater than 500 m from the coast. In this study, we based this distance on Mahoney et al.'s (2007a) determination of the geolocation accuracy of Radarsat-1 imagery to be 500 m. This distance prevented misidentifying landfast ice caused by geolocation inaccuracy.

Stable Ice occurs when grounded pressure ridges anchor the landfast ice to the seabed. Grounding pressure ridges occur beneath the landfast ice surface and therefore cannot be directly detected with SAR imagery, although interferometric SAR (InSAR) has shown promise for identifying the stabilized landfast ice that forms behind grounded ridges (Dammann et al., 2018). Since InSAR data are not available for our study region and period, we instead rely on water depth as a proxy for stability. Barry et al. (1979) and Mahoney et al. (2007a 2014) used a water depth of 15 *m* for this purpose, noting that once the SLIE this water depth, it rarely retreated shoreward until the end of winter. In our study area, we use the modal water depth at the SLIE to account for comparatively shorter widths over shallower water depths. The modal water depth varies by study region. Thus, in this study, *Stable Ice* conditions occur when the SLIE reaches the 13 *m* isobath in Northern Section, the 7 *m* isobath in Central Section, and the 8.5 *m* isobath in the Southern Section. *Break Up* events occur when landfast ice rapidly retreats toward the coastline, and is identified as the most temporal negative gradient in measured landfast ice width when the gradient remains less than or equal to zero. *Ice Free* coastlines occur when the SLIE retreats to less than 500 m from the coast, a distance again based on the geolocation accuracy of Radarsat-1.

We identified these four key events on a year-by-year basis then used linear regression methods to identify interannual trends. These annual cycle events generally occur successively in a landfast ice annual cycle, however it should be noted that landfast ice on Western Alaskan coastlines do not always fit this pattern (Mahoney et al., 2014).

4. Results

We created 274 digitized SLIEs over our study area, covering the Northern, Central, and Southern Sections of the Eastern Bering Sea. Intersecting the digitized SLIEs with the coastal vectors resulted in 877,836 SLIE data points.

4.1. Landfast ice spatial distribution on Alaskan Bering Sea coastlines

The spatial distribution of SLIEs in the Eastern Bering Sea is visually identifiable in Fig. 5, which depicts all SLIEs created from 1996 to 2008. In this figure landfast ice extends north beyond our study area into the Chukchi Sea, and south to the mouth of the Kuskokwim River on the YK Delta. Note that a gap in Radarsat-1 coverage prevented the identification of SLIEs in the southeast portion of the Norton Sound.

Spatial distributions of the SLIE are distinct by geographic region within our study area. Generally, the SLIE extends further from the coastline in Central Section and along the Southern Section than it does on the Northern Section. The differences in SLIE width by geographic region pertain to the relationship between landfast ice and bathymetry that is addressed in section 2. The differences in SLIE spatial distribution by geographic region are additionally evident in histograms of landfast ice widths, as shown in Fig. 6. These histograms indicate that each region has distinct distributions of landfast ice width. Notably, not only is the average landfast ice width different in each region, but the average width in the Central Section approximately corresponds to the 90th percentile width in the Southern Section and, similarly, the average width in the Southern Section approximately corresponds to the 90th percentile in Norton (Table 1). This separation of distributions supports the basis on which were selected these sub regions for our study. Further inspection of SLIEs on the Northern Section show increased SLIE widths in the Koyuk Inlet and Norton Bay that account for the right tails that extend to 30 km. Additional quantitative parameters distinguishing the three study regions are further explored in Table 1.

4.2. Landfast ice spatial distribution and Bering Sea physical geography

Landfast ice widths relate to physical geographic features in the study area. Previous studies have shown the location of the SLIE – and thus the landfast ice width – is influenced by stabilizing physical features such as shoals and barrier islands that promote the formation of grounded pressure ridges (Granskog et al., 2003, 2004, 2006; Mahoney et al., 2007, 2014). Fig. 7 shows line density maps of the SLIE in our study area, depicting the probability of a SLIE occurring within 1 km of a given point. Closer inspection of high-density areas of SLIE presence sometimes reveals proximate coastal islands acting as stabilizing features (Fig. 6a, b, c), either by providing grounding features for pressure ridges, or by sheltering landfast ice from shearing forces (e.g. wind/wave action, collisions with drift ice). Landfast ice widths averaged approximately 4.2 km on the Northern Section, 18.8 km on the Central Section, and 8.9 km on the KY Delta.

Water depths at the SLIE were found to vary by geographic region in our study area (Fig. 8). Water depths at the SLIE exhibited modal values of -13 m on the Northern Section, −7 m in the Central Section, and − 8.5 m in the Southern Section. Visual comparison of the SLIEs and the 15 m isobath contour (as can be seen in Fig. 5) suggests that bathymetry influences landfast ice width in the Bering Sea. This contour extends further from the coastlines of the Central Section and Southern Section than it does from the Northern Section. Correspondingly, the widths of SLIEs extend further from the Central Section and Southern Section than from the Northern Section. The relationship between landfast ice width and bathymetry is further explored with monthly plots in Fig. 9. When plotting the water depth at the SLIE in all three

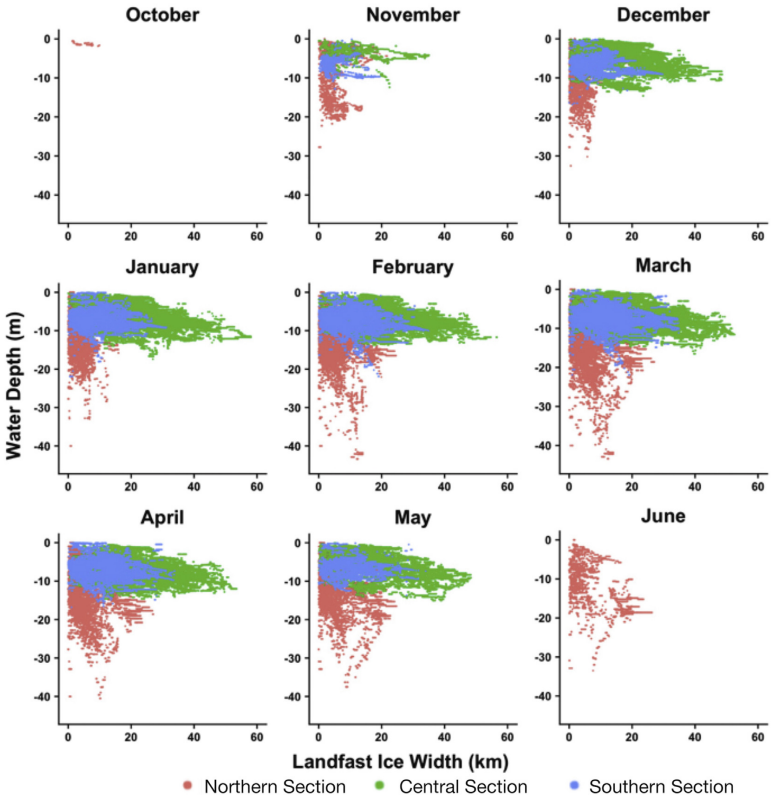

Fig. 9. Monthly plots depicting the relationship between SLIE width and water depth. Each region has distinguishable width/water depth values. Note that how water depth extends up to 40 m at the SLIE, despite its relatively short width. This suggests a steep bathymetric gradient beyond the coastline, beyond where grounding pressure ridges may form.

geographic regions, it becomes evident that shallower water depths enable greater landfast ice widths throughout the annual cycle. SLIEs on the Northern Section can extend to water depths of up to 40 *m* with relatively short widths, suggesting the existence of a steep seafloor gradient beyond the formation of grounded pressure ridges. Unlike landfast ice in Northern Section and further north in the Chukchi and Beaufort Seas, the water depths at the SLIEs on the Central Section and Southern Section coastlines rarely reach the 15 m isobath.

4.3. Spatial and interannual variability of landfast ice annual cycle

Over our 1996–2008 study period, we derived 12 annual cycles of landfast ice width at 3204 locations along the Alaskan coasts of the Bering Sea. These results allow us to characterize spatial and temporal variability of landfast ice extent, formation, and duration throughout the study area. Additionally, the SLIE widths are averaged by year within each geographic region to identify the mean occurrence of annual cycle events in our study area.

Generally for the entirety of our study area, *First Ice* occurs between December and January; *Stable Ice* occurs between mid-February and late Marcy; *Break Up* occurs between March and May; *Ice Free* occurs between April and early June (Fig. 10). Despite its more southerly setting, landfast ice forms earlier around the shores of the Southern Section than in the Northern and Central Sections, but it also breaks-up earlier so that the total length of the landfast ice season is very similar to that on the Northern Section. On average, landfast ice lasts longest on the Central Section and thereby has the longest landfast ice season of our three subregions. Landfast ice in the Central Section is also the first to become stable in our study area as well. In addition to regional variability, there is also interannual variability in the timing of landfast ice events in the Bering Sea (Table 2). Over the course of the study period 1996 to 2008, there are positive trends in the occurrence of *First Ice* in our study area, meaning that landfast ice is forming later in the year. These trends are consistent with those reported elsewhere in the Arctic (Galley et al., 2012; Mahoney et al., 2014; Selyuzhenok et al., 2015; Stringer et al., 1978). *Stable Ice and Break Up* events exhibit modest negative trends (Slopes $\leq$0.58 days / year), meaning they are occurring earlier in the year. The coasts of the Northern Section and the Southern Section are becoming *Ice Free* earlier in the year. However, our results show a significant positive trend along the coast of the Central Section, such that *Ice Free* conditions are occurring 15 days later from 1996 to 2008. On average, landfast ice formed 5 days later in the

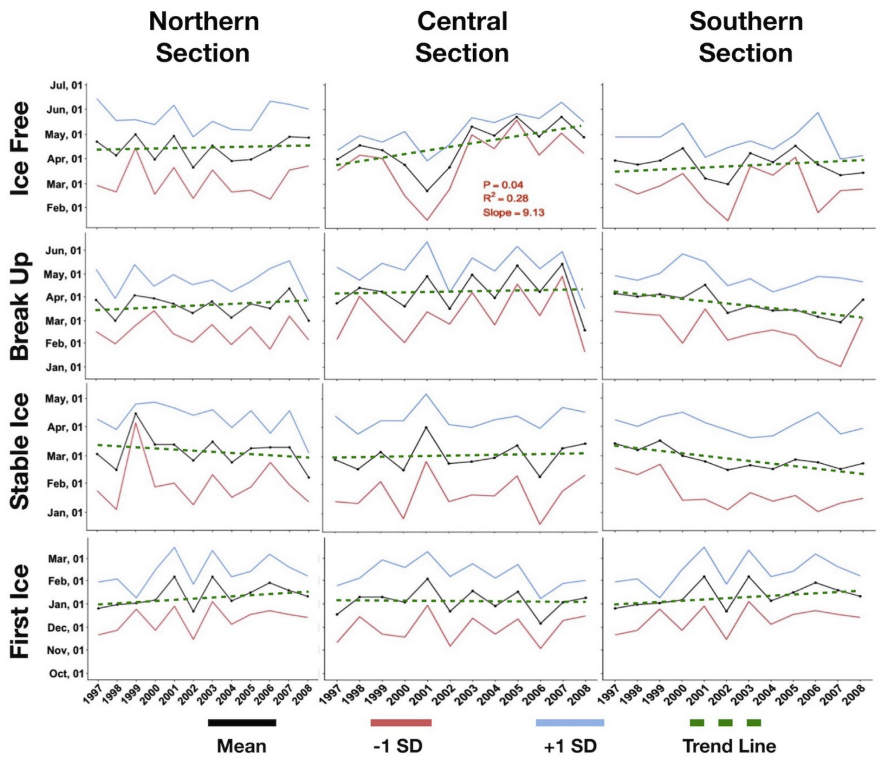

Fig. 10. Timeseries of mean occurrence date for three key events in the landfast ice annual cycle (First Ice, Stable Ice, Ice Free) from 1996 to 2008. Black lines represent mean occurrence dates, blue lines represent +1 standard deviation, and purple lines represent −1 standard deviation. Green dashes represent linear regressions for plots where the trend was found to be statistically significant. (For interpretation of the references to colour in this figure legend, the reader is referred to the web version of this article.)

Table 2
Statistical parameters of annual cycle events in the Eastern Bering Sea from 1996 to 2008.

	Parameter	Northern Section	Central Section (S)	Southern Section
First Ice	Minimum	October 16	November 01	November 16
	Maximum	February 19	February 25	February 21
	Mean	January 12	January 04	January 06
	Standard deviation	32 days	35 days	31 days
Stable Ice	Minimum	January 13	January 29	January 12
	Maximum	April 20	April 25	April 08
	Mean	March 06	March 01	February 26
	Standard deviation	39 days	40 days	34 days
Break Up	Minimum	February 11	February 03	January 26
	Maximum	May 05	May 09	May 04
	Mean	March 20	April 08	March 22
	Standard deviation	26 days	31 days	36 days
Ice Free	Minimum	March 07	February 25	February 19
	Maximum	June 12	May 17	May 08
	Mean	April 13	April 17	March 27
	Standard deviation	39 days	20 days	27 days

year, and broke up 4 days earlier on average in the eastern Bering Sea region

It is important to note that Fig. 10's mean occurrence dates throughout our study area can mask other annual cycle trends. The monthly density maps of all SLIEs in Figs. 11 and *11b* demonstrate that although *First Ice* generally takes place in December throughout our study area, this event is preceded by the formation of landfast ice in sheltered embayments and lagoons. We consider embayments to be concave sections of the coast, whereas lagoons are sections of coast behind barrier islands. For example, on the Northern Section, landfast ice first occurs in Golovnin Lagoon and Koyuk Inlet as early as October. Generally, *First Ice* events in sheltered embayments/lagoons preceded the geographic region's *First Ice* events by an average of 18.2 days on the Northern Section, 12.95 days in the Central Section, and 6.09 days on the Southern Section. *Ice Free* events in sheltered embayments/lagoons followed the geographic region's *Ice Free* events by an average of 13.96 days on the Northern Section, 4.97 days on the Central Section, and 8.34 days in the Southern Section.

5. Discussion

This study contributes to the broader synthesis of landfast ice conditions on Alaskan coastlines in the Chukchi and Beaufort seas

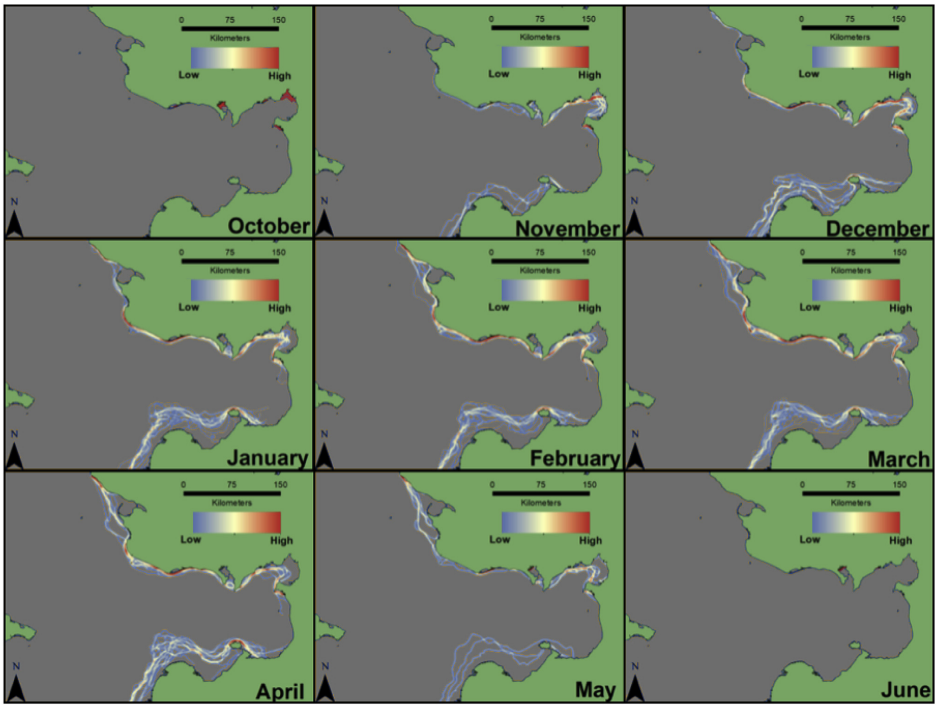

Fig. 11. Line density maps by month over the Northern/Central Sections (11a) and Southern Section (11b), respectively. Note how the onset of landfast ice conditions generally occur along a north-to-south latitudinal gradient. Also note how landfast ice width reaches its maximum extent for all study area regions during the month of March.

completed by Mahoney et al. (2014), and further investigates the relationship between landfast ice and local physical geography explored by Mahoney et al. (2007). Consistent with these studies, we find that the spatial and temporal characteristics of the landfast ice annual cycle to be influenced by the physical geography of our study area. Coastal features such as lagoons and sheltered embayments provide of shallow bathymetry and protection from shearing forces, influencing the location of landfast ice annual cycle onset and conclusions. For example, along the Northern Section landfast ice generally appears in the Koyuk Inlet and Golovnin Lagoon in late October, and persists in these areas until June. However, elsewhere on the Northern Section, landfast ice generally appears in early to mid December, and persists until the middle or end of May. The SLIE also consistently occurs close to islands proximate to the coastline.

Landfast ice widths were was also influenced by the general bathymetry of the Bering Sea. Landfast ice attached to coastlines contiguous with steep bathymetric gradients had correspondingly narrower widths, whereas moderate bathymetric gradients enabled greater landfast ice widths. Furthermore, previous studies have observed that, as a rule of thumb, the 15 -m isobath is a measure for where grounding pressure ridges are likely to occur (Mahoney et al., 2007a, 2014). All SLIEs fall within the 15-m isobath in Fig. 5. Although the failure of the SLIE to reach the 15 m isobath distinguishes landfast ice the Bering Sea from that in the Chukchi and Beaufort Seas (Mahoney et al., 2014), it is similar to observations the Baltic Sea (Granskog et al., 2003, 2006) and western Kara Sea (Divine et al., 2004).

Together, the Bering, Baltic, and western Kara Seas are notable for being shallow water bodies and possess similar climatology conditions that may account for their relatively shallower water depths at the SLIE. The Baltic region experiences strong winds and low-pressure storms in the winter (Hallegatte et al., 2011) that may contribute to confining landfast ice in sheltered locations with shallower water depths (Granskog et al., 2003, 2004, 2006). The western Kara Sea likewise experiences frequent winter storms and strong winds that confine landfast ice widths to shallower water depths (Divine et al., 2004; Pavlov and Pfirman, 1995). The Bering Sea experiences frequent winter storms as well, with high-speed winds characterizing the northern Bering Sea (Overland, 1981). The occurrence of strong winds resulting from wintertime storms in these three regions may place stress on portions of landfast ice that would otherwise extend to greater water depths in calmer conditions, and increase shearing activity from circulating drift ice. The shallower water depths at the SLIE in these regions suggests that the application of the 15 m rule-of-thumb for *Stable Ice* conditions first requires a consideration of regional climatology.

Comparing our results to Mahoney et al.' (2014) work reveals different landfast ice annual cycles between the Alaskan Bering Sea and Alaskan Chukchi and Beaufort Seas. The mean occurrence dates of *First Ice* and *Ice Free* events in the Alaskan Bering Sea are notable as being respectively later and earlier than the mean occurrence dates in the Chukchi and Beaufort Seas. Although Mahoney et al. (2014) did not find any statistically significant interannual trends of annual cycle events at the 5% level, trends in *Ice Free* events were statistically

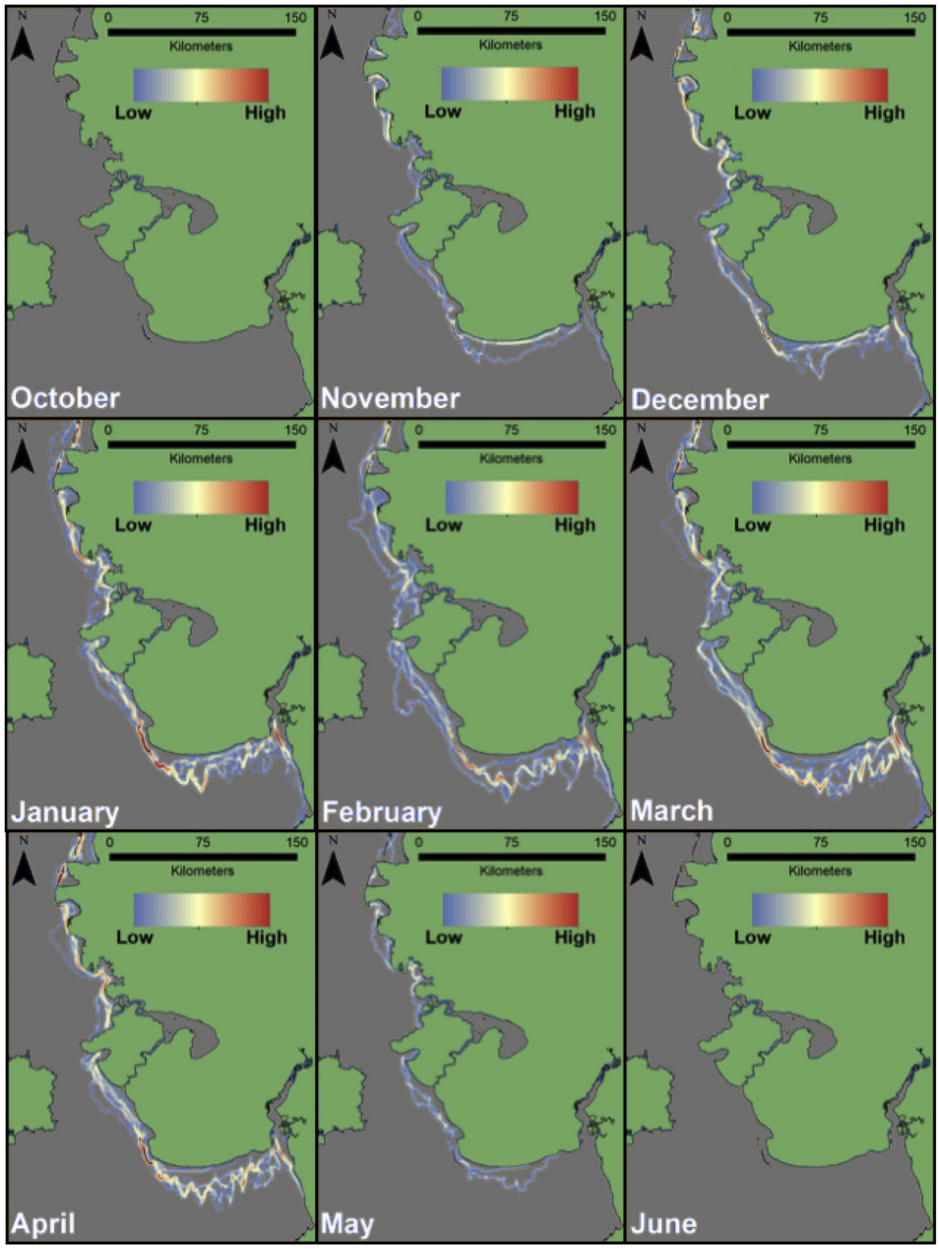

Fig. 11. (*continued*)

significant at the same level on the Central Section coastlines. The distinction between sea ice regimes is similar to observations made Frey et al.'s (2015) study of general sea ice conditions, where Bering Sea ice was found to exhibit a more complex interannual variability in areal extent and seasonal onset/duration than conditions in Chukchi and Beaufort Seas. It is also important to note that pack ice that accretes to the coast in the Northern Chukchi and Beaufort Seas is significantly thicker than in the Bering Sea (Amundrud et al., 2004), which would influence different outcomes in landfast ice areal extent and seasonal duration.

The trend toward later *Ice Free* conditions by 15 days from 1996 to 2008 in the Central Section region is notable. To our knowledge, this runs counter to every other coastline for which the annual cycle of landfast ice has been studied. The landfast ice in this region is wider than in the adjacent Northern Section and Southern Section regions. Additionally, the coastline is oriented differently with respect to prevailing winds and ocean currents, which may results in the landfast ice in Central Section responding differently to ongoing atmospheric and oceanic changes than neighboring coastlines. It is also worth noting that landfast ice in the Central Section lies immediately downstream of the outflow from the Yukon River Delta, which can flood the landfast ice surface during peak discharge and initiate or accelerate melt (Dean et al., 1994; Weingartner et al., 2017). However, observations at Pilot Station, approximately 200 km up the Yukon River from the coast, indicate trends toward increased and earlier occurrence of peak discharge (Ge et al., 2013), which would seem to promote earlier break-up of landfast ice in Central Section. Hence, the underlying cause of the positive trend we observe in *last ice* occurrence in this region remains a topic for future research.

The variability surrounding the seasonal duration of the landfast ice annual cycle from 1996 to 2008 is consistent with other observations of sea ice conditions in the Bering Sea (Kawerak 2013; Oceana and Kawerak, 2014), as well as findings on biogeophysical processes where sea ice in coastal zones is a necessary consideration (Grebmeier et al., 2006; Mueter and Litzow, 2008). However, warmer southerly air circulations increasing surface temperatures and preventing the transport of sea ice into the Bering Sea region have contributed to low sea ice coverage from 2017 to 2019 (Perovich et al., 2019). Our study does not account for trends in landfast ice cover during recent periods of sea ice decline in the Bering Sea, but serves as a reference point for future studies, being particularly relevant to the ongoing challenges of subsistence communities in the Bering Sea region, where landfast ice provides a means to access and harvest resources (Kawerak 2013; Ray et al., 2016; Robards et al., 2013). Further, the datasets created in our study are at a spatial scale relevant to human activities where landfast ice is an important consideration. Ongoing changes in Bering Sea ice cover necessitates further investigations of the annual cycle, causes of its change, and implications for human and biogeophysical processes in the region.

6. Conclusion

Using data derived from Radarsat-1 imagery, we have characterized the spatial and temporal patterns of the landfast ice annual cycle in the eastern Bering Sea, as well as its interannual change. This study is the most comprehensive analysis to date of landfast ice on Bering Sea Alaskan coastlines, and expands upon Mahoney et al. 's (2014) similar study in the Chukchi and Beaufort Seas to complete the analysis of landfast ice conditions on Alaskan coastlines from 1996 to 2008.

We found that the physical geography of the Bering Sea region influenced the spatial distribution and seasonal duration of landfast ice in our study area. Consistent with other landfast ice studies (Dammann et al., 2018; Mahoney et al., 2007a, 2014), we found coastal morphology features to influence the seasonal duration and physical properties of landfast ice; areas with sheltered embayments and lagoons extended the seasonal duration of the annual cycle. Further, the occurrence of the SLIE at shallow water depths is consistent with other studies that note a bathymetric constraint on landfast ice width (Divine et al., 2004; Granskog et al., 2003, 2006; Mahoney et al., 2007, 2014; Zubov, 1945). We also found that the 15 m rule-of-thumb isobath used by previous studies (Mahoney et al., 2007, 2014) to identify the onset of *Stable Ice* conditions was not applicable to stable landfast ice in the Bering Sea. This finding suggests that the utility of the 15 m isobath metric for identifying *Stable Ice* events varies by study region; SLIEs in regions that experience frequent winter storms and strong winds (i.e. Kara Sea, Baltic Sea, Bering Sea) generally do not reach the 15 m isobath. Thus, prior consideration of regional climatology is necessary before using the 15 m isobath metric.

On an interannual basis, the Northern Section, Central Section, and Southern Section coastlines to have distinct spatial distributions and seasonal durations. The annual cycle on the Northern Section and Southern Section are interannually decreasing in seasonal duration: the *First Ice* events occur later and the *Ice Free* events occur earlier. This trend is consistent with those found in landfast ice studies the Beaufort and Chukchi Seas (Mahoney et al., 2014). However, the annual cycle is shifting on the Central Section, with statistically significant positive interannual trends in both *First Ice* and *Ice Free* events. There is no parallel for that trend in the existing literature.

This study broadly contributes to future research where landfast ice is a relevant consideration. Changes in the landfast ice annual cycle can contribute to changes in broader biogeophysical processes in the Bering Sea region that merit further study. For example, changing landfast ice conditions in the Bering Sea have been cited as influencing changes in wildlife habitat and behavior (Laidre et al., 2008; Kawerak 2013) and coastal geomorphology (USACE, 2009; Oceana and Kawerak, 2014). Characterization of landfast ice annual cycle changes can inform how these aforementioned changes are characterized as well. Further, landfast ice research is especially relevant to the challenges faced by Bering Sea coastal communities, including changing subsistence practices (ACIA-Arctic Climate Impact Assessment et al., 2005; Kawerak 2013; Oceana and Kawerak, 2014), shifting marine food webs (Brown et al., 2011; Grebmeier et al., 2006; Mueter and Litzow, 2008), and accelerated coastal erosion that are underway in this region (Mesquita et al., 2010; Pingree-Shippee et al., 2016; Terenzi et al., 2014). Characterizing the landfast ice annual cycle in the Bering Sea region can enable future research avenues that integrate social metrics relevant to community challenges.

Declaration of Competing Interest

The authors declare that they have no known competing financial interests or personal relationships that could have appeared to influence the work reported in this paper.

References

ACIA-Arctic Climate Impact Assessment, Arctic Monitoring, Assessment Programme, Program for the Conservation of Arctic Flora, International Arctic Science Committee, 2005. Arctic Climate Impact Assessment-Scientific Report. Cambridge University Press.

Amundrud, T.L., Melling, H., Ingram, R.G., 2004. Geometrical constraints on the evolution of ridged sea ice. J. Geophys. Res. Oceans 109 (C6).

Antonova, S., 2011. Spatial and temporal variability of the fast ice in the Russian Arctic (Doctoral dissertation, Master thesis, State University of St. Petersburg, Russia and University of Hamburg, Germany).

Attard, K.M., Søgaard, D.H., Piontek, J., Lange, B.A., Katlein, C., Sørensen, H.L., ... Glud, R.N., 2018. Oxygen fluxes beneath Arctic land-fast ice and pack ice_ towards estimates of ice productivity. Polar Biol. 41 (10), 2119–2134.

Barnhart, K.R., Overeem, I., Anderson, R.S., 2014. The effect of changing sea ice on the physical vulnerability of Arctic coasts. Cryosphere 8 (5).

Barry, R.G., Moritz, R.E., Rogers, J.C., 1979. The fast ice regimes of the Beaufort and Chukchi Sea coasts, Alaska. Cold Reg. Sci. Technol. 1 (2), 129–152.

Bhatt, U.S., Walker, D.A., Raynolds, M.K., Comiso, J.C., Epstein, H.E., Jia, G., Rudiger, G., Pinzon, J., Tucker, C., Tweedie, C., Webber, P.J., 2010. Circumpolar Arctic tundra vegetation change is linked to sea ice decline. Earth Interact. 14 (8), 1–20.

Brown, Z.W., Van Dijken, G.L., Arrigo, K.R., 2011. A reassessment of primary production

and environmental change in the Bering Sea. J. Geophys. Res. Oceans 116 (C8).
Dammann, D.O., Eriksson, L.E., Mahoney, A.R., Eicken, H., Meyer, F.J., 2018. Landfast Sea Ice Stability-Mapping Pan-Arctic Ice Regimes with Implications for Ice Use, Subsea Permafrost and Marine Habitats. Cryosphere Discuss.
Danielson, S., Johnson, M., Solomon, S., Perrie, W., 2008. 1 km Gridded Bathymetric Dataset Based on Ship Soundings: A research tool for the waters of eastern Russia, Alaska & western Canada, Poster presentation at the 2008 Alaska Marine Science Symposium, Anchorage, Alaska.
Dean, K.G., Stringer, W.J., Ahlnas, K., Searcy, C., Weingartner, T., 1994. The influence of river discharge on the thawing of sea ice, Mackenzie River Delta: albedo and temperature analyses. Polar Res. 13 (1), 83–94.
Divine, D.V., Korsnes, R., Makshtas, A.P., 2004. Temporal and spatial variation of shorefast ice in the Kara Sea. Cont. Shelf Res. 24, 1717–1736.
Drake, D.E., Cacchione, D.A., Muench, R.D., Nelson, C.H., 1980. Sediment transport in Norton Sound, Alaska. Marine Geol. 36 (1-2), 97–126.
Druckenmiller, M.L., Eicken, H., Johnson, M.A., Pringle, D.J., Williams, C.C., 2009. Toward an integrated coastal sea-ice observatory: System components and a case study at Barrow. Alaska. Cold Reg. Sci. Technol. 56 (2-3), 61–72.
Dumas, J., Carmack, E., Melling, H., 2005. Climate change impacts on the Beaufort shelf landfast ice. Cold Reg. Sci. Technol. 42 (1), 41–51.
Duffy-Anderson, J.T., Stabeno, P., Andrews, A.G., Cieciel, K., Deary, A., Farley, E., ... Kuletz, K., 2019. Responses of the northern Bering Sea and southeastern Bering Sea pelagic ecosystems following record-breaking low winter sea-ice. Geophys. Res. Lett. 46 (16), 9833–9842.
Eisner, L., 2018. The Bering Sea: Current status and recent trends. PICES Press 26 (1), 29–36.
Forbes, D.L., Taylor, R.B., 1994. Ice in the shore zone and the geomorphology of cold coasts. Prog. Phys. Geogr. 18 (1), 59–89.
Fraser, A.D., Massom, R.A., Michael, K.J., 2009. A method for compositing polar MODIS satellite images to remove cloud cover for landfast sea-ice detection. IEEE Transactions on Geoscience and Remote Sensing 47 (9), 3272–3282.
Fraser, A.D., Massom, R.A., Michael, K.J., 2010. Generation of high-resolution East Antarctic landfast sea-ice maps from cloud-free MODIS satellite composite imagery. Remote. Sens. Environ. 114 (12), 2888–2896.
Fraser, A.D., Massom, R.A., Michael, K.J., Galton-Fenzi, B.K., Lieser, J.L., 2012. East Antarctic landfast sea ice distribution and variability, 2000–08. J. Clim. 25 (4), 1137–1156.
Frey, K.E., Moore, G.W.K., Cooper, L.W., Grebmeier, J.M., 2015. Divergent patterns of recent sea ice cover across the Bering, Chukchi, and Beaufort seas of the Pacific Arctic Region. Prog. Oceanogr. 136, 32–49.
Galley, R.J., Else, B.G., Howell, S.E., Lukovich, J.V., Barber, D.G., 2012. Landfast sea ice conditions in the Canadian Arctic: 1983-2009. Arctic 133–144.
Ge, S., Yang, D., Kane, D.L., 2013. Yukon River Basin long-term (1977–2006) hydrologic and climatic analysis. Hydrol. Process. 27 (17), 2475–2484.
Granskog, M.A., Martma, T.A., Vaikmäe, R.A., 2003. Development, structure and composition of land-fast sea ice in the northern Baltic Sea. J. Glaciol. 49 (164), 139–148.
Granskog, M.A., Leppäranta, M., Kawamura, T., Ehn, J., Shirasawa, K., 2004. Seasonal development of the properties and composition of landfast sea ice in the Gulf of Finland, the Baltic Sea. J. Geophys. Res. Oceans 109 (C2).
Granskog, M., Kaartokallio, H., Kuosa, H., Thomas, D.N., Vainio, J., 2006. Sea ice in the Baltic Sea–a review. Estuar. Coast. Shelf Sci. 70 (1–2), 145–160.
Grebmeier, J.M., Overland, J.E., Moore, S.E., Farley, E.V., Carmack, E.C., Cooper, L.W., Frey, K., Helle, J., McLaughlin, F., McNutt, S.L., 2006. A major ecosystem shift in the northern Bering Sea. Science 311 (5766), 1461–1464.
Hallegatte, S., Ranger, N., Mestre, O., Dumas, P., Corfee-Morlot, J., Herweijer, C., Wood, R.M., 2011. Assessing climate change impacts, sea level rise and storm surge risk in port cities: a case study on Copenhagen. Clim. Chang. 104 (1), 113–137.
Hamilton, C.D., Kovacs, K.M., Ims, R.A., Aars, J., Lydersen, C., 2017. An Arctic predator–prey system in flux: climate change impacts on coastal space use by polar bears and ringed seals. J. Anim. Ecol. 86 (5), 1054–1064.
Huntington, H.P., Noongwook, G., Bond, N.A., Benter, B., Snyder, J.A., Zhang, J., 2013. The influence of wind and ice on spring walrus hunting success on St. Lawrence Island, Alaska. Deep-Sea Res. II Top. Stud. Oceanogr. 94, 312–322.
Kawerak, Inc., 2013. Seal and walrus harvest and habitat areas for nine Bering Strait Region communities. Kawerak, Inc., Social Science Program, Nome, AK.
Kovacs, A., 1976. Grounded Ice in the Fast Ice Zone along the Beaufort Seacoast of Alaska (No. CRREL-76-32). Cold Regions Research And Engineering Lab, Hanover NH.
Kwok, R., Rignot, E., Holt, B., Onstott, R., 1992. Identification of sea ice types in spaceborne synthetic aperture radar data. J. Geophys. Res. Oceans 97 (C2), 2391–2402.
Laidre, K.L., Stirling, I., Lowry, L.F., Wiig, Ø., Heide-Jørgensen, M.P., Ferguson, S.H., 2008. Quantifying the sensitivity of Arctic marine mammals to climate-induced habitat change. Ecol. Appl. 18 (sp2), S97–S125.
Lantuit, H., Pollard, W.H., 2008. Fifty years of coastal erosion and retrogressive thaw slump activity on Herschel Island, southern Beaufort Sea, Yukon Territory, Canada. Geomorphology 95 (1–2), 84–102.
Lovvorn, J.R., Rocha, A.R., Mahoney, A.H., Jewett, S.C., 2018. Sustaining ecological and subsistence functions in conservation areas: eider habitat and access by Native hunters along landfast ice. Environ. Conserv. 45 (4), 361–369.
Mahoney, A., Eicken, H., Graves, A., Shapiro, L., Cotter, P., 2004 September. Landfast sea ice extent and variability in the Alaskan Arctic derived from SAR imagery. In IGARSS 2004. 2004. IEEE International Geoscience and Remote Sensing Symposium 3, 2146–2149 IEEE.
Mahoney, A., Eicken, H., Shapiro, L., Graves, A., 2006. Defining and locating the seaward landfast ice edge in northern Alaska. In: 18th International Conference on Port and Ocean Engineering under Arctic Conditions (POAC'05), Potsdam, NY, pp. 991–1001.
Mahoney, A.R., Eicken, H., Shapiro, L., 2007. How fast is landfast sea ice? A study of the at- tachment and detachment of nearshore ice at Barrow, Alaska. Cold Reg. Sci. Technol. 47 (3).
Mahoney, A.R., Eicken, H., Gaylord, A.G., Shapiro, L., 2007a. Alaska landfast sea ice: links with bathymetry and atmospheric circulation. J. Geophys. Res. Oceans 112 (C2). https://doi.org/10.1029/2006jc003559. (C02001).
Mahoney, A.R., Eicken, H., Gaylord, A.G., Gens, R., 2014. Landfast Sea ice extent in the Chukchi and Beaufort Seas: the annual cycle and decadal variability. Cold Reg. Sci. Technol. 103, 41–56.
Mesquita, M.S., Atkinson, D.E., Hodges, K.I., 2010. Characteristics and variability of storm tracks in the North Pacific, Bering Sea, and Alaska. J. Clim. 23 (2), 294–311.
Meyer, F.J., Mahoney, A.R., Eicken, H., Denny, C.L., Druckenmiller, H.C., Hendricks, S., 2011. Mapping arctic landfast ice extent using L-band synthetic aperture radar interferometry. Remote Sens. Environ. 115 (12), 3029–3043.
Mueter, F.J., Litzow, M.A., 2008. Sea ice retreat alters the biogeography of the Bering Sea continental shelf. Ecol. Appl. 18 (2), 309–320.
Oceana and Kawerak, 2014. Bering Strait Marine Life and Subsistence Use Data Synthesis. Oceana and Kawerak, Juneau, AK.
Overland, J.E., 1981. Marine climatology of the Bering Sea. The Eastern Bering Sea Shelf: Oceanogr. Resour. 1, 15–22.
Pavlov, V.K., Pfirman, S.L., 1995. Hydrographic structure and variability of the Kara Sea: implications for pollutant distribution. Deep-Sea Res. II Top. Stud. Oceanogr. 42 (6), 1369–1390.
Perovich, D., Meier, W., Tschudi, M., Farrell, S., Hendricks, S., Gerland, S., Haas, C., Krumpen, T., Polashenski, C., Ricker, R., Webster, M., 2019. Sea ice cover [in "State of the Climate in 2018"]. Bull. Amer. Meteor. Soc. 100 (9), S146–S150.
Pingree-Shippee, K.A., Shippee, N.J., Atkinson, D.E., 2016. Overview of Bering and Chukchi sea wave states for four severe storms following common synoptic tracks. J. Atmos. Ocean. Technol. 33 (2), 283–302.
Post, E., Bhatt, U.S., Bitz, C.M., Brodie, J.F., Fulton, T.L., Hebblewhite, M., Kerby, J., Kutz, S., Stirling, I., Walker, D.A., 2013. Ecological consequences of sea-ice decline. Science 341 (6145), 519–524.
Ray, G.C., Hufford, G.L., Overland, J.E., Krupnik, I., McCormick-Ray, J., Frey, K., Labunski, E., 2016. Decadal Bering Sea seascape change: consequences for Pacific walruses and indigenous hunters. Ecol. Appl. 26 (1), 24–41.
Reimnitz, E., Toimil, L., Barnes, P., 1978. Arctic continental shelf morphology related to sea-ice zonation, Beaufort Sea, Alaska. Marine Geology 28 (3-4), 179–210.
Robards, M.D., Kitaysky, A.S., Burns, J.J., 2013. Physical and sociocultural factors affecting walrus subsistence at three villages in the northern Bering Sea: 1952–2004. Polar Geography 36 (1–2), 65–85.
Selyuzhenok, V., Krumpen, T., Mahoney, A., Janout, M., Gerdes, R., 2015. Seasonal and interannual variability of fast ice extent in the southeastern Laptev S ea between 1999 and 2013. J. Geophys. Res. Oceans 120 (12), 7791–7806.
Stabeno, P.J., Bell, S.W., 2019. Extreme conditions in the Bering Sea (2017–2018): record-breaking low sea-ice extent. Geophys. Res. Lett. 46 (15), 8952–8959.
Stabeno, P.J., Bond, N.A., Salo, S.A., 2007. On the recent warming of the southeastern Bering Sea shelf. Deep-Sea Res. II Top. Stud. Oceanogr. 54 (23–26), 2599–2618.
Stringer, W.J., Barrett, S.A., Schreurs, L., 1978. Morphology of Beaufort, Chukchi and Bering Seas near shore ice conditions by means of satellite and aerial remote sensing. In: Environmental Assessment of the Alaskan Continental Shelf. Annual Reports of Principal Investigators for the Year Ending March 1978, 10.
Stroeve, J., Holland, M.M., Meier, W., Scambos, T., Serreze, M., 2007. Arctic sea ice decline: faster than forecast. Geophys. Res. Lett. 34 (9).
Stroeve, J., Serreze, M., Drobot, S., Gearheard, S., Holland, M., Maslanik, J., ... Scambos, T., 2008. Arctic sea ice extent plummets in 2007. EOS Trans. Am. Geophys. Union 89 (2), 13–14.
Terenzi, J., Jorgenson, M.T., Ely, C.R., Giguère, N., 2014. Storm-surge flooding on the Yukon-Kuskokwim delta. Alaska. Arctic 360–374.
U.S. Fish and Wildlife Service, 2008. Endangered and threatened wildlife and plants; determination of threatened status for the polar bear (Ursus maritimus) throughout its range; final rule. Fed. Regist. 73 (95).
USACE, 2009. Alaska Baseline Erosion Assessment: Study Findings and Technical Report. U.S. Army Corps of Engineers, Alaska District.
Vermaire, J.C., Pisaric, M.F., Thienpont, J.R., Courtney Mustaphi, C.J., Kokelj, S.V., Smol, J.P., 2013. Arctic climate warming and sea ice declines lead to increased storm surge activity. Geophys. Res. Lett. 40 (7), 1386–1390.
Weingartner, T.J., Danielson, S.L., Potter, R.A., Trefry, J.H., Mahoney, A., Savoie, M., Irvine, C., Sousa, L., 2017. Circulation and water properties in the landfast ice zone of the Alaskan Beaufort Sea. Cont. Shelf Res. 148, 185–198.
World Meteorological Organization, 1970. WMO Sea-Ice Nomenclature, Terminology, Codes and Illustrated Glossary. Secretariat of the WMO, Geneva.
Yu, Y., Stern, H., Fowler, C., Fetterer, F., Maslanik, J., 2014. Interannual variability of Arctic landfast ice between 1976 and 2007. J. Clim. 27 (1), 227–243.
Zubov, N.N., 1945. Arctic Sea Ice (in Russian), 366 pp., Izd. Glavsevmorputi, Moscow. (English translation). 491 pp. 1963 U.S. Navy Oceanogr. Off., Springfield, VA.

Appendix B. Interannual Declines of St. Lawrence Island Landfast Ice Cover

Interannual Declines of St. Lawrence Island Landfast Ice Cover

David Jensen[1], Andrew R. Mahoney[2], Lynn M. Resler[1]

1. Department of Geography; College of Natural Resources and Environment; Virginia Polytechnic Institute and State University; Blacksburg, Virginia
2. Geophysical Institute; University of Alaska Fairbanks; Fairbanks, Alaska

Corresponding Author:
David Jensen
Department of Geography
Virginia Tech
220 Stranger Street
Blacksburg, VA 24061, USA
(ajdavid6@vt.edu; 301-523-8812)

Highlights:

- Most comprehensive analysis to date of landfast ice in the Northern Bering Sea from 1996 – 2019
- St. Lawrence Island landfast ice regime does not conform to annual cycle events used to study landfast ice regimes in the Chukchi and Beaufort Seas
- Landfast ice conditions are undergoing strong interannual declines that match recent reductions in Bering Sea Ice cover.

Keywords:
Landfast; sea ice; Bering Sea; Subarctic

Abstract
Seasonal sea ice in the Bering Sea, AK has undergone declines in areal extent and seasonal duration. On St. Lawrence Island, seasonal ice becomes locked into a stationary position against the coastline to provide a protective buffer against coastal erosion, habitat for migratory marine mammals, and a substrate for travel and subsistence activities. A thorough understanding of how stationary coastal ice on St. Lawrence Island, termed *landfast ice*, is affected by broader sea ice trends is limited by a lack of data on landfast ice areal coverage, seasonal duration, and interannual variability. Here, we created a comprehensive spatial dataset to provide an observational baseline for landfast ice conditions on St. Lawrence Island from 1996–2019. Our results show statistically significant interannual declines in landfast ice spatial extent. The strongest trends occur in the years of 2016–2019, corresponding more broadly to recent sea ice declines in the Bering Sea. No similarly significant interannual shifts in the seasonal timing of landfast ice formation and break up occurred within our study period. The dataset created for this study provides a baseline understanding of landfast ice that can contributes to future research on associated biogeophysical processes on St. Lawrence Island, where changing landfast ice conditions are a relevant consideration.

1. Introduction

The areal extent of sea ice is declining with climatic shifts in Arctic and Subarctic environments. Specifically, the extent of perennial ice and the seasonal duration of first year ice is diminishing (Serreze and Stroeve 2015). The loss of sea ice cover is significant for myriad global processes, including climate regulation (Liu et al. 2012; Screen & Simmonds 2010; Vihma 2014), shifting ecotones (Bhatt et al. 2010; Oceana and Kawerak 2014; Post et al. 2013) and wildfire regimes (Knapp and Soulé 2017). Additionally, human access to global transportation routes (Stephenson et al. 2011, 2013) and natural resource exploration (Whiteman et al. 2013) are fostered by sea ice loss. In these cases, global processes are influenced by shifts in the spatial extent and seasonal duration of ice cover. Understanding the global consequences of sea ice loss necessitates the scientific study of its spatial and temporal trends.

The degree of reduction in sea ice extent has been found to vary geographically, with consequences for localized biogeophysical processes. For example, changing sea ice conditions in the Beaufort, Chukchi, and Bering seas have exhibited differing changes in areal extent and seasonal duration (Frey et al. 2015). In the Bering Sea, seasonal ice cover has exhibited greater interannual variability than adjacent seas in the Arctic Circle, characterized by unpredictable seasonal duration, areal extent, and multiyear ice transport through the Bering Strait (ANC et al. 2012; Frey et al. 2015; Stabeno et al. 2007). Between 2018 and 2019, the Bering Sea has experienced record-setting lows in sea ice areal extent and seasonal duration (Cornwall 2019; Eisner 2018; Stabeno et al. 2018). Sea ice loss in the northern Bering Sea has influenced broader ecological shifts. Until recently, northern Bering Sea ecosystems were structured by the seasonal presence of continuous ice cover to support diverse benthic communities and bottom-feeding megafauna such as migratory marine mammals (Grebmeier et al. 2006, Kovacs et al. 2011, Oceana and Kawerak 2014). The northward retreat of the Arctic isothermal boundary has altered these ecosystems, primarily by affecting the consistency of seasonal ice cover presence. These broad ecological shifts carry associated consequences for subsistence hunting and commercial fishing (Grebmeier et al. 2006; Haynie and Huntington 2016; Sigler et al. 2010). Changes in Bering Sea ice cover also carry

consequences for ice conditions that serve specific biogeophysical functions, such as in coastal zones where sea ice becomes locked into a stationary position.

Stationary coastal sea ice, termed *landfast ice,* is important for its seasonal influence on broader biogeophysical processes in the Bering Sea. It can provide habitat for marine mammals (Kawerak 2013; Oceana and Kawerak 2014), act as a substrate for human mobility and subsistence practices (Ray et al. 2016; Robards et al. 2013), and protect coastlines from erosive wind and wave action (Lantuit & Pollard 2008). Some studies suggest that Bering Sea landfast ice changed along with broader sea ice shifts in the region (ACIA 2005; Oceana and Kawerak 2014). Changing landfast ice regimes carry consequences for the broader biogeophysical processes they influence. On St. Lawrence Island in the northern Bering Sea, landfast ice is an integral component of the northern Bering Sea ecosystem, and is important for the subsistence livelihoods of the island's two Yupik communities: Gambell and Savoonga (Oceana and Kawerak 2014). In recent decades, the location and timing of coastal ice surrounding the island have been observed to be increasingly variable, affecting wildlife habitat and behavior as well as subsistence activities (Benson and Trites 2002; Noongwook et al. 2007). Further, Savoonga residents have observed accelerated coastal erosion that has been partially attributed to changing coastal ice conditions (USACE 2007). These observations coincide with rising air temperatures over the island and earlier onsets of ice melt conditions (Grebmeier et al. 2006). Understanding interannual landfast ice change on St. Lawrence Island is important for ongoing and future research that characterizes broader biogeophysical shifts in the northern Bering Sea region.

Here, we present the most comprehensive analysis of interannual landfast ice change on St. Lawrence Island to date. Specifically, our research objectives are to: 1) identify patterns in the spatial distribution and seasonal duration of St. Lawrence Island's landfast ice cover; 2) observe how St. Lawrence Island and the northern Bering Sea's physical features such as nearshore bathymetry and coastal morphometry/orientation influence patterns observed from Objective 1; and 3) characterize interannual change in the spatial distribution and seasonal duration of St. Lawrence Island's landfast ice cover from 1996–2019.

2. Study Area

St. Lawrence Island (Figure 1) is a volcanic island situated in the northern Bering Sea at approximately~ 60° N latitude, ~200 kilometers to the west of mainland Alaska. At its widest points, St. Lawrence Island spans 160 km east to west, and 55 km north to south (Patton et al. 2011). The dominant vegetation cover is Arctic tundra (approximately 70% cover). Topography is characterized by low mountains, reaching a maximum elevation of 673 m a.s.l. (Nakeo et al. 1986). The nearshore bathymetry, an essential physical feature for understanding landfast ice, varies on the island by geographic region (Danielson et al. 2008; Figure 1). Water depths range from 0-25 meters in the Northwest region, 0-35 meters in the Northeast Region, 0-60m in the Southwest region, and 0-50m in the Southeast region. Two small communities are located on the northern and northwest coasts: Savoonga (population: 705) and Gambell (population: 700), respectively (U.S. Census Bureau 2018). The communities are culturally St. Lawrence Island Yupik and host subsistence economies based the migratory patterns of marine mammals (Kawerak 2013; Oceana and Kawerak 2014).

Sea ice is a seasonal feature in the Bering Sea region that is introduced when the combination of reduced solar intensity and the wind-driven transport of sea ice induce freezing ocean temperatures. From winter to late spring/early summer, St. Lawrence island is encircled by a combination of landfast ice and high concentrations of mobile, drifting ice (known as pack ice). Landfast ice forms on St. Lawrence Island through the process of in-situ freezing of open-water in sheltered areas, such as bays and lagoons, and the accretion of incoming pack ice against the seaward edge of the landfast ice, a process analogous to those discussed by Mahoney et al. (2007a) in the Chukchi and Beauforts Seas. Coastal sea ice conditions on the island vary by location. During winter, the northern coast is typically bordered by several kilometers of landfast ice with little or no open water at its edge where it meets the drifting pack ice, which frequently separates from the coast in large sheets throughout the winter and spring (Oceana and Kawerak 2014). By contrast, landfast ice on the southern coast is much narrower and is typically bordered by polynyas (persistent areas of open water in sea ice conditions) and low-concentration drift ice define conditions on the southern coast (Kapsch et al. 2010;

Kawerak 2013).

The spatial and seasonal patterns of St. Lawrence Island's landfast ice cover influence many of the islands biogeophysical processes. For example, the seasonal onset and retreat of sea ice generally coincide with migratory patterns of marine mammals near St. Lawrence Island, such as walrus, seal, bowhead whale, and occasionally polar bear (Kawerak 2013; Noongwook et al. 2007; Oceana and Kawerak 2014). Bottom-feeding pinnipeds have been known to interact with sea ice proximate to the island as part of their seasonal foraging and haul-out behavior (Kawerak 2013; Oceana and Kawerak 2014). Access to the sea floor under the ice by way of polynyas and leads (linear cracks formed in the ice by the separation or shearing of ice floes), provide rich foraging opportunities for bottom-feeding mammals. Further, landfast ice provides platforms for ringed seals to rest, give birth, and nurse young (Oceana and Kawerak 2014). The seasonal presence of marine mammals proximate to landfast ice enables subsistence opportunities for Gambell and Savoonga hunters. Subsistence hunters generally use snow machines to travel over and hunt on landfast ice, as well as haul boats over the island to access the polynyas on the southern coast (Kapsch et al. 2010). Walrus is a predominant component of subsistence diet for residents of Gambell and Savoonga. A 2009 subsistence harvest survey in Savoonga found walrus to comprise 66% of all locally-harvested food, and 75% of harvested marine mammals (Fall et al. 2013; Huntington et al. 2013). Community elders and hunters have cited ice conditions as a major influence of the undertaking and success of walrus harvesting (Huntington et al. 2013).

Sea ice decline in the Bering Sea manifests as diminished areal cover, shortening seasonal durations, and reduced multiyear ice transports through the Bering Strait (ANC et al. 2012; Stabeno et al. 2007; Robards et al. 2013). Some studies suggest that landfast ice has similarly changed with unpredictable seasonal durations and spatial extents (ACIA 2005; Oceana and Kawerak 2014). Changing landfast ice conditions has consequences for wildlife migratory behavior and subsistence activities similar to those found on St. Lawrence Island (Robards et al. 2013; USFWS 2008).

3. Methods

3.1 Designating Study Regions on St. Lawrence Island

In order to assess geographic differences in landfast ice distributional patterns, we divided the study area of St. Lawrence Island into four regions for analysis: Northwest, Northeast, Southwest, and Southeast (Figure 1). Delineations of these regions were based upon the island's distinctive coastal features and near shore ice conditions. Each region represents a concave section of coastline, separated physically by capes, or convex areas that transition into other concave coastlines, whereby the process of landfast ice formation and accumulation is largely independent from other regions. The Northwest region spans the coast from the community of Savoogna on the northern coast to the community of Gambell on the Northwest Cape. The coastline between these communities takes the form of a single large embayment, where drift ice transported from northern latitudes accumulates during the winter months (Oceana and Kawerak 2014). The Northeast region extends eastward from Savoonga to the eastern tip of the island and comprises multiple headlands, bays and lagoons. The Southeast region extends between the eastern tip of the island and the Southeastern Cape (the southernmost tip of the island) and is again dominated by a single large embayment. The Southwest region includes the most coastline of the four sub regions and extends from the Southeastern Cape to the Northwestern Cape. Coastal polynyas occur along the southern coast of the island (Kawerak 2013; Oceana and Kawerak 2014).

3.2 Defining and Locating Landfast Ice

We used primary and secondary datasets to track the location of landfast ice from 1996 to 2019. A time series of synthetic aperture radar (SAR) satellite imagery served as the primary dataset. SAR imagery is not compromised by adverse weather and prolonged polar nights, enabling year-round observation of polar environments. Further, sea ice generally has a higher backscatter coefficient compared to open water (Kwok et al. 1992), making it useful in identifying landfast ice. SAR imagery has been used successfully for identifying landfast ice using the aforementioned two-criteria definition (Mahoney et al. 2004, 2007a, 2014). We selected three SAR imagery datasets to cover the majority of our 1996 – 2019 study period: 1) moderate resolution Radarsat-1

ScanSAR wide beam imagery (1996 – 2008); 2) ENVISAT ASAR Wide-Swath Mode imagery (2008 – 2012); 3) Sentinel-1 Interferometric Wide Swath imagery (2016 – 2019). We are able to combine these sensors for continuous observations throughout our study period because all three sensors use C-band radar with comparable repeat intervals. Note that the sensor selection for this study results a data gap from 2013-2015. No freely-accessible SAR imagery over our study area is available for this time period. All images were resampled to 100 m to match the coarsest spatial resolution of Radarsat-1.

Seafloor bathymetry obtained from the Alaska Region Bathymetric Digital Elevation Model (ARBDEM, Danielson et al. 2008) served as a secondary dataset. Landfast ice can be anchored by pressure ridges that occur when the ice floes converge and pile together to form grounded pressure ridges in shallow water (Mahoney et al. 2007b). Thus, water depth can be used as a proxy for understanding when and where landfast ice is stabilized by grounded pressure ridges. Because average water depth at the landfast ice edge varies with geographic region (Divine et al. 2004; Granskog et al. 2003, 2006; Zubov 1945); the relationship between stable landfast ice and bathymetry proximate to St. Lawrence Island were explored. We use the ARBDEM (Danielson et al. 2008) to record water depth values. The ARBDEM covers the Arctic and Pacific Oceans between 130° E to 12° W and 45° N to 75° N. We reprojected this dataset to NAD 1983 Alaska Albers, and resampled it to match the 100m spatial resolution of the SAR imagery in our primary dataset. To further explore how landfast ice position is influenced by coast line shape morphometry (a component of Objective 1) we obtained a shapefile of the State of Alaska from the Alaska State Geospatial Clearinghouse to aid visual identification of sheltered coastal regions, such as lagoons.

We used a two-criteria definition advanced by Mahoney et al. (2006) to identify landfast ice in satellite imagery: 1) the sea ice is contiguous with the coastline, and 2) the sea ice exhibits no detectible motion for approximately 20 days. The criteria allowed us to distinguish between areas of moving and stationary sea ice; areas of coast-contiguous sea ice that has remained stationary for 20 days was classified as landfast ice. The 20-day threshold for stationary sea ice excludes drift ice that is motionless, but not held fast against the coastline or seabed. This criteria has been used successfully in identifying areas of landfast ice, as well as observing interannual variation of its physical properties

and annual cycle (Lovorn et al. 2018; Mahoney et al. 2007a, 2014).

Landfast ice is not distinguishable from drift ice using a single satellite image since its stationary nature over time is a defining feature. Generally, multiple consecutive images over a predetermined time and place is necessary to identify motionless, coast-contiguous sea ice as landfast (Fraser et al. 2012; Mahoney et al. 2004, 2006, 2007a, 2014; Meyer et al. 2011). We apply a method described in detail by Mahoney et al. (2004, 2006) to identify sea ice properties that are consistent with our previously-referenced two-criteria definition of landfast ice. Our selected method entails using three consecutive SAR images acquired within a ~20-day period to distinguish moving and stationary sea ice. Landfast ice is highlighted by calculating the horizontal and vertical gradient fields of each image, and determining the "net gradient difference" between the three images. The gradient fields are necessary to account for differences in consecutive backscatter values that are unrelated to motion, such as differing incidence angles between the sensors and illuminated areas. Homogenous coast-contiguous regions of low net gradient difference represent regions that have minimally changed in the ~20-day period, and indicate the presence of landfast ice (Figure 2). Landfast ice regions pass on to linear regions of high net-gradient difference that represent the seaward landfast ice edge (SLIE) — the area where landfast ice transitions to drift ice or open-ocean**.** We use the regions highlighted by the gradient difference image as well as the consecutive SAR images to visually identify landfast ice, and digitize these regions into shapefiles using ArcMap 10.6.1. We complete our data collection by repeating this process over 20-day intervals for the entirety of the 1996 – 2019 study period.

3.3 Analysis of Landfast Ice Spatial Distribution, Interannual Change, and Physical Geography

Our analysis of landfast ice spatial distribution and interannual change was based on techniques advanced by Mahoney et al. (2007a). We first intersect SLIE polylines with coast-normal vectors positioned at 200 m intervals along the island (Figure 3). We created these vectors by finding the closest point at 200 m intervals between a created coast-parallel polyline and the islands coastline. We repeated this process from the island

coastline to the coast-parallel polyline for concave sections of the coast where points are more than 200 m apart. We simplify coastal morphometry by excluding barrier islands and land spits that shelter lagoons; coastal vectors intersect these land features as they span from the main island to the coast-parallel polyline.

Because the shapefile represents the minimum landfast ice edge within a 20-day period, we assigned the date of the first input image to the SLIE when it is advancing from the coastline, and the date of the last input image when it is retreating, following the approach described by Mahoney et al. (2007a, 2014). Intersecting the SLIE with the coastal vectors and ARBDEM result in data points containing information of landfast ice width, water depth, and date of occurrence. We used linear regression methods to assess interannual change in the width of landfast ice and water depth at the SLIE. Statistical analysis in this study is accomplished using built-in functions in RStudio 3.5.3, an open-access IDE for the R programming language.

We also considered how sinuosity, fetch distance, and nearshore bathymetry of the coastline influenced outcomes in landfast ice width on St. Lawrence Island Coastlines (Table 1) using simple linear regression models. Nearshore bathymetry was incorporated into the model using the ARBDEM discussed in the previous section. Sinuosity refers to a scalar number between 0 and 1 that describes how sinuous a path is compared to a straight line distance. A sinuosity value of 1 corresponds to a straight line, and a value of 0 corresponds to an infinitely convoluted path. Sinuosity is calculated using ArcGIS's *Calculate Sinuosity* tool on manually designated sections of concave coast no greater than 5 kilometers in length. Fetch distance measures the unobstructed distance from a given point at the SLIE. The maximum fetch distance measured is 80km. Fetch vectors extending to their maximum length signify that the coastline is exposed to open ocean. Fetch distances less than the maximum values represent areas adjacent to coastlines. Fetch distances are calculated for each coastal vector using RStudios *FetchR* package, and sampled at 5 kilometer intervals to avoid multicollinearity. Independent variable data was stored in the coastal vectors intersecting with SLIEs. We sampled the coastal vectors at 5 km intervals to alleviate problems with multicollinearity. No correlations between independent variables exceeded 0.8.

3.4 Analysis of Landfast Ice Seasonal Duration and Interannual Change

To measure the seasonal duration of landfast ice, we use an approach described by Mahoney et al. (2007a, 2014) to analyze the landfast ice annual cycle on St. Lawrence Island from 1996 – 2019. *Annual Cycle* refers to the seasonal process by which landfast ice forms in the winter, interacts with the surrounding environment, and melts in the spring/summer. Following the work of Mahoney et al. (2007a, 2014), we identify four key events within the annual cycle that can be quantified from our primary and secondary datasets: *First Ice, Stable Ice, Break Up, and Ice Free.* By determining the timing of these events throughout our study period, we can assess interannual changes in landfast ice the seasonal duration of landfast ice presence and stable conditions.

First ice events occur when the SLIE extends further than 500 m from the coastline, and signifies the onset of landfast ice conditions. We selected this distance based on Mahoney et al.'s (2007a) determination of the geolocation accuracy of Radarsat-1 imagery, and thus prevents the misidentification of landfast ice condition caused by geolocation error. *Stable Ice* events occur when grounded pressure ridges anchor the landfast ice to the seabed. Water depths at the SLIE serve as a proxy for *Stable Ice* conditions because grounded pressure ridges cannot be detected with SAR imagery. We identify the onset of stable conditions when the SLIE reaches the 15 m isobath, as this measurement has been used as the rule of thumb for *Stable Ice* events in previous studies (Barry et al. 1979; Mahoney et al. 2014). *Break Up* events occurs when landfast ice rapidly retreats toward the coastline, and is identified as the most negative gradient in measured landfast ice width in a given season. *Ice Free* events occur in the late spring or early summer when the SLIE recedes to less than 500 m from the coastline, and signifies the end of the annual cycle. The geolocation accuracy of our primary dataset informed the selection of this distance as well.

The timing of these events was calculated for each coastal vector, and then the date of event-occurrence was converted to Unix time (the number of seconds between the recorded date and January 1st 1970), averaged by study region to identify when mean occurrence dates for annual cycle events occur. We used the same linear regression

methods described in Section 3.3 to identify interannual trends in mean occurrence dates of annual cycle events from 1996 – 2019.

4. Results

4.1: Spatial distribution of SLIEs

Stacked SLIEs in our study area (Figure 5) reveal distinct spatial patterns of landfast ice among the four study regions. SLIES generally exhibit greater widths in the Northwest (Mean = 6.5km; Upper Decile = 16.6km) and Northeast (Mean = 5.1km; Upper Decile = 11.3km) regions compared to the Southwest (Mean = 3.6km; Upper Decile = 7.6km) and Southeast (Mean = 5km; Upper Decile = 10.1km). Of the four study regions, SLIEs in the Northwest region exhibit the widest mean SLIE width with the greatest variation (+/- 5.6 km); SLIEs in the Southwest region exhibit the smallest SLIE width (3.6 km) with the least variation (+/-3 km). The highest densities of SLIEs occur proximate to the coastline (Figure 6), with the notable exception of the Southeast region, where landfast ice extends to the Punuk islands to form a "hook" shape in the stacked SLIEs.

The distinct regional landfast ice regimes on St. Lawrence Island, as defined by width, are associated with distributions of water-depth values at the SLIE (Figure 7). These distributions are further explored in Table 2. Of the four study regions, SLIEs in the Northeast region occupy the deepest water depths with the greatest variation; SLIEs in the shallowest water depths occur in the Southeast region, and the least amount of variation in water depth at the SLIE occur in the Northwest region. The interrelation between landfast ice width and water depth varies by geographic region. Generally, greater SLIE widths and water depths occur in the Northwest and Northeast regions, whereas SLIEs in the Southwest and Southeast regions exhibit modest widths at comparable water depths (Figures 8a-d). SLIE widths in the Southeastern region are generally wider at shallower water depths than in the Southwest region.

Linear regression was used to assess how the physical geographic factors of St. Lawrence Island and the northern Bering Sea influenced landfast ice spatial distributions. The regression models used four independent variables (water depth (m), concave sinuosity, convex sinuosity, fetch distance (km)) to predict the outcome of landfast ice

widths (Tables 3a-d). Mean water depth values at the SLIE were generally found to have a negative influence on mean landfast ice width. Concave sinuosity had a positive influence on mean landfast ice width in the Northwest and Southwest regions, and a negative influence in the Northeast and Southeast regions. Fetch distances by coastline orientation had varying degrees of positive and negative influence with landfast ice. Generally, fetch distances had a negative influence on mean landfast ice width where the coastline was oriented in the same direction as the overall region (e.g. Northeast fetch vectors in the Northeast region). Our regression models explain differing amounts of variation in mean landfast ice width by region. Adjusted R^2 values ranged from 0.04 - 0.24. The models explained 9% of mean landfast ice width variability in the Northwest region, 17% in the Northeast region, 4% in the Southwest region, and 24% in the Southeast region.

4.2: Interannual Change

Analysis of interannual trends reveal declines in width (Figure 9). All of these trends are statistically significant ($\alpha = 0.05$) (Table 4). The sharpest declines in width and water depth at the SLIE occur from 2016 – 2019. Further, interannual declines in landfast ice width are evident for the entire island as well. For the entirety of St. Lawrence Island from 1996 – 2012, mean landfast ice width was 5.2 km; from 2016 – 2019, mean landfast ice width was 2.8 km.

We also analyzed interannual trends of four annual cycle events, *First Ice, Stable Ice, Break Up, Ice Free,* from 1996 – 2019 (Table 5). We found these events to occur chronologically in our study area, with the exception of *Break Up* events (Figure 10). In all four study regions, mean *Break Up* dates sometimes precede *Stable Ice* and *First Ice* dates, and occur after *Ice Free* dates. The relatively low R^2 indicate a high level of variability around mean occurrence dates. *First Ice* events have been occurring later in the year in the Northeast, Southwest, and Southeast regions. *Stable Ice* and *Break Up* events have been occurring earlier in all four study regions. *Ice Free* events have been generally occurring earlier, in the Northwest, Northeast, and Southeast regions. The earlier occurrence of *Ice Free* events in the Northeast region is the only statistically

significant interannual trend in our analysis of the annual cycle. The mean occurrence of annual cycle events varies by coastal morphometry (Table 6). Generally, *First Ice* events occur earlier in sheltered coastlines, with the exception of the Southwest region. *Ice Free* events occur earlier in sheltered areas in the Northwest and Northeast regions, but later in the Southwest and Southeast regions.

5. Discussion

5.1. Spatial Distribution of St. Lawrence Island Landfast Ice

We characterized physical and seasonal landfast ice conditions by its spatial distribution as it relates to width, and water depth at the SLIE. Consistent with landfast ice research in other study areas (Divine et al. 2004; Granskog et al. 2003, 2006; Mahoney et al. 2007a, 2014; Zubov 1945) we found the width of landfast ice to vary by geographic region on St. Lawrence Island. We found landfast ice on northern coastlines of St. Lawrence Island to be comparatively wider than the southern coastlines. The observed differences in landfast ice width on northern and southern coastlines are likely to be attributable to St. Lawrence Island's geography's influence on landfast ice formation. In particular, it is likely that the north-facing coasts receive the wind-driven transport of pack ice from northern latitudes in the winter, which accrete into larger sheets of landfast ice, contributing to the relatively longer widths observed in this study. The southern coastlines do not receive similar quantities of pack ice, and landfast ice widths are further constrained by the presence of polynyas (Cooper et al. 2002; Kawerak 2013).

Despite relatively large maximum landfast ice widths, the mean widths fall within a comparatively narrower range of 3.6-6.5 km (Table 2). Along with the high variability of *Break Up* events throughout our study period (Figure 10), these findings suggest that the upper decile widths (11.3-16.6 km) in the Northwest and Northeast regions are not sustained throughout a given season. Instead, large ice sheets can break off from the landfast ice shortly after forming. This is consistent with previous observations characterizing the northern coast as becoming locked in by large ice sheets that frequently attach and separate from the coast throughout a given season (Oceana and

Kawerak 2014). However, the high variability of widths and *Break Up* events on St. Lawrence Island (Figure 10) does not indicate unstable landfast ice conditions. Visual inspection of SAR imagery of early *Break Up* events reveal an initial rapid advance of the SLIE, followed by the detachment of large ice sheets and comparatively shorter widths for the remainder of the season. The SLIEs after such *Break Up* events generally remain positioned over water depths greater than 15 m, signifying the continuation of *Stable Ice* conditions. These occurrences support Mahoney et al.'s (2014) observation that *Break Up* events do not necessarily coincide with the conclusion of *Stable Ice* conditions. Despite variable *Break Up* events, Figure 10 shows mean water depths at the SLIE to generally exceed the 15m isobath used as a proxy for identifying stable conditions for all four study regions. Further, the highly variable occurrence of *Break Up* events suggests the St. Lawrence Island landfast ice annual cycle does not conform to typical patterns of gradual advance and rapid retreat. Previous studies in the Chukchi and Beaufort seas considered non-consecutive occurrences of annual cycle events to be failed identifications (Mahoney et al. 2007, 2014). The term *Breakout* has been used to describe the occurrence of rapid mid-season SLIE retreats (Jones et al. 2016), and is a more applicable term for SLIE retreats on St. Lawrence Island.

5.2. The Influence of Island Physical Features on Landfast Ice Spatial Distribution

Comparing the shape of the coastline to the shape and position of the SLIE, we found the landfast ice regime on St. Lawrence Island to exhibit a number of similarities to those in the Chukchi and Beaufort Seas. One example is the tendency of landfast ice to appear first in sheltered coastal zones. Mahoney et al. (2014) found landfast ice to form first in sheltered coastal zones along the Chukchi and Beaufort Sea coastlines. Similarly, we found landfast ice on St. Lawrence island to first appear in sheltered areas within the Northwest, Northeast, and Southeast regions. Further, we found SLIEs to cluster around land spits and barrier islands enclosing sheltered regions in our study area, as well as the Punuk Islands off the coast of the Southeast region. These areas experienced the most consistent clustering of SLIEs on an interannual basis, with the exception of the last two years of our study (2018 and 2019) when SLIEs failed to reach the Punuk Islands.

Water depth values also influenced patterns in landfast ice cover by limiting the advance of the SLIE over progressively greater water depths (Figures 8a-d). Mean water depths and widths varied by region on the island, with the lowest mean depth occurring in the Southeast region (13.1m), and the largest occurring in the Northeast (26.9m) (Table 2). Regional variation in mean water depth at the SLIE is in keeping with previous observations that the relationship between landfast ice and water depth can vary by geographic region. For example, SLIEs on the Siberian coast occupy mean depths of 20-25m (Zubov 1945); 5-15m in the Baltic Sea (Granskog et al. 2003, 2006); and 10m in the western Kara Sea, 20-30m in the east (Divine et al. 2004).

The results from our linear regression demonstrate how the physical geography, specifically coastal orientation, morphometry, and nearshore bathymetry of St. Lawrence Island and the northern Bering Sea influence landfast ice width. Independent variables had varying degrees of positive influence by study region. Water depth was found to positively influence landfast ice width, which is consistent with our expectation that the landfast ice edge occupies greater water depths as width increases.

The relationship between sinuosity and landfast ice width varied depending on whether the dependent variable was on concave or convex coastlines. The occurrence of positive relationships between sinuosity and landfast ice width was greater in concave sections than convex sections, and is consistent with previous studies observing concave regions such as sheltered embayments and lagoons to enable earlier formations and greater landfast ice widths by providing shelter from wind and wave action (Mahoney et al. 2007a). However, in the Southeast region, sinuosity had a stronger negative relationship with width in concave regions than convex regions. The negative relationship between width and sinuosity in concave regions may be influenced by the grounding of landfast ice from a convex portion of coastline on the Punuk Islands (Figure 6). The landfast ice extending between the convex coastline and the Punuk Islands may be positioned to prevent incoming pack ice from accumulating in the concave coastlines further south, resulting in shorter landfast ice widths and a negative relationship.
Fetch lengths were added as independent variables to determine if unobstructed coastlines oriented towards to prevailing Northeasterly winds would result in greater accumulations of pack ice and thus positively influence mean landfast ice width. We

generally did not find coastlines oriented toward prevailing winds to have a greater positive relationship with landfast ice widths compared to coastlines oriented elsewhere. Instead, we found that fetch distances had a negative relationship with mean landfast ice width where the coastline was oriented in the same direction as the overall region (e.g. Northeast fetch vectors in the Northeast region), as well as oriented towards prevailing winds. Fetch distances below the 80km maximum value most frequently occurred on concave coastlines, suggesting the coastline is somewhat sheltered, and generally had a positive relationship with mean landfast ice width. The positive relationship between mean landfast ice width and fetch distances below the 80km maximum value suggests that the orientation of a coastline to prevailing winds — although relevant to the transport of drift ice that is necessary for landfast ice formation and growth — may restrict landfast ice widths if the morphometry of the coastline does not shelter the accumulated ice from wind/ocean energy. The frequency of winter storms in the Bering Sea (Overland 1981), and linkages between weather and coastal ice conditions on St. Lawrence Island (Huntington et al. 2013), may increase the negative influence of coastal exposure on mean landfast ice width. It is also notable that Northeastern orientations of the coastline did not strongly influence landfast ice width compared to orientations in other directions, suggesting that orientation toward prevailing wind conditions alone do not influence greater landfast ice widths.

Our models explained 24% of the variability in mean landfast ice width. The models include independent variables related to the physical geography of St. Lawrence Island and the northern Bering Sea, but not of meteorological events matching the occurrence dates of our dependent variables. Sea surface temperature and overall sea ice concentration also affect the formation and growth of landfast ice (Mahoney et al. 2014), and their inclusion as independent variables could improve the explanatory power of future regression models.

5.3. Seasonal Duration of St. Lawrence Island Landfast Ice

Based on the mean-occurrence of *First Ice* and *Ice Free* dates the seasonal duration of landfast ice generally spans from mid-January to late-April / early-May. This

timeframe is notably shorter than the seasonal durations of landfast ice regimes in higher latitudes. In comparison to Mahoney et al.'s (2014) time series analysis, the seasonal duration of landfast ice in the Chukchi and Beaufort Seas which has been characterized as forming in the months of October – November, and retreating in the months of May – June. The mean occurrence dates of annual cycle events in the Chukchi and Beaufort season generally occur in chronological order: *First Ice, Stable Ice, Break Up,* and *Ice Free*. These mean occurrence dates are distinct and well separated. On St. Lawrence Island, *First Ice, Stable Ice,* and *Ice Free* events generally occur in chronological order. However, *Break Up* events are highly variable in all four regions, qualifying these occurrences as *breakouts* — the mid-season retreat of SLIEs. Highly variable mean occurrence dates suggest the St. Lawrence Island annual cycle is more complex than the annual cycle criteria created by Mahoney et al. (2007, 2014) to study landfast ice conditions in the Chukchi and Beaufort Seas. This comparatively higher variability is consistent with broader comparisons of sea ice coverage in the Bering Sea versus the Chukchi and Beaufort Seas (Frey et al. 2015).

5.4 Interannual Variability from 1996 – 2019

The spatial distribution of St. Lawrence Island landfast ice shows strong interannual variability by every metric used in this study: width, SLIE water depth, and proximity to coastal features. The strongest interannual variability occurs in the final years of 2016 – 2019. During this period, mean landfast ice widths (Figure 9) sharply decrease. The prevalence of statistically significant interannual trends of landfast ice width and water depth at the SLIE contrasts with the absence of statistically significant trends in annual cycle events, with the exception of *Ice Free* events in the Northeast region (Tables 2 & 3). However, the standard deviation regions of all annual cycle events cluster from 2016 – 2019 (Figure 10), similar to the clustering of standard deviation regions of physical landfast ice conditions (Figures 8, 9, & 10). This clustering suggests that although the mean occurrence dates of annual cycle events exhibit no statistically significant trends overall, the annual cycle is shortening.

The relatively recent decline of St. Lawrence Island landfast ice from 2016 – 2019

matches recent observations of broader sea ice variability in the Bering Sea. Sea ice extent during the winter and spring of 2018 was at the lowest observed in the Bering Sea since satellite observations began in 1972 (Eisner 2018; Stabeno et al. 2018). In the winter of 2019, sea ice areal coverage diminished to the lowest levels seen in 40 years (Cornwall 2019). Whether this trend represents an unusual anomaly or a sustained climatic regime shift continues to be debated. Previous sea ice minimums in the Bering Sea have been attributed to shifts in atmospheric circulation patterns that strongly influence sea sea surface temperature and atmospheric pressure, such as the Pacific Decadal Oscillation (Walsh et al. 2017) and Arctic Oscillation (Kapsch et al. 2010). However, researchers have not ruled out the possibility of recent unprecedented sea ice minimums to be the result of sustained climatic shifts in the Bering Sea region (Cornwall 2019). Regardless, the broader implications of recent sea ice conditions in the Bering Sea are represented in landfast ice conditions on St. Lawrence Island. Continued monitoring of landfast ice is necessary to determine if the trends observed in this study represent an anomaly in landfast ice conditions or a sustained regime shift.

6. Conclusion

This study is the most comprehensive analysis to date of landfast ice on St. Lawrence Island, and contributes to the broader study of landfast ice conditions in the northern Bering Sea. In doing so we have expanded on past work characterizing landfast ice conditions on Alaskan coastlines in the Chukchi and Beaufort Seas (Mahoney et al. 2014). We have also characterized the seasonal duration of landfast ice on St. Lawrence Island by tracking the mean occurrence of annual cycle events, measured by the timing and spatial distribution of SLIEs. We found that the seasonal duration of landfast ice varies by study region, yet generally spans from mid-January to late-April / early-May, which is notably shorter than landfast ice seasonal durations in the Chukchi and Beaufort Seas (Mahoney et al. 2014). The shorter seasonal duration of St. Lawrence Island's annual cycle involves a relatively rapid succession of annual cycle events, and is notable for *Break Up* events to occur throughout this cycle rather than near the conclusion. Despite the frequent occurrence of *Breakout* events, the remaining landfast ice still

occupies water depths used as a proxy for stable ice conditions. The variability of annual cycle events on St. Lawrence Island suggests that annual cycle models applied to the Chukchi and Beaufort Seas (Mahoney et al. 2014) may not be applicable in the Bering Sea. The high variability and short seasonal duration that characterizes St. Lawrence Island's annual cycle is consistent with broader characterizations of sea ice conditions in the northern Bering Sea overall (Frey et al. 2015). This observation matches a similar conclusion made by Mahoney et al. (2014) where landfast ice variability responds to regional processes that influence similar variability in drift ice conditions. Recent declines of drift ice extent in the Bering Sea (Cornwall 2019; Eisner 2019; Stabeno et al. 2018) may have influenced similar declines in overall landfast ice cover for the region.

Our analysis of interannual variability in landfast ice width, water depth at the SLIE, and annual cycle events reveal statistically significant trends. The strongest interannual changes occurred from 2016 – 2019 in our study period, and were not gradual. During these years, all four study regions experienced sharp declines in width and water depth at the SLIE. Interannual declines in water depth at the SLIE generally did not fall below 15m, with the exception of the Southeast region, where the mean SLIE values fell below 10m in the 2018-2019 annual cycle year. Interannual trends were evident in the mean occurrence dates of annual cycle events as well. Generally, *First Ice* dates are occurring later and *Ice Free* dates are occurring earlier, suggesting an interannual reduction in landfast ice seasonal duration. Both *Stable Ice* and *Break Up* events were found to be occurring earlier as well. However, none of these trends were found to be statistically significant, except in the case of increasingly early occurrence of *Ice Free* events on the Southeastern region.

Previous periods of comparably diminished sea ice over in the Bering Sea have been attributed to shifts in the Pacific Decadal Oscillation (PDO) and the Arctic Oscillation (AO) (Kapsch et al. 2010; Walsh et al. 2017). It is presently unclear if recent declines in sea ice cover, including landfast ice in our study area, are attributable to decadal oscillations in atmospheric circulation, or are the result of a sustained climatic regime shift (Cornwall 2019). Continued monitoring of landfast ice on St. Lawrence Island would distinguish between whether interannual trends observed in this study represent a sustained decline of landfast sea ice, or are part of the complex multiyear

variation that characterizes seasonal ice cover in the Bering Sea.

7. References

ACIA-Arctic Climate Impact Assessment, Arctic Monitoring, Assessment Programme, Program for the Conservation of Arctic Flora, & International Arctic Science Committee. (2005). Arctic Climate Impact Assessment-Scientific Report. Cambridge University Press.

ANC, H. Voorhees, and R. Sparks. 2012. Nanuuq: Local and Traditional Ecological Knowledge of Polar Bears in the Bering and Chukchi Seas. Alaska Nanuuq Commission, Nome, AK.

Barry, R.G., Moritz, R.E., Rogers, J.C., 1979. The fast ice regimes of the Beaufort and Chukchi Sea coasts, Alaska. Cold Regions Science and Technology, 1 (2), 129–152.

Benson, A. J., & Trites, A. W. (2002). Ecological effects of regime shifts in the Bering Sea and eastern North Pacific Ocean. Fish and Fisheries, 3(2), 95-113.

Bhatt, U. S., Walker, D. A., Raynolds, M. K., Comiso, J. C., Epstein, H. E., Jia, G., Rudiger, G., Pinzon, J., Tucker, C., Tweedie, C., & Webber, P. J. (2010). Circumpolar Arctic tundra vegetation change is linked to sea ice decline. Earth Interactions, 14(8), 1-20.

Coachman, L. K., & Aagaard, K. (1988). Transports through Bering Strait: Annual and interannual variability. *Journal of Geophysical Research: Oceans*, *93*(C12), 15535-15539.

Cooper, L. W., Grebmeier, J. M., Larsen, I. L., Egorov, V. G., Theodorakis, C., Kelly, H. P., & Lovvorn, J. R. (2002). Seasonal variation in sedimentation of organic materials in the St. Lawrence Island polynya region, Bering Sea. Marine Ecology Progress Series, 226, 13-26.

Cornwall, W. (2019). Vanishing Bering Sea ice poses climate puzzle.

Danielson, S., Johnson, M., Solomon, S., & Perrie, W. (1). km Gridded bathymetric dataset based on ship soundings: a research tool for the waters of eastern Russia. In Alaska & western Canada, Poster presentation at the 2008 Alaska Marine Science Symposium, Anchorage, Alaska.

DeMaster, D. P., & Rauch III, S. D. (2018). Final environmental impact statement for

issuing annual quotas to the Alaska Eskimo Whaling Commission for a subsistence hunt on bowhead whales for the years 2013 through 2018.

Divine, D.V., Korsnes, R., Makshtas, A.P., 2004. Temporal and spatial variation of shore-fast ice in the Kara Sea. Continental Shelf Research, 24, 1717–1736. \

Eisner, L. (2018). The Bering Sea: Current status and recent trends. PICES Press, 26(1), 29-36.

Fraser, A. D., Massom, R. A., Michael, K. J., Galton-Fenzi, B. K., & Lieser, J. L. (2012). East Antarctic landfast sea ice distribution and variability, 2000–08. Journal of Climate, 25(4), 1137-1156.

Frey, K. E., Moore, G. W. K., Cooper, L. W., & Grebmeier, J. M. (2015). Divergent patterns of recent sea ice cover across the Bering, Chukchi, and Beaufort seas of the Pacific Arctic Region. Progress in Oceanography, 136, 32-49.

Granskog, M. A., Martma, T. A., & Vaikmäe, R. A. (2003). Development, structure and composition of land-fast sea ice in the northern Baltic Sea. Journal of Glaciology, 49(164), 139-148.

Granskog, M., Kaartokallio, H., Kuosa, H., Thomas, D. N., & Vainio, J. (2006). Sea ice in the Baltic Sea–a review. Estuarine, Coastal and Shelf Science, 70(1-2), 145-160.

Grebmeier, J. M., Overland, J. E., Moore, S. E., Farley, E. V., Carmack, E. C., Cooper, L. W., ... & McNutt, S. L. (2006). A major ecosystem shift in the northern Bering Sea. *Science*, *311*(5766), 1461-1464.

Hansen, Kathryn, "Historic Low Sea Ice in the Bering Sea" Climate.nasa.gov. https://climate.nasa.gov/news/2726/historic-low-sea-ice-in-the-bering-sea/ (accessed September 2018)

Haynie, A., & Huntington, H. (2016). Strong connections, loose coupling: the influence of the Bering Sea ecosystem on commercial fisheries and subsistence harvests in Alaska. Ecology and Society, 21(4).

Huntington, H. P., Noongwook, G., Bond, N. A., Benter, B., Snyder, J. A., & Zhang, J. (2013). The influence of wind and ice on spring walrus hunting success on St. Lawrence Island, Alaska. Deep Sea Research Part II: Topical Studies in Oceanography, 94, 312-322.

Huntington, H. P., Daniel, R., Hartsig, A., Harun, K., Heiman, M., Meehan, R., ... & Stetson, G. (2015). Vessels, risks, and rules: planning for safe shipping in Bering Strait. Marine Policy, 51, 119-127.

J. Fall. (2013). Subsistence harvests in the BSIERP communities, 94, 274-291.

Jones, J., Eicken, H., Mahoney, A., Rohith, M. V., Kambhamettu, C., Fukamachi, Y., ... & George, J. C. (2016). Landfast sea ice breakouts: Stabilizing ice features, oceanic and atmospheric forcing at Barrow, Alaska. *Continental Shelf Research*, *126*, 50-63.

Kapsch, M. L., Eicken, H., & Robards, M. (2010). Sea ice distribution and ice use by indigenous walrus hunters on St. Lawrence Island, Alaska. In SIKU: Knowing Our Ice (pp. 115-144). Springer, Dordrecht.

Kawerak, Inc. 2013. Seal and walrus harvest and habitat areas for nine Bering Strait Region communities. Nome, AK: Kawerak, Inc., Social Science Program

Knapp, P. A., & Soulé, P. T. (2017). Spatio-temporal linkages between declining Arctic sea-ice extent and increasing wildfire activity in the western United States. *Forests*, *8*(9), 313.

Kovacs, K. M., Lydersen, C., Overland, J. E., & Moore, S. E. (2011). Impacts of changing sea-ice conditions on Arctic marine mammals. Marine Biodiversity, 41(1), 181-194.

Kwok, R., Rignot, E., Holt, B., & Onstott, R. (1992). Identification of sea ice types in spaceborne synthetic aperture radar data. Journal of Geophysical Research: Oceans, 97(C2), 2391-2402.

Lantuit, H., & Pollard, W. H. (2008). Fifty years of coastal erosion and retrogressive thaw slump activity on Herschel Island, southern Beaufort Sea, Yukon Territory, Canada. Geomorphology, 95(1-2), 84-102.

Liu, J., Curry, J. A., Wang, H., Song, M., & Horton, R. M. (2012). Impact of declining Arctic sea ice on winter snowfall. Proceedings of the National Academy of Sciences, 109(11), 4074-4079.

Lovorn, J. R., Rocha, A. R., Mahoney, A. H., & Jewett, S. C. (2018). Sustaining ecological and subsistence functions in conservation areas: eider habitat and access by Native hunters along landfast ice. Environmental Conservation, 45(4), 361-369.

Macklin, S. A. (1983). Wind drag coefficient over first‐year sea ice in the Bering Sea. *Journal of Geophysical Research: Oceans*, *88*(C5), 2845-2852.

Mahoney, A., Eicken, H., Graves, A., Shapiro, L., & Cotter, P. (2004, September). Landfast sea ice extent and variability in the Alaskan Arctic derived from SAR imagery. In Geoscience and Remote Sensing Symposium, 2004. IGARSS'04. Proceedings. 2004 IEEE International (Vol. 3, pp. 2146-2149). IEEE.

Mahoney, A., Eicken, H., Shapiro, L., & Graves, A. (2006). Defining and locating the seaward landfast ice edge in northern Alaska. In 18th International Conference on Port and Ocean Engineering under Arctic Conditions (POAC'05), Potsdam, NY (pp. 991-1001).

Mahoney, A.R., Eicken, H., Gaylord, A.G., Shapiro, L., 2007a Alaska landfast sea ice: links with bathymetry and atmospheric circulation. Journal of Geophysical Research Oceans 112 (C2).

Mahoney, A.R., Eicken, H., Shapiro, L., 2007b. How fast is landfast sea ice? A study of the at- tachment and detachment of nearshore ice at Barrow, Alaska. Cold Regions Science and Technology, 47 (3)

Mahoney, A. R., Eicken, H., Gaylord, A. G., & Gens, R. (2014). Landfast sea ice extent in the Chukchi and Beaufort Seas: The annual cycle and decadal variability. Cold Regions Science and Technology, 103, 41-56.

Meyer, F. J., Mahoney, A. R., Eicken, H., Denny, C. L., Druckenmiller, H. C., & Hendricks, S. (2011). Mapping arctic landfast ice extent using L-band synthetic aperture radar interferometry. Remote sensing of environment, 115(12), 3029-3043.

Noongwook, G., Huntington, H. P., & George, J. C. (2007). Traditional knowledge of the bowhead whale (Balaena mysticetus) around St. Lawrence Island, Alaska. Arctic, 60(1), 47-54.

Oceana and Kawerak. 2014. Bering Strait Marine Life and Subsistence Use Data Synthesis. Oceana and Kawerak, Juneau, AK.

Overland, J. E. (1981). Marine climatology of the Bering Sea. *The eastern Bering Sea shelf: Oceanography and resources*, *1*, 15-22.

Post, E., Bhatt, U. S., Bitz, C. M., Brodie, J. F., Fulton, T. L., Hebblewhite, M., Kerby, J., Kutz, S., Stirling, I., & Walker, D. A. (2013). Ecological consequences of sea-ice decline. Science, 341(6145), 519-524.

Ray, G. C., Hufford, G. L., Overland, J. E., Krupnik, I., McCormick‐Ray, J., Frey, K., & Labunski, E. (2016). Decadal Bering Sea seascape change: consequences for Pacific walruses and indigenous hunters. Ecological Applications, 26(1), 24-41.

Robards, M. D., Kitaysky, A. S., & Burns, J. J. (2013). Physical and sociocultural factors affecting walrus subsistence at three villages in the northern Bering Sea: 1952–2004. Polar Geography, 36(1-2), 65-85.

Salo, S. A., Schumacher, J. D., & Coachman, L. K. (1983). Winter currents on the eastern Bering Sea shelf.

Screen, J. A., & Simmonds, I. (2010). The central role of diminishing sea ice in recent Arctic temperature amplification. Nature, 464(7293), 1334.

Serreze, M. C., & Stroeve, J. (2015). Arctic sea ice trends, variability and implications for seasonal ice forecasting. *Philosophical Transactions of the Royal Society A: Mathematical, Physical and Engineering Sciences*, *373*(2045), 20140159.

Sigler, M. F., Harvey, H. R., Ashjian, J., Lomas, M. W., Napp, J. M., Stabeno, P. J., & Van Pelt, T. I. (2010). How does climate change affect the Bering Sea ecosystem?. Eos, Transactions American Geophysical Union, 91(48), 457-458.

Simpkins, M. A., Hiruki-Raring, L. M., Sheffield, G., Grebmeier, J. M., & Bengtson, J. L. (2003). Habitat selection by ice-associated pinnipeds near St. Lawrence Island, Alaska in March 2001. Polar Biology, 26(9), 577-586.

Stabeno, P. J., Bond, N. A., & Salo, S. A. (2007). On the recent warming of the southeastern Bering Sea shelf. Deep Sea Research Part II: Topical Studies in Oceanography, 54(23-26), 2599-2618.

Stabeno, P. J., & Bell, S. W. (2019). Extreme Conditions in the Bering Sea (2017–2018): Record‐Breaking Low Sea‐Ice Extent. *Geophysical Research Letters*.

Stephenson, S. R., Smith, L. C., & Agnew, J. A. (2011). Divergent long-term trajectories of human access to the Arctic. *Nature Climate Change*, *1*(3), 156.

Stephenson, S. R., Smith, L. C., Brigham, L. W., & Agnew, J. A. (2013). Projected 21st-century changes to Arctic marine access. *Climatic Change*, *118*(3-4), 885-899.

Stroeve, J., Holland, M. M., Meier, W., Scambos, T., & Serreze, M. (2007). Arctic sea ice decline: Faster than forecast. Geophysical research letters, 34(9).

Stroeve, J., Serreze, M., Drobot, S., Gearheard, S., Holland, M., Maslanik, J., ... & Scambos, T. (2008). Arctic sea ice extent plummets in 2007. Eos, Transactions American Geophysical Union, 89(2), 13-14.

USACE 2007. Erosion Information Paper - Savoonga, Alaska. U.S. Army Corps of Engineers, Alaska District.

U.S. Fish and Wildlife Service, 2008. Endangered and threatened wildlife and plants; determination of threatened status for the polar bear (Ursus maritimus) throughout its range; Final rule. Federal Register 73 (95)

Vihma, T. (2014). Effects of Arctic sea ice decline on weather and climate: A

review. Surveys in Geophysics, 35(5), 1175-1214.

Walsh, J. E., Fetterer, F., Scott Stewart, J., & Chapman, W. L. (2017). A database for depicting Arctic sea ice variations back to 1850. Geographical Review, 107(1), 89-107.

Whiteman, G., Hope, C., & Wadhams, P. (2013). Climate science: Vast costs of Arctic change. *Nature*, *499* (7459), 401.
Zubov, N. N. (1945), Arctic Sea Ice (in Russian), 366 pp., Izd. Glavsevmorputi, Moscow. (English translation), 491 pp., U.S. Navy Oceanogr. Off., Springfield, Va., 1963

Conflict of Interest Statement

The authors whose names are listed immediately below certify that they have NO affiliations with or involvement in any organization or entity with any financial interest (such as honoraria; educational grants; participation in speakers' bureaus; membership, employment, consultancies, stock ownership, or other equity interest; and expert testimony or patent-licensing arrangements), or non-financial interest (such as personal or professional relationships, affiliations, knowledge or beliefs) in the subject matter or materials discussed in this manuscript. Author names:

David A Jensen
Dr. Andy Mahoney
Dr. Lynn Resler

Tables

Table 1: Details of predictor variables used in models.

Parameter	Definition	Data Source	Resolution	Units	Justification
Nearshore Bathymetry	Measured distance between the ocean floor and the surface	Alaska Regional Bathymetric Digital Elevation Model. Created by Danielson et al. (2008).	100m raster	Meters	Landfast ice is generally confined to shallower water depths that enable the formation of stabilizing features (e.g. grounded pressure ridges) (Mahoney et al. 2007b). We expect greater extents of shallow bathymetry from the coastline to positively influence landfast ice widths.
Sinuosity	A scalar number between 0 and 1 that describes how sinuous a path is compared to the straight line distance. A value of 1 corresponds to a straight line, and a value of 0	Geospatial processing on Alaska Coast Shapefile - Alaska State Geo-spatial Clearinghouse	NA - vector data	0-1 range	The concavity/convexity of a given section of coastline may influence landfast ice width by affecting the amount of landfast ice accumulation (concave) or exposure to shearing forces (convex). Concave regions are often sheltered regions that protect landfast ice

	corresponds to an infinitely convoluted path.				from shearing forces (Mahoney et al. 2007a, 2007b). We expect sinuosity values to have a positive relationship with landfast ice width on concave coastlines, and a negative relationship on convex coastlines.
Fetch Distance	Measurements of unobstructed distance in a given direction from a coast vector (See *Figure 4*). Eight fetch distances were measured for each coastal vector: North, Northeast, East, Southeast, South, Southwest, West, and Northwest.	Geospatial processing on coastal vectors - using fetchR package in R Studio 3.5.3	NA - vector data	Kilometers	Fetch distances determine orientation of a coastline relative to prevailing winds transporting pack ice into coastal zones. Pack ice is generally circulated into the Bering Sea through Northeasterly winds (Coachman & Aagaard 1988; Macklin 1983; Salo et al. 1983).

Table 2: Quantitative parameters of landfast ice width and water depth by region on St. Lawrence Island.

Region	Quantitative Parameters	Width (km)	Water Depth (m)
NW	Mean	6.5	23.8
	Standard Deviation	5.6	4.4
	Upper Decile	16.6	19.3
	Skewness	0.98	-0.71
NE	Mean	5.1	26.9
	Standard Deviation	4	8.8
	Upper Decile	11.3	15.8
	Skewness	1.59	-0.03
SW	Mean	3.6	24.3
	Standard Deviation	3	4.7
	Upper Decile	7.6	18.9
	Skewness	1.78	0.07
SE	Mean	5	19.6
	Standard Deviation	3.6	5.2

	Upper Decile	10.1	13.1
	Skewness	1.43	0.33

Table 3a: Regression outputs for Northwest region

Northwest	Coefficient	Std. Error	T-Value	P-Value
Intercept	13.2	0.21	62.85	<0.05*
Water Depth	-0.43	0.01	-43	<0.05*
Concave Sinuosity	4.21	0.32	13.15	<0.05*
Convex Sinuosity	-1.01	0.29	-3.48	0.12
North Fetch	-0.02	0.01	2	<0.05*
Northeast Fetch	-0.05	0.01	5	<0.05*
East Fetch	0.01	0.01	1	<0.05*
Southeast Fetch	0.01	0.01	1	<0.05*
South Fetch	NA	NA	NA	NA
Southwest Fetch	0.01	0.17	0.06	0.11
West Fetch	-0.01	0.01	-1	0.09
Northwest Fetch	0.01	0.01	3	<0.05*
		F-stat = 612.8	**df** = 405278	

Table 3b: Regression outputs for Northeast region

Northeast	Coefficient	Std. Error	T-Value	P-Value
Intercept	-4.6	0.05	-92	<0.05*
Water Depth	-0.46	0.01	-46	<0.05*
Concave Sinuosity	-2.33	0.04	-58.25	0.07
Convex Sinuosity	-0.87	0.09	-9.66	0.16
North Fetch	-0.03	0.01	-3	<0.05*
Northeast Fetch	-0.04	0.01	-4	<0.05*
East Fetch	0.03	0.01	3	<0.05*
Southeast Fetch	-0.01	0.01	-1	0.13
South Fetch	NA	NA	NA	
Southwest Fetch	NA	NA	NA	
West Fetch	NA	NA	NA	<0.05*
Northwest Fetch	0.01	0.01	1	
		F-stat = 1017	**df** = 963806	

Table 3c: Regression outputs for Southwest region

Southwest	Coefficient	Std. Error	T-Value	P-Value
Intercept	7.43	0.1	74.3	<0.05*
Water Depth	-0.31	0.01	-31	<0.05*
Concave Sinuosity	3.31	0.13	25.46	<0.05*
Convex Sinuosity	-2.28	0.11	20.71	<0.05*
North Fetch	NA	NA	NA	NA
Northeast Fetch	NA	NA	NA	NA
East Fetch	NA	NA	NA	NA
Southeast Fetch	0.01	0.01	1	<0.05*
South Fetch	0.01	0.01	1	<0.05*
Southwest Fetch	-0.02	0.01	-2	<0.05*
West Fetch	-0.01	0.01	-1	0.08
Northwest Fetch	-0.02	0.01	-2	0.14
		F-stat = 530.5	**df** = 296558	

Table 3d: Regression outputs for Southeast region

Southeast	Coefficient	Std. Error	T-Value	P-Value
Intercept	6.76	0.08	84.5	<0.05*
Water Depth	-0.49	0.01	-49	<0.05*
Concave Sinuosity	-1.47	0.13	-11.31	<0.05*
Convex Sinuosity	0.43	0.08	5.37	<0.05*
North Fetch	-0.01	0.01	-1	0.16
Northeast Fetch	0.08	0.01	8	<0.05*
East Fetch	0.06	0.01	6	<0.05*
Southeast Fetch	0.12	0.01	12	<0.05*
South Fetch	0.09	0.04	2.25	<0.05*
Southwest Fetch	-0.01	0.01	-1	0.12
West Fetch	NA	NA	NA	NA
Northwest Fetch	NA	NA	NA	NA
		F-stat = 7024	**df** = 396542	

Table 4: Statistical parameters for interannual trends in landfast ice width and water depth at the SLIE from 1996 – 2019

Region	Statistical parameters	Width (km)	Water Depth (m)
NW	Adj. R^2	0.03	0.009
	Slope	0.001	0.105
	Significance [p-value]	<.05*	<.05*
NE	Adj. R^2	0.014	0.005
	Slope	-0.002	0.04
	Significance [p-value]	<.05*	<.05*
SW	Adj. R^2	0.03	0.003
	Slope	0.002	0.05
	Significance [p-value]	<.05*	<.05*
SE	Adj. R^2	0.001	0.002
	Slope	1.59	0.04
	Significance [p-value]	<.05*	<.05

Table 5: Statistical parameters for interannual trends in annual cycle events from 1996 – 2019

Region	Statistical Parameters	First-Ice	Stable Ice	Break-Up	Ice-Free
NW	Adj. R^2	-0.05	-0.05	-0.02	0.04
	Slope	-2.3	-2.93	-5.45	-1.05
	Statistical Significance [p-value]	0.76	0.78	0.49	0.18
NE	Adj. R^2	-0.05	0.01	-0.03	0.16
	Slope	2.75	-1.3	-1.3	-1.66
	Statistical Significance [p-value]	0.75	0.28	0.55	<.05*
SW	Adj. R^2	-0.02	-0.01	-0.03	-0.05
	Slope	5.7	-8.7	-6.68	2.3
	Statistical Significance [p-value]	0.47	0.42	0.51	0.98
SE	Adj. R^2	-0.05	0.001	-0.05	0.07
	Slope	2.21	-1.22	-2.3	-1.3
	Statistical Significance [p-value]	0.8	0.32	0.73	0.14

Table 6: Comparison of mean occurrence dates for First-Ice and Ice-Free events on Sheltered and Not Sheltered coastlines.

Study Area	Coast Type	Mean First-Ice Onset	Mean Ice-Free Onset
NW	Sheltered	February 27	March 9
	Not Sheltered	March 11	March 13
	Δ Days	-12 days	-4 days
NE	Sheltered	March 3	March 18
	Not Sheltered	March 6	March 26
	Δ Days	-3 days	-8 days
SW	Sheltered	March 25	April 11
	Not Sheltered	March 16	April 6
	Δ Days	+9 days	+5 days
SE	Sheltered	March 4	April 17
	Not Sheltered	March 5	Apr 8
	Δ Days	-1 day	+9 days

Figures

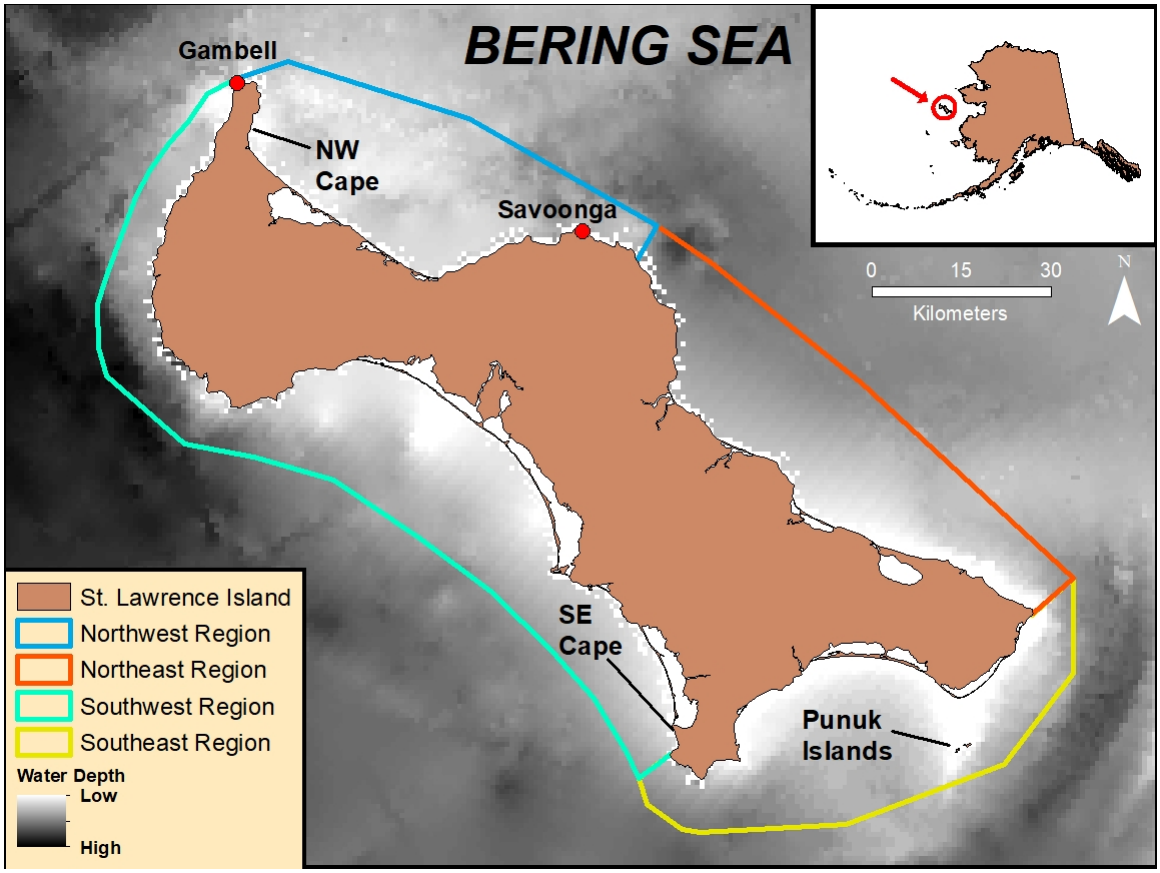

Figure 1

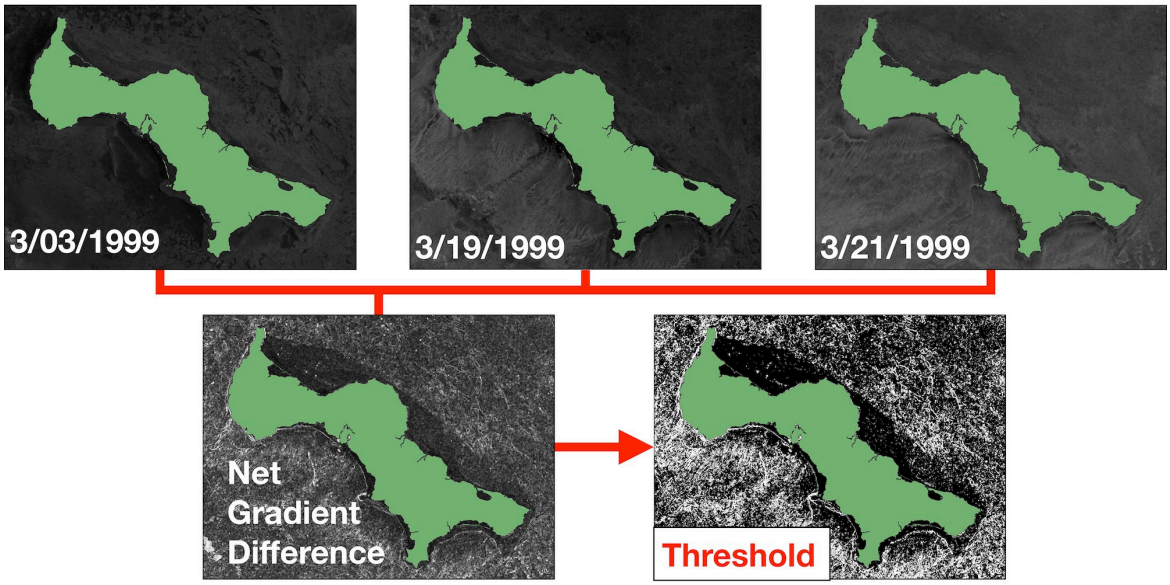

Figure 2

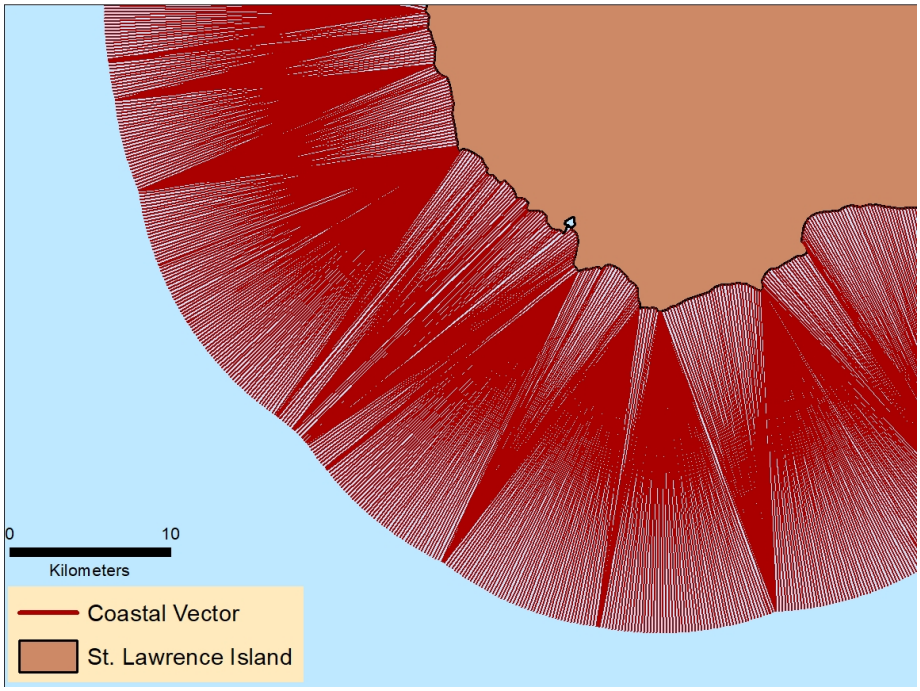

Figure 3

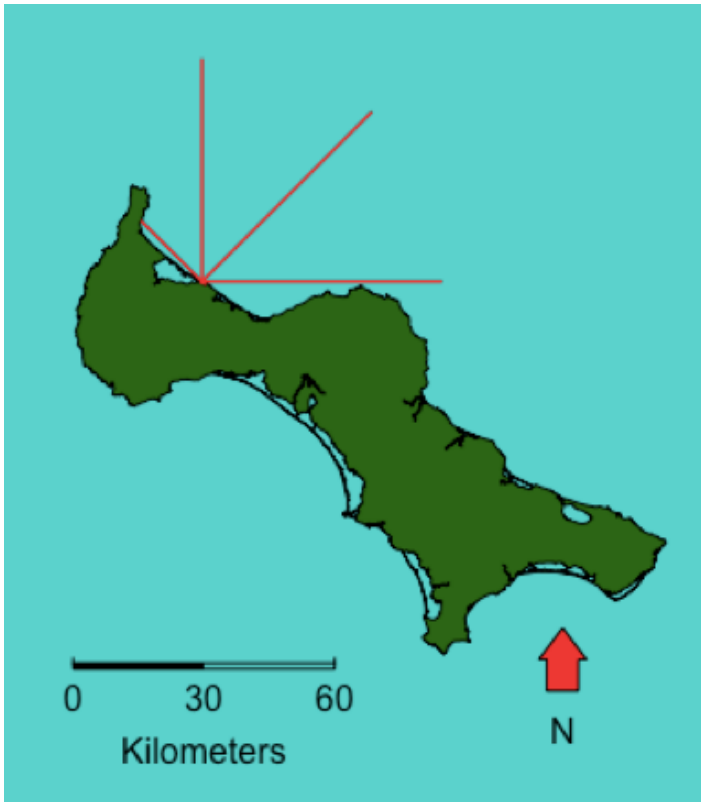

Figure 4

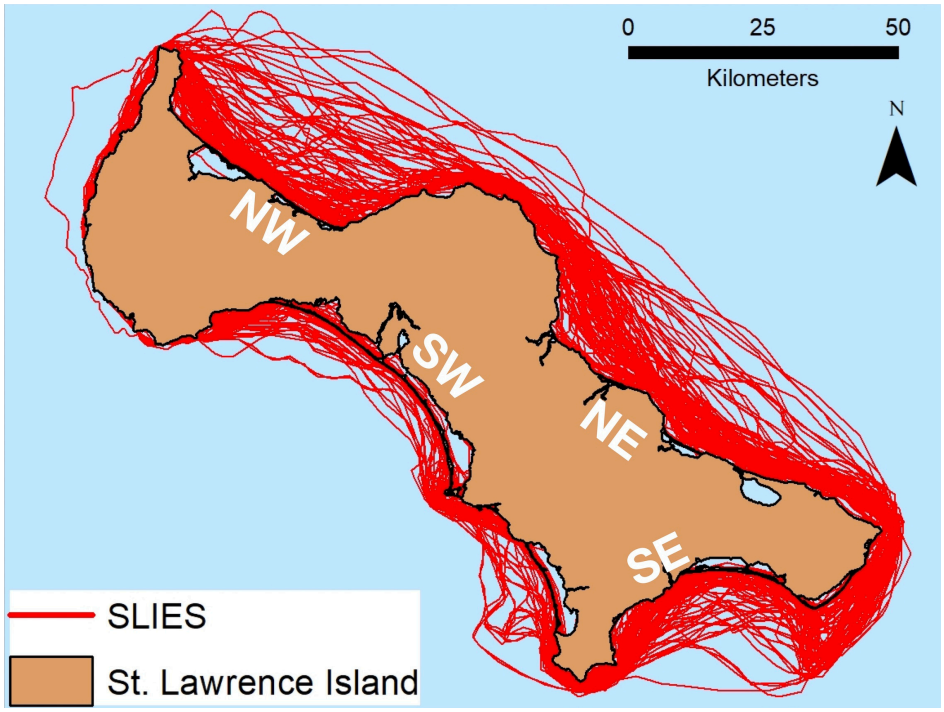

Figure 5

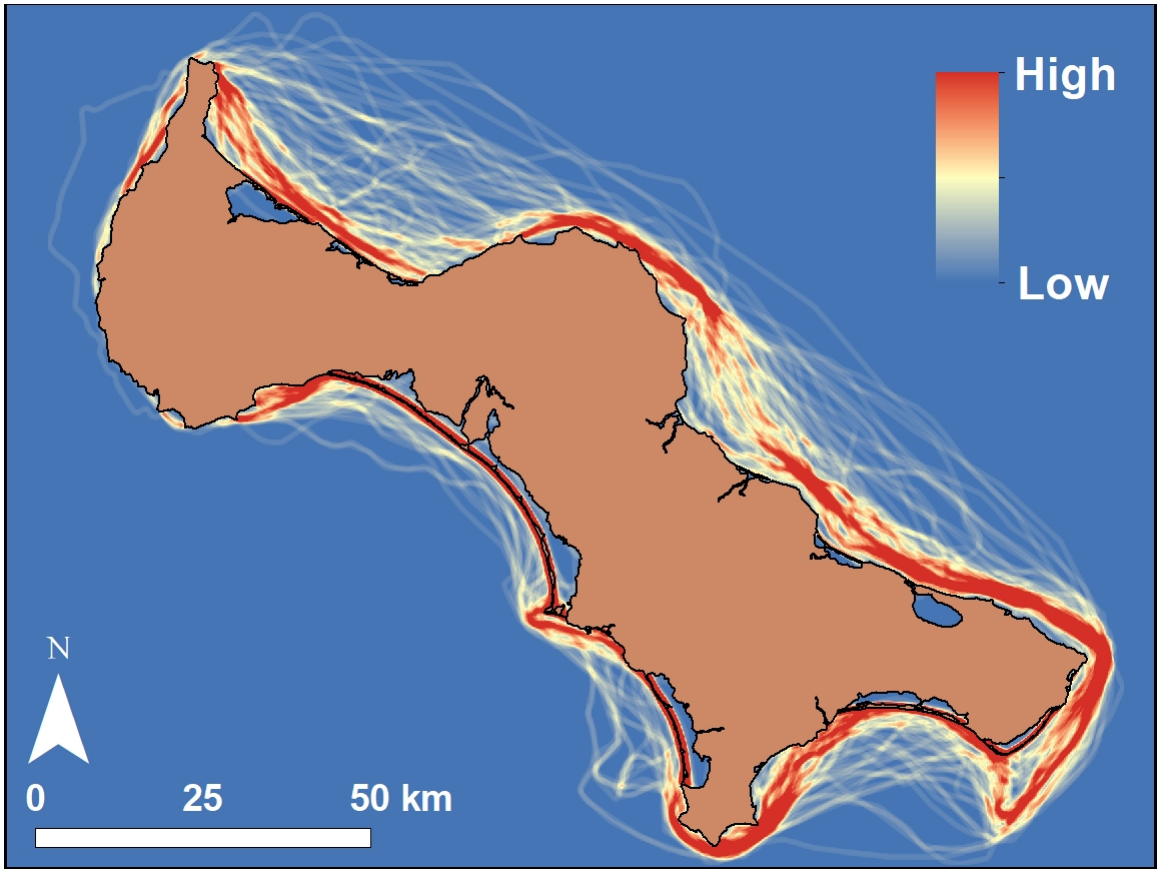

Figure 6

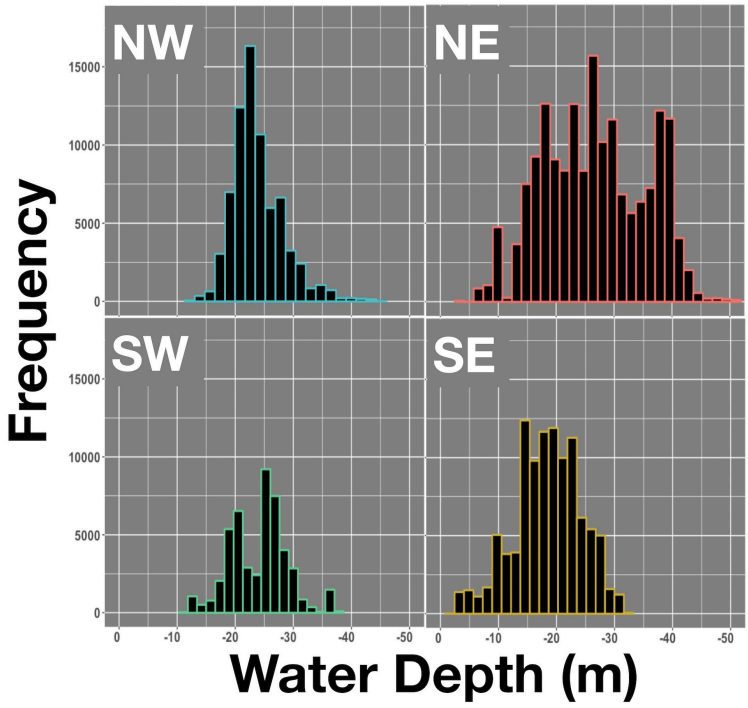

Figure 7

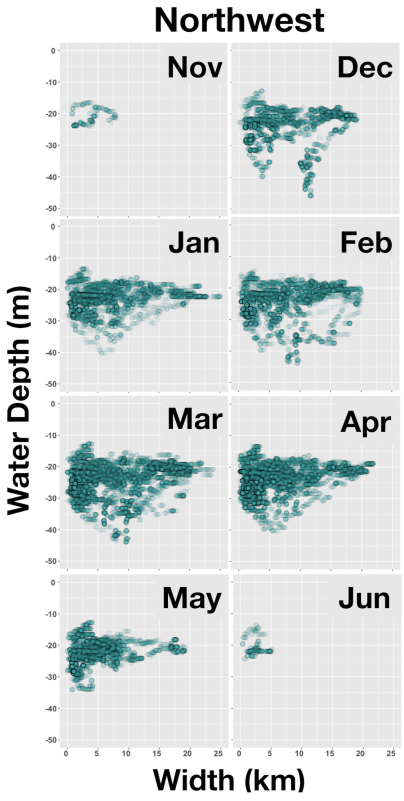

Figure 8a

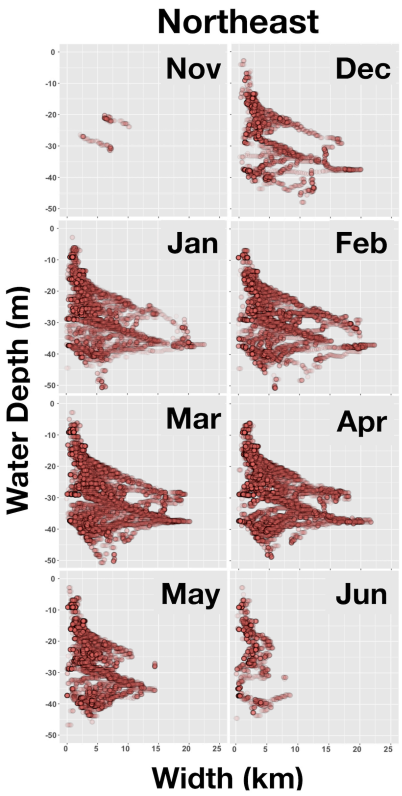
Northeast
Nov
Dec
Jan
Feb
Mar
Apr
May
Jun
Water Depth (m)
Width (km)

Figure 8b

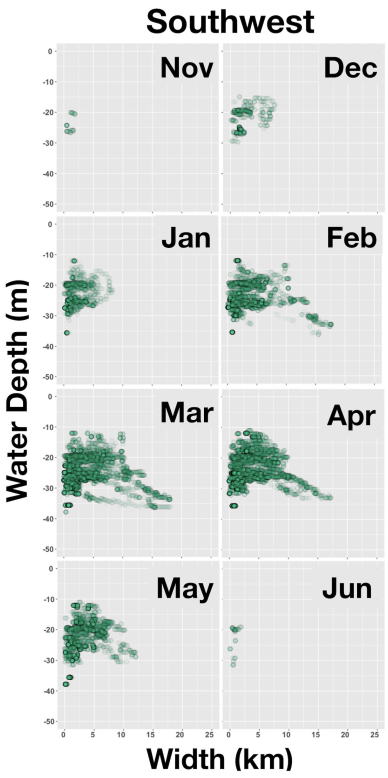
Southwest
Nov
Dec
Jan
Feb
Mar
Apr
May
Jun
Water Depth (m)
Width (km)

Figure 8c

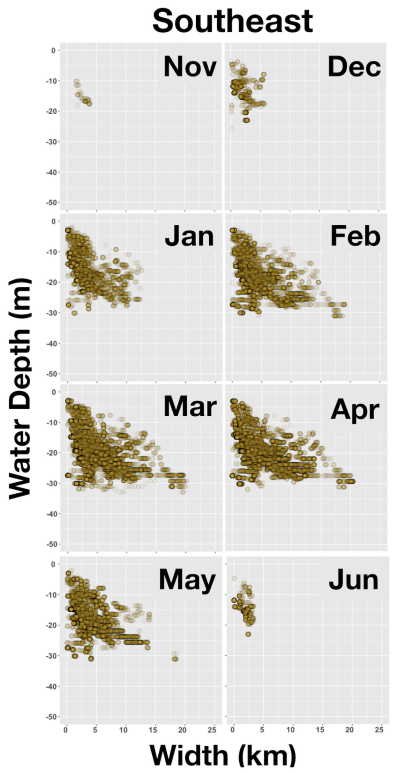

Figure 8d

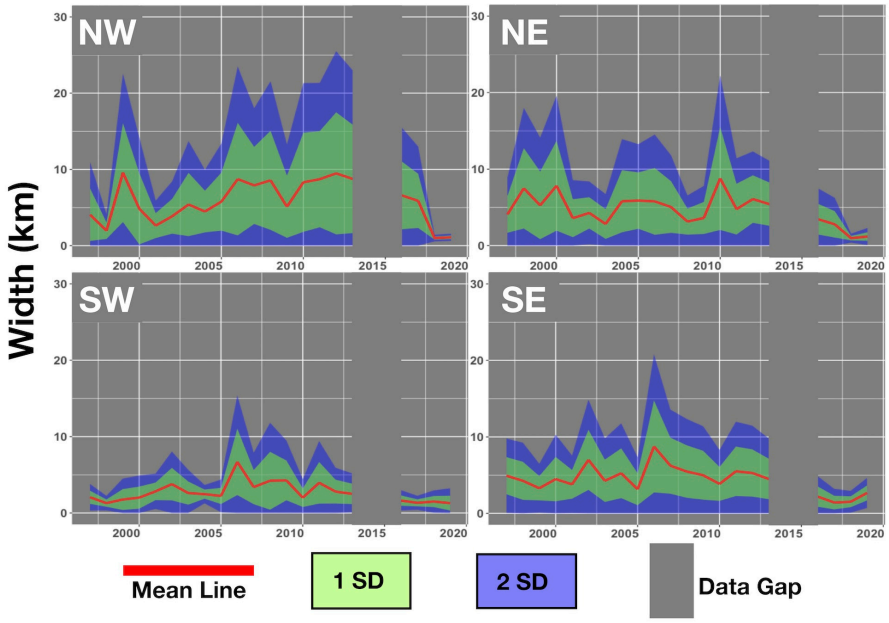

Figure 9

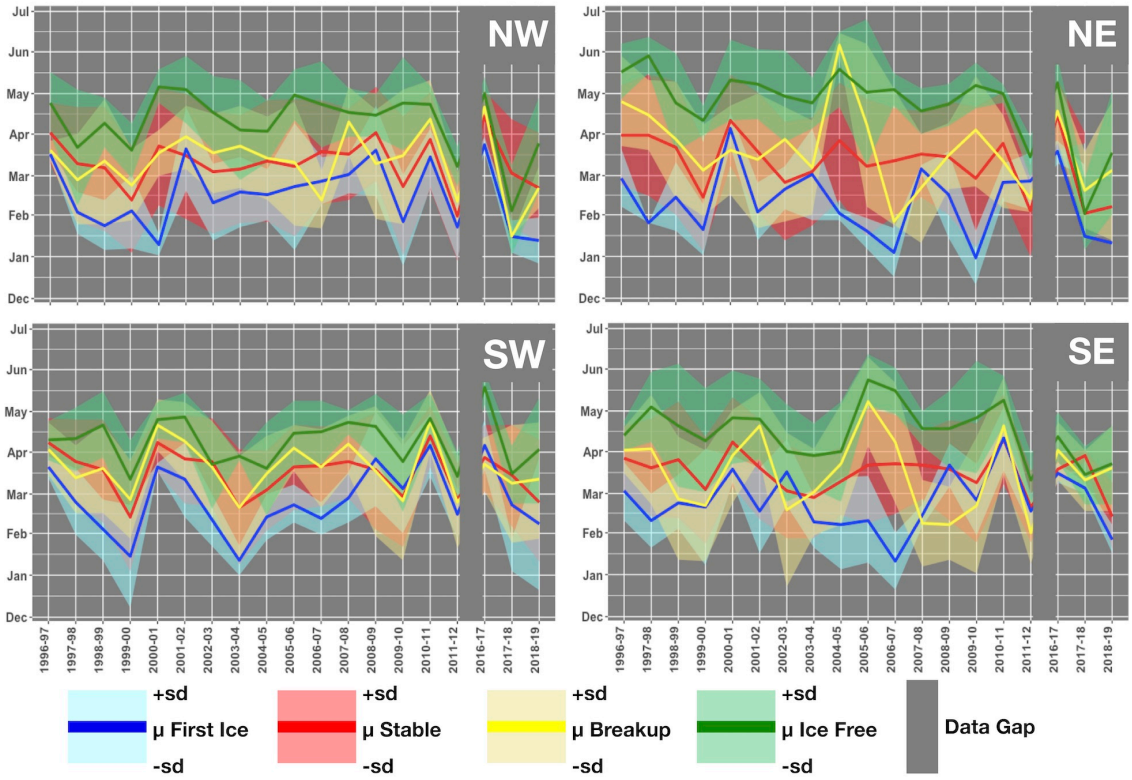

Figure 10

Figure Captions

Figure 1: St. Lawrence Island in the northern Bering Sea. Each region is a distinctly concave section of coastline, where landfast ice independently forms. The study regions are assigned designated colors (e.g. Northwest Region is Blue). For clarity, these color designations are used throughout the figures in this study. Yellow diamonds represent areas we designated as sheltered regions, and are typically characterized by….

Figure 2: Method for identifying landfast ice using SAR imagery. The top three images represent the input SAR imagery, obtained within a ~20 day window. Vertical and horizontal gradient fields are calculated for each image and subtracted, resulting in a "Net Gradient Difference" image visible on the bottom left. Darker homogenous regions of low net gradient difference in the image represent areas of landfast ice. Landfast ice are accentuated by applying a threshold to net gradient difference values, as exemplified by the image on the bottom right.

Figure 3: Coastal vectors for measuring SLIE width. Vectors are separated by 200 meter intervals and connect between the island's coastline and a coast-parallel polyline. Vectors

extend from the island's coastline to the coast-parallel polyline, and vice versa to account for concave sections of coast where coastal vectors are greater than 200 meters apart at the point of origin.

Figure 4: An example of fetch distances on a single grid point. The fetch distances radiate outward in red. Note the North to East fetch distances extend to the maximum distance, while the Southeast to Northwest fetch distances extend until reaching another section of coastline, and are thus below the maximum distance.

Figure 5: All created SLIEs on St. Lawrence Island from 1996 – 2019.

Figure 6: Line-density plot depicting the likelihood of an SLIE to occur within 500m of a given point. Red regions represent high-density SLIE areas. SLIE density has been used as a proxy for identifying the location of grounding features such as grounded pressure ridges (Mahoney et al. 2014), as well as islands. An example of the latter is evident in the southeast region, where SLIEs cluster around the Punuk Islands to form a "hook" shape.

Figure 7: Histograms representing water depth at the SLIE by region. Regional differences in landfast ice width and near-shore bathymetry result in unique distributions of water depth values.

Figures 8a-d: The relationship between width and water depth at the SLIE by region throughout the annual cycle. Note that greater water depths can constrain widths, whereas shallower water depths can enable greater widths. For example, in the Northeast region, water depths exceeding 40m generally do not surpass 15km in width; in the Northwest region, widths surpassing 20km generally do not exceed 20m in water depth at the SLIE.

Figure 9: Interannual change of landfast ice width by region from 1996 – 2019. Note that despite the distinct variation around the mean, all four regions experience the greatest interannual declines from 2016 – 2019. The clustering of standard deviations accompanies this trend. Statistical parameters of this trend is available in Table 2.

Figure 10: Mean occurrence dates for annual cycle events in all four study regions from 1996 – 2019. Mean occurrence dates are depicted by solid color lines, with transparent regions representing one standard deviation above and below the mean. Note the clustering of standard deviation regions in all four plots from 2016 – 2019.

Appendix C. Modeling Landfast Ice Cover on St. Lawrence Island, AK, USA

Modeling the Location of Landfast Ice Cover on St. Lawrence Island, AK, USA

David Jensen[1], Lynn M. Resler[1], Yang Shao[1]

1. Department of Geography; College of Natural Resources and Environment; Virginia Polytechnic Institute and State University; Blacksburg, Virginia

Corresponding Author:
David Jensen
Department of Geography
Virginia Tech
220 Stranger Street
Blacksburg, VA 24061, USA
(ajdavid6@vt.edu; 301-523-8812)

Highlights:

- Introduces a modeling approach that expedites the estimation of landfast ice cover location using freely accessible data.
- Model performance is better on St. Lawrence Island's northern coastlines compared to southern coastlines.
- Sea surface temperature, water depth, and coastline concavity most important in predicting areas of landfast ice cover.

Keywords:
Landfast; sea ice; Bering Sea

Abstract

The spatial distribution of landfast ice — sea ice locked into a stationary position against a coastline — is an important component for many human and biogeophysical processes on Arctic and Subarctic coastlines. Landfast ice regimes are generally governed by underlying geographic and climatic factors that promote its formation and growth. As these underlying factors continue to shift with climate change, understanding their influence on the location of landfast ice cover is an increasingly important endeavor. The purpose of this study is to understand how climate and the physical environment affects landfast ice cover location using a logistic regression modeling approach. We selected four regions on St. Lawrence Island, AK in the northern Bering Sea as our study location due to the existence of continuous (1996 – 2019) landfast ice spatial data, as well as readily available geographic and meteorological data. Our models were able to predict the location of landfast ice cover with 70% - 93.1% accuracy. Sea surface temperature, nearshore bathymetry, and the concavity of coastlines were the most important variables for model accuracy. High omission errors in the models suggest the future inclusion of additional geographic/meteorological variables is necessary to improve model performance and provide a reliable tool for expediting the estimation of landfast ice cover location.

1. Introduction

The spatial distribution of landfast ice — sea ice locked into a stationary position against a coastline — is important for human activities and biogeophysical processes in Arctic and Subarctic environments. Landfast ice provides a platform for human mobility and subsistence activities (Ray et al. 2016; Robards et al. 2013), and habitat and hunting grounds for marine mammals (Kawerak 2013; Oceana and Kawerak 2014). Landfast ice also influences nutrient dispersal from freshwater inputs into ocean environments (Eicken et al. 2005; Nalimov 1995; Reimnitz 2000), and protects coastal infrastructure and coastlines from erosive energy (e.g. wind/wave action) and storm surges (Lantuit and Pollard 2008; Vermaire et al. 2013). The provision of these benefits to ecosystems and human communities are enabled by underlying geographic and climatic factors that promote the formation and growth landfast ice. As these underlying factors continue to shift with climate change, understanding their influence on the location of landfast ice cover is an increasingly important endeavor.

Broadly characterizing the spatial distribution of landfast ice cover is complicated by its unique relationships with geographic (e.g. coastal morphology, nearshore bathymetry) and meteorological (e.g. temperature, sea ice concentration) conditions that vary by region. Efforts to characterize landfast ice spatial distribution in a given region generally rely on remote sensing methods, where algorithms designed to locate regions of landfast ice are applied to satellite imagery. Remote sensing methodologies have been used to generate continuous landfast ice spatial datasets, and infer relationships between landfast ice spatial distribution and geographic/meteorological conditions (Dammann et al. 2019; Fraser 2012, 2019; Giles 2008; Mahoney et al. 2007a, 2014; Meyer et al. 2011). Results from these studies show the spatial distribution of landfast ice cover to be governed by geographic conditions of the coastline as well as meteorological conditions relevant to ice formation and duration. However, the process to acquire landfast ice data using remote sensing methods in order to make such inferences is generally labor-intensive and difficult to automate. As a result, landfast ice datasets are generally confined to a particular region of study (Barry et al. 1979; Divine et al. 2004; Mahoney et

al. 2007a, 2014), and can result in the absence of landfast ice data for a region of interest. Modeling the influence of geographic and meteorological conditions on landfast ice spatial distribution using easily-accessible metrics could expedite the estimation of landfast ice location for future research in a given area.

The purpose of this study is to understand how climate and the physical environment affects landfast ice cover location. We use logistic regression modeling approaches to estimate landfast ice location using readily available data. Specifically, our study objective is to determine geographic and meteorological correlates of landfast ice cover distribution on St. Lawrence Island, AK, USA. We select St. Lawrence Island in the northern Bering Sea as our study area due to the existence of continuous (1996 – 2019) landfast ice spatial data (Jensen, in progress). We use this dataset along with geographic and meteorological variables to train and test a logistic GLM model. The influence of regional geographic and meteorological variables on seasonal sea ice cover in the Bering Sea is generally well understood (Brown et al. 2011; Douglas 2010; Frey et al. 2015; Stabeno et al. 2007). However, due to limited fine-resolution landfast ice spatial datasets in this region, quantifying the influence of meteorological and geographic variables on Bering Sea landfast ice cover, in particular, is understudied.

2. Background

2.1. Conditions Enabling Landfast Ice Cover

Landfast ice refers to sea ice that is locked into a stationary position against a coastline (WMO 1970), and generally occurs in Arctic and Subarctic coastal areas. The difference between landfast and drifting sea ice is important because stationary sea ice conditions in coastal zones uniquely influence human activities and biogeophysical processes. Landfast ice can provide habitat and hunting grounds for marine mammals such as certain pinniped species and polar bears (Kawerak 2013; Oceana and Kawerak 2014), acts as a substrate for human mobility and subsistence practices (Ray et al. 2016; Robards et al. 2013), and protects coastlines and infrastructure from erosive winds/wave action as well as storm surges (Lantuit and Pollard 2008; Vermaire et al. 2013). Changes

in landfast ice conditions (i.e. seasonal duration, spatial distribution of areal coverage) potentially alter these processes as a consequence of shifts of broader environmental conditions.

The spatial distribution of landfast ice cover is generally influenced by a combination of geographic and meteorological conditions that vary spatially and temporally. Geographic conditions refer to unchanging (over decadal time scales) features proximate to land, such as coastal morphology and nearshore bathymetry. Meteorological conditions refer to average weather events that coincide with, and influence the presence of, landfast ice cover on a given day. Landfast ice forms through a combination of in-situ freezing of open-water in sheltered areas, such as bays and lagoons, and the accretion of incoming pack ice against the seaward edge of landfast ice, a process analogous to those discussed by Mahoney et al. (2007a) in the Chukchi and Beaufort Seas. While the continued growth of landfast ice is facilitated by the continued accretion of pack ice and sustained freezing temperatures, its growth is generally constrained by the distribution of nearshore bathymetry. Shallower water depths enable the formation of grounded pressure ridges (i.e. vertical piles of ice that connect with the seabed) that contribute to stabilizing landfast ice against shearing forces (e.g. wind/wave action, collisions with drift ice) (Mahoney et al. 2007b). Therefore, coastlines with a steeper seafloor slope can be expected to experience lesser quantities of landfast ice cover with shorter widths than areas with shallower seafloor conditions. Average water depths at the landfast ice edge are generally used as a proxy for stable landfast ice conditions — conditions where the ice is anchored to the seabed by grounded pressure ridges (Mahoney et al. 2007a, 2014), although the average water depth serving as a proxy for stable conditions vary by region (Divine et al. 2004; Granskog et al. 2003, 2006; Zubov 1945). Finally, average temperature and pack ice conditions enabling landfast ice cover vary by study region as well. Geographic location is thus important in considering site-specific relationships between landfast ice cover and geographic and meteorological conditions. based.

2.2 Study Area

The study area, St. Lawrence Island, AK is situated in the northern Bering Sea (*Figure 1*). The northern Bering Sea is characterized by alternating seasonal periods of sea ice cover in the winter and a highly productive benthic/pelagic ecosystem in the summer (Grebmeier et al. 2006; Oceana and Kawerak 2014). Sea ice conditions occur in this region with the onset of freezing temperatures resulting from seasonally diminished solar intensity and the wind-driven introduction of drift ice through the Bering Strait (Robards et al. 2013; Stabeno et al. 2007). Changing conditions in Bering Sea temperatures (Grebmeier et al. 2006) and atmospheric circulation patterns (Perovich et al. 2018) have influenced changes in the areal extent and seasonal duration of sea ice cover, as well as changes in biological communities that characterize the Bering Sea ecosystem (Oceana and Kawerak 2014).

For the purpose of assessing geographic differences in the relationship between landfast ice distribution and geographic and meteorological variables, we divided the St. Lawrence Island into four regions (Northwest, Northeast, Southwest, and Southeast regions, *Figure 1*). Each region represents a unique concave section of coastline where landfast ice formation and growth are independent from other regions. Capes, defined as a headland extending into a body of water, or convex coastlines physically separate the study regions. From winter to late spring / early summer, St. Lawrence Island is generally encircled by a combination of landfast ice and high concentrations of mobile, drifting ice (known as pack ice). Pack ice is introduced and circulated into the northern Bering Sea by a persistent Northeasterly wind throughout the winter and spring months (Coachman & Aagaard 1988; Macklin 1983; Salo et al. 1983). As a result, the distribution of ice in the island's coastal zones varies by location. During winter, the northern coast (Northwest and Northeast regions) is typically bordered by several kilometers of landfast ice that transitions directly to drifting pack ice, and frequently attaches and separates from the coast in large sheets (Oceana and Kawerak 2014). Landfast ice on the southern coast (Southwest and Southeast regions) is typically much narrower by contrast, and bordered by polynyas — persistent areas of open water in sea ice conditions — and low-concentration drift ice (Kapsch et al. 2010; Kawerak 2013).

The surface air temperature generally ranges between -20° and 8° Celsius at Savoogna, one of the island's two coastal communities situated on the northern coastlines, though these temperatures have been steadily increasing (Grebmeier et al. 2006). The presence of coastal ice is important for the subsistence livelihoods of the St. Lawrence Island's two Yupik communities: Gambell and Savoonga (Oceana and Kawerak 2014), as well as the habitat and behavior of wildlife (Benson and Trites 2002; Noongwook et al. 2007). Savoonga residents have linked coastal ice conditions on the island to accelerated coastal erosion conditions on the island (USACE 2007).

3. Methods

3.1 Data creation

This study combines existing datasets to determine spatially coinciding landfast ice and geographic/meteorological conditions. The landfast ice data used in this study was previously created byJensen et al. (in progress) using a two-criteria definition advanced by Mahoney et al. (2006) to identify landfast ice in satellite imagery: 1) the sea ice is contiguous with the coastline, and 2) the sea ice exhibits no detectible motion for approximately 20 days. Based on a method advanced by Mahoney et al. (2004), we identified regions of landfast ice cover on St. Lawrence Island using three Synthetic Aperture Radar (SAR) images taken within a ~20 day period to generate maps distinguishing landfast ice from moving drift ice. Landfast ice regions are digitized into polygons in ArcMap 10.6 (ESRI 2011). This process was repeated every ~20 days from 1996 – 2019 using imagery obtained by a combination of C-band SAR sensors: Radarsat-1 (1996 – 2008), ENVISAT ASAR (2008 – 2012), and Sentinel-1 (2015 – 2019).

Modeling how the location of landfast ice cover is influenced by independent variables required the creation of a spatial dataset where the overlapping areas of landfast ice cover and geographic/meteorological conditions can be stored. We created a grid of points at 1-kilometer intervals around St. Lawrence Island to record the location of landfast ice cover and relevant variables using ArcMap 10.6 (*Figure 1*). Using ArcMap's *Create Fishnet* tool, we generated a grid of rectangular cells, then used the *Find*

Centroids tool to produce a grid of point features representing the center of each cell. We applied a 40 kilometer buffer around a shapefile of the island obtained from the Alaska State Geospatial Clearinghouse, and clipped the point grid within this boundary for analysis. Our decision to clip within a 40-kilometer buffer was informed by the distribution of landfast ice cover in our study area. A 40 kilometer buffer allows us to track landfast ice cover ranging from heavy coverage to consistently non-landfast ice conditions. Divided among our four study regions, there are 4,459 grid points in the Northwest Region, 4,469 grid points in the Northeast Region, 9,052 grid points in the Southwest Region, and 5,215 grid points in the Southeast Region. Differences in point distributions is proportional to the size of the study region area.

We extracted the location and time of occurrence of relevant variables for each data point and exported the point grid to a table. Each table row represents a point on the grid containing information on landfast ice coverage (1 = landfast ice cover; 0 = landfast ice absence), and relevant geographic and meteorological conditions. We repeated this process for each landfast ice spatial dataset. There are 127 landfast ice spatial datasets covering the years 1996 – 2019 and a total of 2,945,765 data points, indicating the presence/absence of landfast ice (N = 566,293 in the Northwest region, N= 567563 points in the Northeast region, N= 1,149,604 points in the Southwest region, N= 662,305 in the Southeast region). These datasets were aggregated into a single table for regression analysis. We gave special consideration to minimize risk of temporal and spatial autocorrelation. To address temporal autocorrelation, we selected a single landfast ice dataset from the month of March for each annual cycle to ensure no two datasets were temporally autocorrelated. The month of March was selected because large landfast ice sheets are a common occurrence during this month. To address spatial autocorrelation, we randomly sampled grid points. Because ice-free grid points (0) greatly outnumbered landfast ice grid points (1), we conducted a stratified random spatial sample of 25% of points from each group.

3.2 Logistic Regression Analysis

We used a logistic regression approach to determine the probability of landfast ice presence at each grid point as a function of geographic and meteorological parameters.

Parameters for this study were selected based on their hypothesized influence on landfast ice cover, and generally fall under two broad categories: geographic and meteorological . Geographic variables are measurements of geographic features that are generally unchanging throughout our 1996 – 2019 study period. Meteorological variables are measurements of natural features and weather events that change on a continual basis throughout our 1996 – 2019 study period. Variable parameters and collection are summarized in *Table 1.* Geographic variables include: Water Depth, Concave Sinuosity, Fetch Distances (*Figure* 2), and Hydrological Input Proximity. Meteorological variables include: Landfast Ice Cover (dependent variable), sea surface temperature, and Sea Ice Concentration (SIC). Parameter descriptions and sources for Water Depth, Sinuosity, and Fetch Distances have been described in Chapter 3 of this dissertation. Hydrological Input Proximity refers to the distance from a given grid point to the nearest freshwater input on St. Lawrence Island's coastline. Freshwater input locations were calculated using a flow accumulation analysis performed on Alaska 2 Arc-second DEM from the USGS National Map 3DEP. Sea ice concentration refers to the amount of sea ice areal coverage per defined space for the ~20 day period of landfast ice coverage. This information was extracted from 25 kilometer rasters provided by the National Snow and Ice Data Center. Sea surface temperature refers to the average temperature per defined space for the ~20 day period of landfast ice coverage. This information was extracted from 0.25-degree rasters provided by the National Centers for Environmental Prediction.

We created one model for each of four study regions: Northwest, Northeast, Southwest, and Southeast (*Tables 2.1 - 2.4*). We performed all modeling in R 3.5.3 (R Core Team 2019) using built-in functions. Parameter inclusion varied by model due to differing outcomes in multicollinearity (exclusion of correlations > 0.8) and statistical significance ($p < .05$) tests. All models retained sea surface temperature metrics, sinuosity, water depth, and some fetch distance parameters. Statistically insignificant fetch distance parameters were removed. Hydrological input proximity parameters were included in the Southwest and Southeast models, but not in the Northwest and Northeast models because they were not statistically significant. To account for multicollinearity, we removed predictors with correlations greater than 0.8. As a result, all models had some SIC parameters removed for having a high correlation with sea surface temperature.

The relationship between the probability (p) of binary outcomes in our dependent variable (landfast ice cover / no landfast ice cover) and predictor independent variables (xi) is expressed as:

$$\hat{p} = e^{(b_0 + b_{1x1} + b_{2x2} + \ldots, b_{nxn})} / (1 + e^{(b_0 + b_{1x1} + b_{2x2} + \ldots, b_{nxn})}$$

Where b0 is the intercept, bi (i = 1, 2, …, n) are regression coefficients, and xi (i = 1, 2, …, n) are the independent variables. To build and validate our models, we divided the landfast ice presence and absence grid points into training (70%) and testing (30%) data. Variable inclusion in the final model was based on statistical significance in regression output summaries and increased values in McFadden R^2 values. We evaluated model performance based on McFadden's pseudo R^2, classification accuracy, and commission as well as omission errors.

4. Results

4.1 Model Parameters

In all four models (*Tables 2.1-2.4*) sea surface temperature metrics, water depth, and concave sinuosity were the most important for explaining landfast ice cover. Fitting the models with these metrics alone resulted in McFadden's Pseudo R^2 values

ranging from (0.45-0.64). Water depth coefficients were all negative; sea surface temperature coefficients varied from positive to negative depending on the metric (e.g. maximum, standard deviation) used. The addition of Concave Sinuosity to the model only increased the McFadden's Pseudo R range by 0.01. Concave Sinuosity coefficients were generally high, and were positive in the Northwest, Northeast, and Southeast models, and negative in the Southwest model. Hydrological input distances resulted in modest increases to McFadden's Pseudo R^2 range. All hydrological input distance coefficients were negative, with the exception of the Southwest model. SIC parameters that were not removed from the final models only increased the McFadden's Pseudo R^2 range by 0.01.

SIC coefficients exhibited positive and negative values that varied by model. Fetch parameters that were not removed from the final models only modestly increased the McFadden's Pseudo R^2. Fetch direction coefficients were generally negative in all four models. All parameters result in a McFadden's Pseudo R^2 range of 0.68 -0.81, indicating a good overall fit. With all parameters included, McFadden's Pseudo R^2 values were highest for the Northeast model (0.81), followed by the Northwest (0.8), Southeast (0.78) and Southwest (0.68) (*Tables 2.1 – 2.4*).

4.2 Model Performance

Classification accuracy of landfast ice cover on St. Lawrence Island ranged from 70.1% (Southwest) −93.1% (Northeast) (Table 3). Commission errors (i.e., errors that reflect an overestimation of landfast ice presence) were generally low with the exception of the Southwest model resulting in an error value of 0.3. Omission errors (i.e., errors that reflect an underestimation of landfast ice presence were generally high, ranging from 0.53 -0.86 in the Southeast, Northwest, and Northeast models. The Southwest model had a comparatively lower omission error of 0.25. We applied a Point Density tool in ArcMap to compare the spatial distribution of our landfast ice predicted outcomes (*Figure 3*), commission error (*Figure 4*), and omission error (*Figure 5*). Each region had some grid points removed due to NoData values, resulting from the coarse spatial resolution of sea surface temperature or SIC rasters. NoData regions appear as gaps in predicted regions of landfast ice cover and commission/omission error. The Southwest region had the largest number of grid points removed due to NoData values, with the majority of grid points confined to the eastern portion near the Southeast cape (*Figures 3-5*).

For St. Lawrence Island's northern coastlines, the northwest and northeast models produced large regions of high landfast ice probability (*Figure 3*). The Northwest model portrayed the highest probabilities of landfast ice in the concave section between the northwest cape and northern central region of the island, with the probability of landfast ice increasing as proximity to the coastline decreases. Regions of high omission error were proximate to the coastline, with the highest density occurring in the southernmost

concave section. There were no comparably high densities of commission error in this region. The Northeast model portrayed the highest probabilities of landfast ice in the concave section between the northern central region to the easternmost sheltered embayment. There is a high probability of landfast ice where the northeastern corner of the region transitions into the Southeast region, though these regions are somewhat reduced when setting higher probability thresholds (i.e. the threshold value by which probabilities are sorted into landfast ice cover (1), or absence (0). A threshold of 0.7 assigns higher probability values a 1, and lower probability values a 0). High densities of omission error coincide with high densities of landfast ice probability, and these density regions are also reduced by increases in probability thresholds. High densities of commission error occur north of the easternmost sheltered embayment.

Models for the southern coastlines on St. Lawrence Island produced smaller regions of probable landfast ice cover compared to northern coastlines. The Southeast model was able to reproduce the grounding of landfast ice on the Punuk Islands to the south, where the highest probabilities of landfast ice presence form a "hook" shape off the northeastern portion of the island. Regions with a high probability of landfast ice presence are consistently centered around the Punuk Islands (*Figure 3*). No high densities of omission error occur in this region, though omission errors occurred more frequently around the Punuk Islands. The highest concentrations of commission errors occur around the Punuk Islands as well, and reduce with increased probability thresholds. The Southwest model had significant gaps in landfast ice probability regions due to large areas of NoData values in sea surface temperature, SIC, and water depth values. No comparable areas of high landfast ice probability occurred in the Southwest model. Predicted areas of landfast ice cover were generally located in the southern portion of the Southwest region when the probability threshold is set from 0.5 to 0.7. There are no predicted areas of landfast ice when the threshold is set beyond 0.8 (*Figure 3*). Low-density regions of omission error occur in the same areas as predicted landfast ice cover when set at the same probability thresholds (*Figure 5*).

5. Discussion

This results of this study contribute an understanding of geographic and meteorological parameters associated with landfast ice location through the use of explanatory and predictive modeling approaches. This study advances a modeling method that will expedite the estimation of landfast ice location using freely accessible data in future studies. This method has future potential in discerning relationships between the location of landfast ice cover and unique geographic/meteorological conditions of a given region. We found that sea surface temperature, water depth, and coastal sinuosity were the three most important parameters for modeling landfast ice cover on St. Lawrence Island. These findings align with previous research that has associated landfast ice cover to freezing air temperatures combined with shallow nearshore bathymetry that enables the formation of stabilizing grounded pressure ridges (Mahoney et al. 2007a, Selyuzhenok et al. 2017). Mahoney et al. (2014) also found that concave sheltered areas such as embayments and lagoons enable landfast ice formation and growth in the Beaufort and Chukchi Seas. Nearshore conditions in sea surface temperature and water depth values at the landfast ice edge have been used successfully to explain some variability in landfast ice cover in the Beaufort and Chukchi Seas (Mahoney et al. 2007). In such cases landfast ice formation and break up were found to coincide with the onset of freezing and thawing temperatures. The incursion of pack ice into coastal zones was also found to coincide with the onset of landfast ice cover (Mahoney et al. 2014). The introduction of pack ice contributes to reductions in sea surface temperature (Robards et al. 2013; Stabeno et al. 2007), and may account for the multicollinearity between SIC and Sea surface temperature parameters.

Fetch distances generally had a negative influence on he probability of landfast ice cover (*Tables 2.1-2.4*). Open water increases the exposure of landfast ice to shearing forces, in contrast to embayments and lagoons that provide shelter (Mahoney et al. 2007a). In our models, maximum fetch distance values of 40 kilometers indicate exposure to open water. Fetch distance values less than 40 kilometers indicate proximity to the coast. Negative fetch distance coefficients suggest coastal proximity increases the probability of landfast ice cover. Coastlines can be oriented to protect landfast ice from offshore or alongshore forcing of wind and wave energy, or facilitate the accumulation of pack ice into coastal zones. For example, the sample grid point in *Figure 2* has maximum

fetch distance values ranging from northwest to east, but shorter fetch distance values ranging from southeast to west. As indicated in *Figure 3* the high-density values in the Northwest region coincide with areas where fetch directions oriented towards other coastlines are shorter. Thus, shorter fetch distances indicate proximity to sections of coast where wind-driven transport of pack ice accumulates to promote landfast ice growth, thereby increasing the probability of landfast ice cover.

Grid point proximity to coastal features was relevant to probability outcomes in landfast ice cover. For example, proximity to hydrological inputs such as rivers increased the probability of landfast ice cover in every model with the exception of Southwest. Generally, proximity to hydrological inputs has been shown to initiate melting conditions by flooding the landfast ice surface with warmer water that reduces surface albedo (Dean et al. 1994; Weingartner et al. 2017). However, many of St. Lawrence Island's hydrological inputs were in concave regions of coastline sheltered by barrier islands and land spits, which promote landfast ice growth (Mahoney et al. 2007a, 2014). The sheltering effect associated with these features may offset the negative influence of surface flooding on St. Lawrence Island. Further, the amount of freshwater discharge into St. Lawrence Island coastal zones is smaller in comparison to Bering Sea coastlines on mainland Alaska with large freshwater inputs from the Yukon-Kuskokwim Rivers.

The influence of concave sinuosity varied by model. Greater sinuosity values (i.e. greater concavity) was positively associated with landfast ice probability in the Northwest and Southeast models, and negatively in the Northeast and Southwest models. This finding may be explained by the differences in broader coastal geographies of the study regions, as well the 'shelteredness' of concave regions. For example, barrier islands and land spits generally sheltered concave sections of coast in the Northwest region from shearing forces, while multiple sections of concave coastline in the Northeast region were exposed to wind and wave energy from the open ocean. Concavity of a coastline may only positively influence landfast ice cover if there is some associated mechanism to provide shelter from shearing forces.

Our evaluation of model performance found similarities between high probability regions of landfast ice cover (*Figure 3*) and the stacked landfast ice polygons used as model inputs (*Figure 6*). With the exception of NoData gaps, high-density regions of

landfast ice probability spatially coincide with high-density regions of stacked landfast ice polygons, and are consistent with previous observations (Kawerak 2013; Oceana and Kawerak 2014) of landfast ice cover on St. Lawrence Island. Model outputs for the Northwest and Northeast regions reveal larger high-density regions of landfast ice probability than the Southwest and Southeast regions. The distribution of landfast ice probability regions is consistent with observations of St. Lawrence Island landfast ice cover. The northern coast of St. Lawrence Island is typically bordered by several kilometers of landfast ice that frequently attaches and separates from the coast (Oceana and Kawerak 2014). By contrast, landfast ice cover on the southern coast is much smaller and is typically bordered by polynyas — persistent areas of open water in sea ice conditions — and low concentration drift ice (Kapsch et al. 2010; Kawerak 2013).

High density regions of commission (*Figure 4*) and omission errors (*Figure 5*) spatially coincided with high density regions of landfast ice probability. It is important to note that high occurrences of commission and omission errors are not equal. The highest occurrence of commission error for a given grid point was 4; the highest occurrence of omission error was 20. The lack of commission and omission error in Southwest and Southeast sheltered regions was not indicative of model inaccuracy, but instead are due to the persistence of NoData regions in these areas. The regions of commission error with the highest densities occurred in the Northwest and Northeast regions. High densities of commission error in the Northeast region were proximate to two large sheltered regions with high sinuosity values. The sinuosity coefficient is positive in the Northeast model, and may contribute to an incorrect prediction of landfast ice cover. High densities of commission error in the Southeast region were proximate to the Punuk Islands. This area occupies relatively shallow water depths and is proximate to high-sinuosity concave regions to the west, which may have contributed to frequent incorrect predictions of landfast ice occurrence.. High density regions of omission errors spatially overlap with high density regions of landfast ice probability. Omission errors generally do not occur outside areas predicted by the model, but are centralized over regions where landfast ice is accurately predicted. The model failing to predict landfast ice cover in high density regions of probability suggests the influence of additional geographic or meteorological variables not being considered.

Additional steps can improve future model performance, such as the inclusion of additional parameters and use of alternative datasets. Wind speed and direction is a key parameter not included in our model that can facilitate and inhibit landfast ice formation and duration. Winds transport pack ice into coastal areas to promote landfast ice growth (Mahoney et al. 2007a). Further, the northern Bering Sea experiences frequent winter storms (Overland 1981). Strong winds from storms have been shown to limit the extent of landfast ice cover (Divine et al. 2004; Pavlov and Pfirman 1995). Wind speed and direction have also been important parameters in modeling stages of landfast ice development (Selyuzhenok et al. 2017). Future models accounting for wind direction and speed relative to St. Lawrence Island could improve model accuracy and reduce commission and omission error. Coarse spatial resolution of sea surface temperature and SIC rasters limited model performance by introducing NoData values. As a consequence, regions where raster cells did not adhere to the coast were excluded. The inclusion of finer resolution sea surface temperature and SIC rasters would result in fewer spatial gaps in model outputs.

Resolving multicollinearity issues between initial parameters would improve model performance, as well. SIC and sea surface temperature parameters were measured at the location of a given grid point and were highly correlated, resulting in the removal of several SIC parameters in all four models. Multicollinearity issues may be reduced by measuring the distance of a given grid point to broader SIC trends. For example, Mahoney et al. (2014) used the same SIC data to correlate the onset of landfast ice cover with the incursion of pack ice 200 kilometers from the coastline. The position or distance of a grid point relative to broader SIC trends could provide additional relevant parameters while avoiding multcollinearity problems with sea surface temperatures.

6. Conclusion

In this study we used spatially overlapping landfast ice data and geographic/meteorological measurements to develop an explanatory spatial logistic regression model on the location of St. Lawrence Island's landfast ice cover. Our models used measurements of four geographic conditions and two meteorological conditions as

input parameters to explain 64 – 75% of the variability of landfast ice cover location. Classification accuracy was generally high in the Northwest, Northeast, and Southeast models (89.54% – 90.39%), and lower in the Southwest model (83.33%). In all four models, commission error was generally low (0.08 – 0.17) and omission error generally high (0.77 – 0.83). The high omission error was likely due to a missing key geographic or meteorological parameter enabling the existence of landfast ice cover. Commission and omission errors would likely be reduced by wind speed and direction parameters, as the direction and intensity of wind has been shown to both enable (Mahoney et al. 2007a, Selyuzhenok et al. 2017) and limit (Divine et al 2004; Pavlolv and Pfirman 1995) landfast ice cover formation and duration. The coarse spatial resolution of meteorological data resulted in large NoData regions. Finer resolution meteorological data would better adhere to the contours of St. Lawrence Island's coastline to reduce gaps in model outputs.

Model outputs are consistent with observations on St. Lawrence Island, and broader observations of relationships between landfast ice and geographic/meteorological conditions. Regions of landfast ice probability are largest on the northern coastlines, which are known to be bordered by several kilometers of fast ice (Oceana and Kawerak 2014). Southern coastlines are characterized by polynyas and low concentrations of drift ice reducing landfast ice cover (Kapsch et al. 2010; Kawerak 2013). Consequentially, southern coastlines exhibit smaller regions of landfast ice probability. Water depth and sea surface temperature were the most influential model parameters, and have demonstrable importance in previous studies on landfast ice formation and seasonal duration (Eicken et al. 2006; Mahoney et al. 2007a, 2014).

Sea ice change is linked to changes in climatology and geographic environment. This study contributes to a growing body of research exploring the changing relationships between landfast ice cover and environmental conditions. We demonstrate the benefits and caveats of using freely accessible data to enable a more expedited and comprehensive approach in assessing landfast ice cover under the influence of geographic and environmental conditions.

7. References

Barry, R.G., Moritz, R.E., Rogers, J.C., 1979. The fast ice regimes of the Beaufort and Chukchi Sea coasts, Alaska. Cold Regions Science and Technology, 1 (2), 129–152.

Benson, A. J., & Trites, A. W. (2002). Ecological effects of regime shifts in the Bering Sea and eastern North Pacific Ocean. Fish and Fisheries, 3(2), 95-113.

Brown, Z. W., Van Dijken, G. L., & Arrigo, K. R. (2011). A reassessment of primary production and environmental change in the Bering Sea. Journal of Geophysical Research: Oceans, 116(C8).

Coachman, L. K., & Aagaard, K. (1988). Transports through Bering Strait: Annual and interannual variability. *Journal of Geophysical Research: Oceans*, *93*(C12), 15535-15539.

Dammann, D. O., Eriksson, L. E., Mahoney, A. R., Eicken, H., & Meyer, F. J. (2019). Mapping pan-Arctic landfast sea ice stability using Sentinel-1 interferometry. *The Cryosphere*, *13*(2), 557-577.

Dean, K. G., Stringer, W. J., Ahlnas, K., Searcy, C., & Weingartner, T. (1994). The influence of river discharge on the thawing of sea ice, Mackenzie River Delta: albedo and temperature analyses. *Polar Research*, *13*(1), 83-94.

Divine, D.V., Korsnes, R., Makshtas, A.P., 2004. Temporal and spatial variation of shore-fast ice in the Kara Sea. Continental Shelf Research, 24, 1717–1736.

Douglas, D.C., 2010. Arctic sea ice decline: projected changes in timing and extent of sea ice in the Bering and Chukchi Seas. U.S. Geological Survey Open-File Report 2010–176 (32 pp.)

Eicken, H., Dmitrenko, I., Tyshko, K., Darovskikh, A., Dierking, W., Blahak, U., ... & Kassens, H. (2005). Zonation of the Laptev Sea landfast ice cover and its importance in a frozen estuary. *Global and planetary change*, *48*(1-3), 55-83.

ESRI 2011. ArcGIS Desktop: Release 10. Redlands, CA: Environmental Systems Research Institute

Fetterer, F., K. Knowles, W. N. Meier, M. Savoie, and A. K. Windnagel. 2017, updated daily. *Sea Ice Index, Version 3*. [Indicate subset used]. Boulder, Colorado USA. NSIDC: National Snow and Ice Data Center. doi: https://doi.org/10.7265/N5K072F8.

Fraser, A. D., Massom, R. A., Michael, K. J., Galton-Fenzi, B. K., & Lieser, J. L. (2012). East Antarctic landfast sea ice distribution and variability, 2000–08. *Journal of Climate*, *25*(4), 1137-1156.

Fraser, A. D., Ohshima, K. I., Nihashi, S., Massom, R. A., Tamura, T., Nakata, K., ... & Willmes, S. (2019). Landfast ice controls on sea-ice production in the Cape Darnley Polynya: A case study. *Remote Sensing of Environment*, *233*, 111315.

Eicken, H., Shapiro, L. H., Gaylord, A. G., Mahoney, A., & Cotter, P. W. (2006). Mapping and characterization of recurring spring leads and landfast ice in the Beaufort and Chukchi seas. *US Department of Interior, Minerals Management Service (MMS), Alaska Outer Continental Shelf Region, Anchorage*.

Frey, K. E., Moore, G. W. K., Cooper, L. W., & Grebmeier, J. M. (2015). Divergent patterns of recent sea ice cover across the Bering, Chukchi, and Beaufort seas of the Pacific Arctic Region. Progress in Oceanography, 136, 32-49.

Giles, A. B., Massom, R. A., & Lytle, V. I. (2008). Fast-ice distribution in East Antarctica during 1997 and 1999 determined using RADARSAT data. *Journal of Geophysical Research: Oceans*, *113*(C2).

Granskog, M. A., Martma, T. A., & Vaikmäe, R. A. (2003). Development, structure and composition of land-fast sea ice in the northern Baltic Sea. *Journal of Glaciology*, *49*(164), 139-148.

Granskog, M., Kaartokallio, H., Kuosa, H., Thomas, D. N., & Vainio, J. (2006). Sea ice in the Baltic Sea–a review. Estuarine, Coastal and Shelf Science, 70(1-2), 145-160.

Hakkinen, S., Proshutinsky, A., & Ashik, I. (2008). Sea ice drift in the Arctic since the 1950s. *Geophysical Research Letters*, *35*(19).

Iijima, Y., Nakamura, T., Park, H., Tachibana, Y., & Fedorov, A. N. (2016). Enhancement of Arctic storm activity in relation to permafrost degradation in eastern Siberia. *International Journal of Climatology*, *36*(13), 4265-4275.

Kapsch, M. L., Eicken, H., & Robards, M. (2010). Sea ice distribution and ice use by indigenous walrus hunters on St. Lawrence Island, Alaska. In SIKU: Knowing Our Ice (pp. 115-144). Springer, Dordrecht.

Kawerak, Inc. 2013. Seal and walrus harvest and habitat areas for nine Bering Strait Region communities. Nome, AK: Kawerak, Inc., Social Science Program

Lantuit, H., & Pollard, W. H. (2008). Fifty years of coastal erosion and retrogressive thaw slump activity on Herschel Island, southern Beaufort Sea, Yukon Territory, Canada. Geomorphology, 95(1-2), 84-102.

Lesack, L. F., Marsh, P., Hicks, F. E., & Forbes, D. L. (2014). Local spring warming

drives earlier river‐ice breakup in a large Arctic delta. *Geophysical Research Letters*, *41*(5), 1560-1567.

Macklin, S. A. (1983). Wind drag coefficient over first-year sea ice in the Bering Sea. *Journal of Geophysical Research: Oceans*, *88*(C5), 2845-2852.

Mahoney, A.R., Eicken, H., Gaylord, A.G., Shapiro, L., 2007a Alaska landfast sea ice: links with bathymetry and atmospheric circulation. Journal of Geophysical Research Oceans 112 (C2). http://dx.doi.org/10.1029/2006jc003559 (C02001).

Mahoney, A.R., Eicken, H., Shapiro, L., 2007b. How fast is landfast sea ice? A study of the at- tachment and detachment of nearshore ice at Barrow, Alaska. Cold Regions Science and Technology, 47 (3)

Mahoney, A. R., Eicken, H., Gaylord, A. G., & Gens, R. (2014). Landfast sea ice extent in the Chukchi and Beaufort Seas: The annual cycle and decadal variability. *Cold Regions Science and Technology*, *103*, 41-56.

Meyer, F. J., Mahoney, A. R., Eicken, H., Denny, C. L., Druckenmiller, H. C., & Hendricks, S. (2011). Mapping arctic landfast ice extent using L-band synthetic aperture radar interferometry. *Remote Sensing of Environment*, *115*(12), 3029-3043.

Najafi, M. R., Zwiers, F. W., & Gillett, N. P. (2015). Attribution of Arctic temperature change to greenhouse-gas and aerosol influences. *Nature Climate Change*, *5*(3), 246-249.

Nalimov, Y. V. (1995). The ice-thermal regime at front deltas of rivers of the Laptev Sea. *Reports on Polar Research*, *176*, 55-61.

Noongwook, G., Huntington, H. P., & George, J. C. (2007). Traditional knowledge of the bowhead whale (Balaena mysticetus) around St. Lawrence Island, Alaska. Arctic, 60(1), 47-54.

Oceana and Kawerak. 2014. Bering Strait Marine Life and Subsistence Use Data Synthesis. Oceana and Kawerak, Juneau, AK.

Overland, J. E. (1981). Marine climatology of the Bering Sea. *The eastern Bering Sea shelf: Oceanography and resources*, *1*, 15-22.

Park, H., Yoshikawa, Y., Oshima, K., Kim, Y., Ngo-Duc, T., Kimball, J. S., & Yang, D. (2016). Quantification of warming climate-induced changes in terrestrial arctic river ice thickness and phenology. *Journal of Climate*, *29*(5), 1733-1754.

Perovich, W. Meier, M. Tschudi, S. Farrell, S. Hendricks, S. Gerland, C. Haas, T. Krumpen, C. Polashenski, R. Ricker, and M. Webster: Sea Ice Cover [in “State of the

Climate in 2018"] *Bull. Amer. Meteor. Soc.*, **100** (9), S146-150

R Core Team (2019). R: A language and environment for statistical computing. R Foundation for Statistical Computing, Vienna, Austria. URL https://www.R-project.org/

Ray, G. C., Hufford, G. L., Overland, J. E., Krupnik, I., McCormick-Ray, J., Frey, K., & Labunski, E. (2016). Decadal Bering Sea seascape change: consequences for Pacific walruses and indigenous hunters. Ecological Applications, 26(1), 24-41.

Robards, M. D., Kitaysky, A. S., & Burns, J. J. (2013). Physical and sociocultural factors affecting walrus subsistence at three villages in the northern Bering Sea: 1952–2004. Polar Geography, 36(1-2), 65-85.

Salo, S. A., Schumacher, J. D., & Coachman, L. K. (1983). Winter currents on the eastern Bering Sea shelf.

Selyuzhenok, V., Mahoney, A., Krumpen, T., Castellani, G., & Gerdes, R. (2017). Mechanisms of fast-ice development in the south-eastern Laptev Sea: a case study for winter of 2007/08 and 2009/10. *Polar Research*, *36*(1), 1411140.

Shiklomanov, A. I., & Lammers, R. B. (2014). River ice responses to a warming Arctic—recent evidence from Russian rivers. *Environmental Research Letters*, *9*(3), 035008.

Stabeno, P. J., Bond, N. A., & Salo, S. A. (2007). On the recent warming of the southeastern Bering Sea shelf. Deep Sea Research Part II: Topical Studies in Oceanography, 54(23-26), 2599-2618.

USACE 2007. Erosion Information Paper - Savoonga, Alaska. U.S. Army Corps of Engineers, Alaska District.

Vermaire, J. C., Pisaric, M. F., Thienpont, J. R., Courtney Mustaphi, C. J., Kokelj, S. V., & Smol, J. P. (2013). Arctic climate warming and sea ice declines lead to increased storm surge activity. *Geophysical Research Letters*, *40*(7), 1386-1390.

Weingartner, T. J., Danielson, S. L., Potter, R. A., Trefry, J. H., Mahoney, A., Savoie, M., ... & Sousa, L. (2017). Circulation and water properties in the landfast ice zone of the Alaskan Beaufort Sea. *Continental Shelf Research*, *148*, 185-198.

World Meteorological Organization, 1970. WMO Sea-ice Nomenclature, Terminology, Codes and Illustrated Glossary. Secretariat of the WMO, Geneva.

Zubov, N. N. (1945), Arctic Sea Ice (in Russian), 366 pp., Izd. Glavsevmorputi, Moscow. (English translation), 491 pp., U.S. Navy Oceanogr. Off., Springfield, Va., 1963

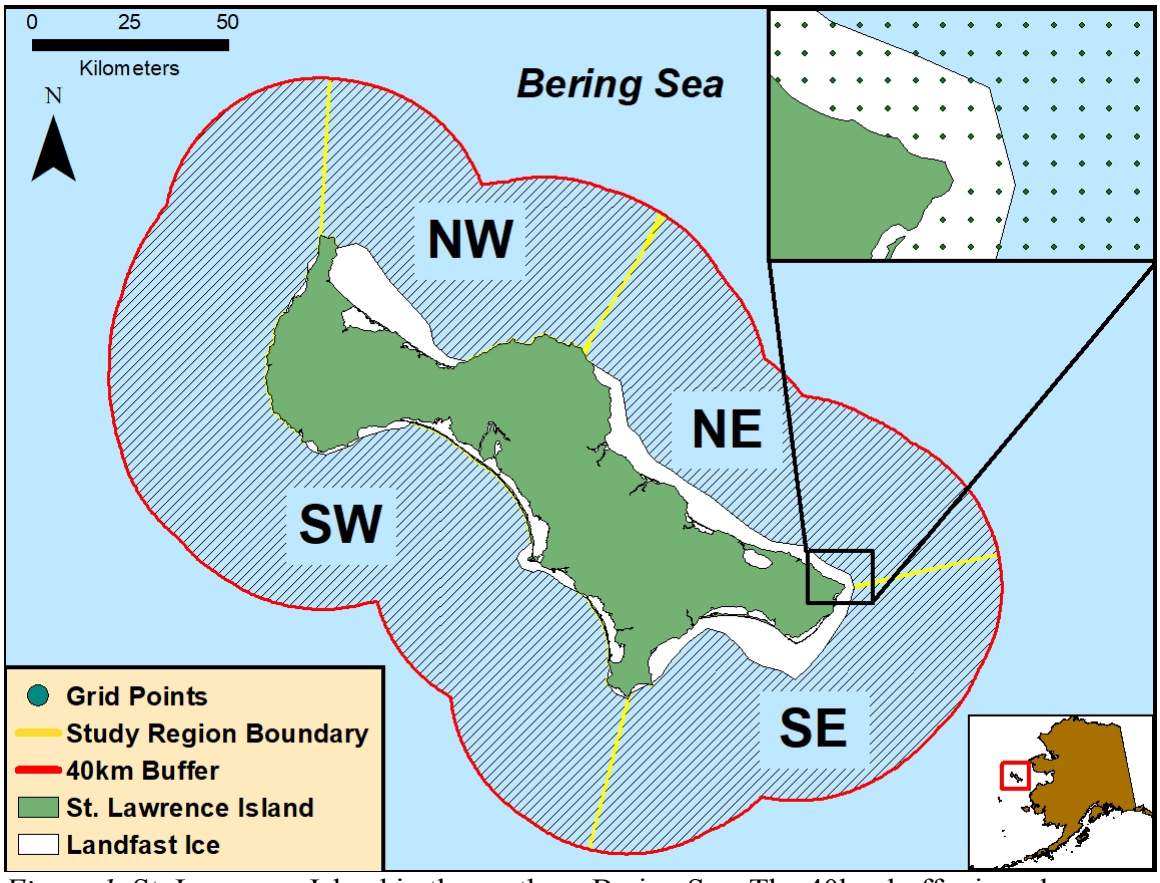

Figure 1: St. Lawrence Island in the northern Bering Sea. The 40km buffer in red contains grid points at 1-km intervals used to extract spatial data of landfast ice cover and physical/meteorological variables.

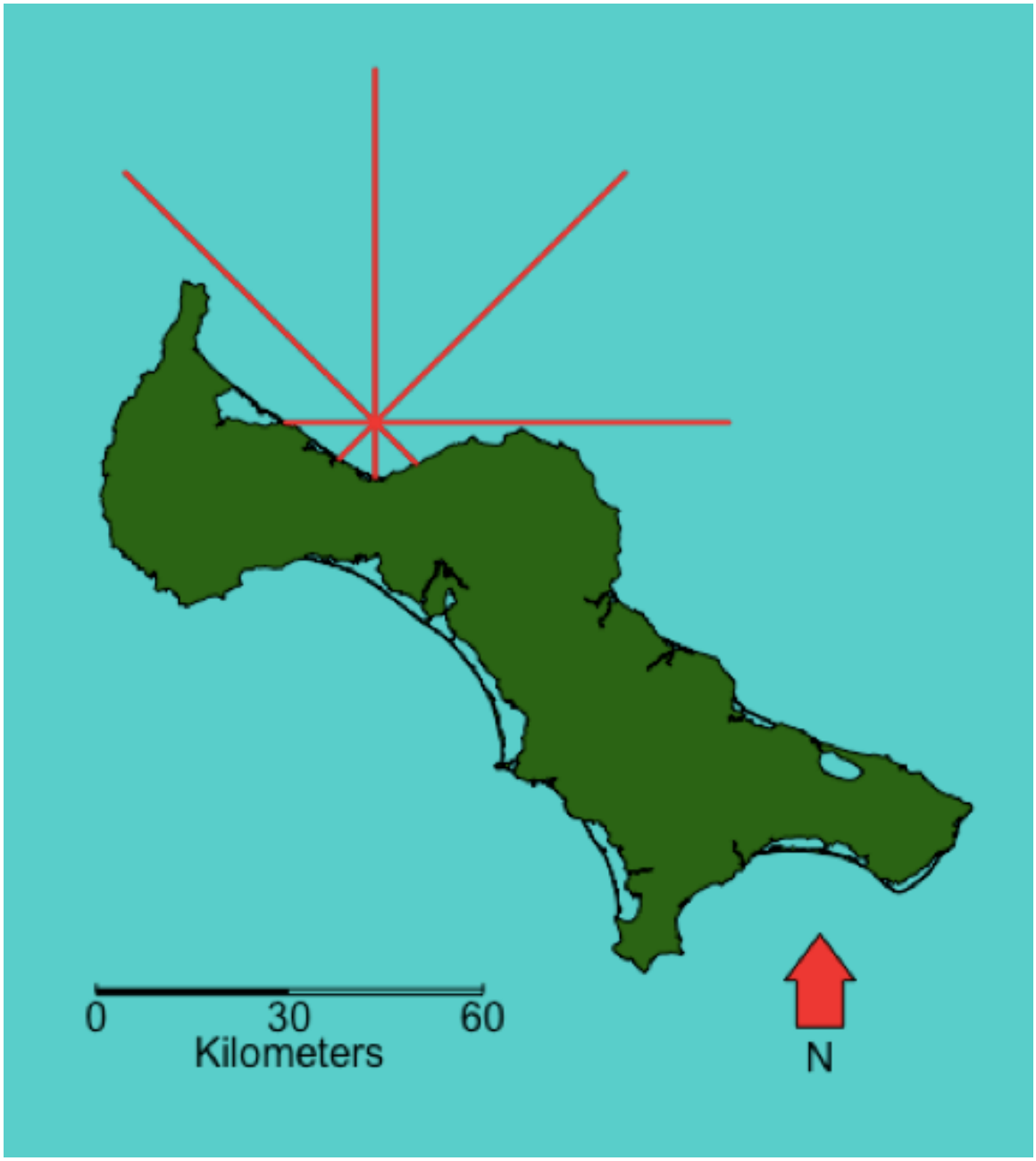

Figure 2: An example of fetch distances on a single grid point. The fetch distances radiate outward in red. Note the Northwest to East fetch distances extend to the maximum distance, while the Southeast to West fetch distances extend until reaching another section of coastline, and are thus below the maximum distance.

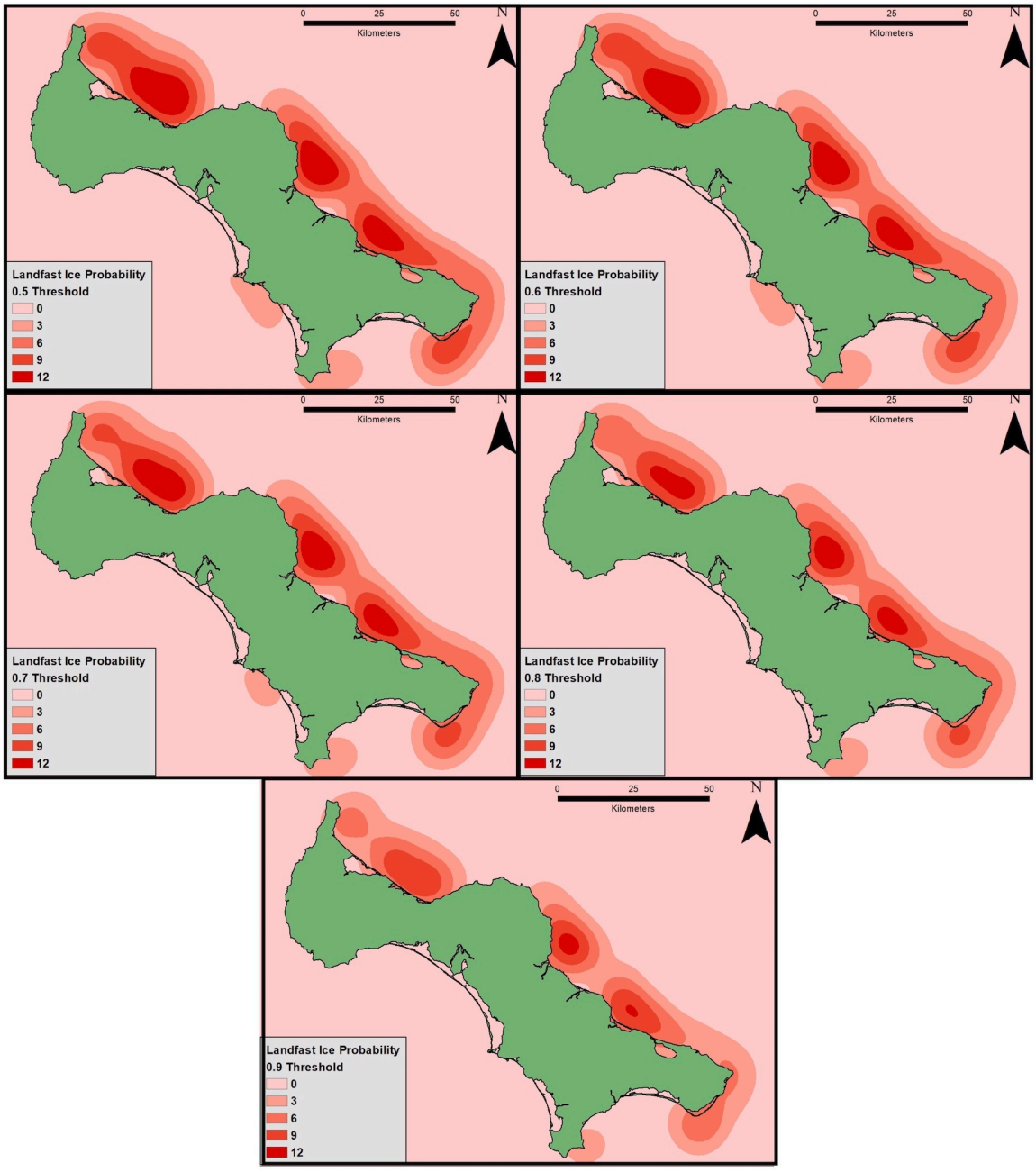

Figure 3: Regions of landfast ice probability depicted using a Point Density tool in ArcMap 10.6. Darker red regions signify grid points with a higher occurrence of predicted landfast ice cover. Note rectangular gaps between high density regions signify grid points removed due to NoData values.

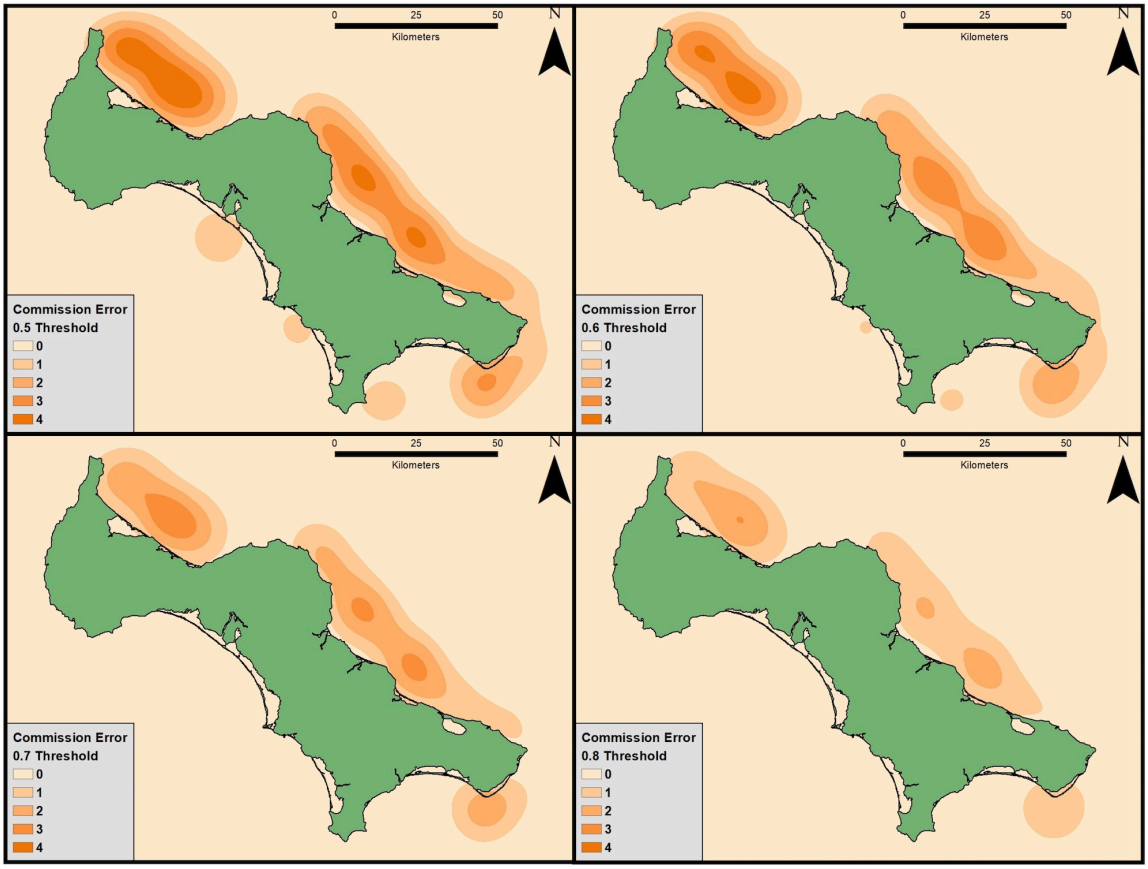

Figure 4: Regions of commission error depicted using a Point Density tool in ArcMap 10.6. Darker orange regions signify grid points with a higher occurrence of commission error (i.e. areas where landfast ice cover was overestimated). Note rectangular gaps between high density regions signify grid points removed due to NoData values.

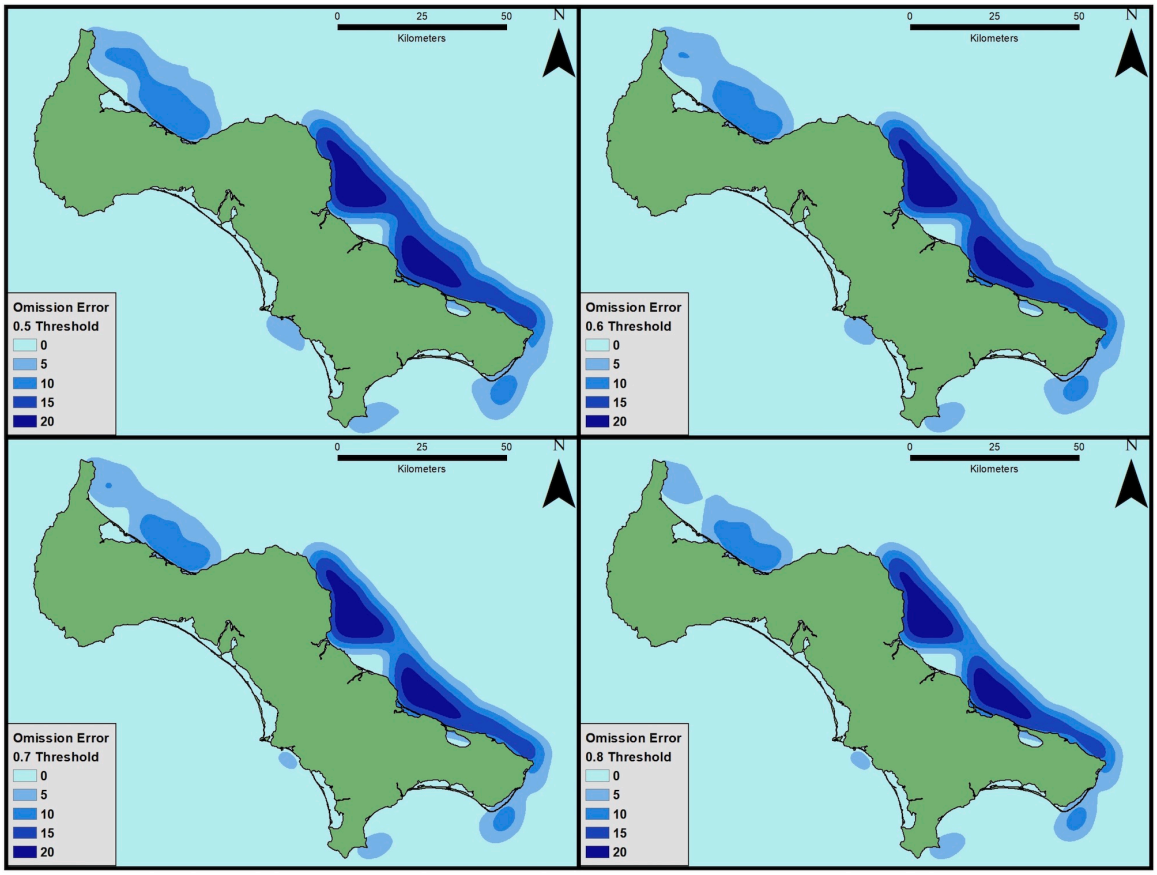

Figure 5: Regions of omission error depicted using a Point Density tool in ArcMap 10.6. Darker blue regions signify grid points with a higher occurrence of omission error (i.e. areas where landfast ice cover was underestimated). Note rectangular gaps between high density regions signify grid points removed due to NoData values.

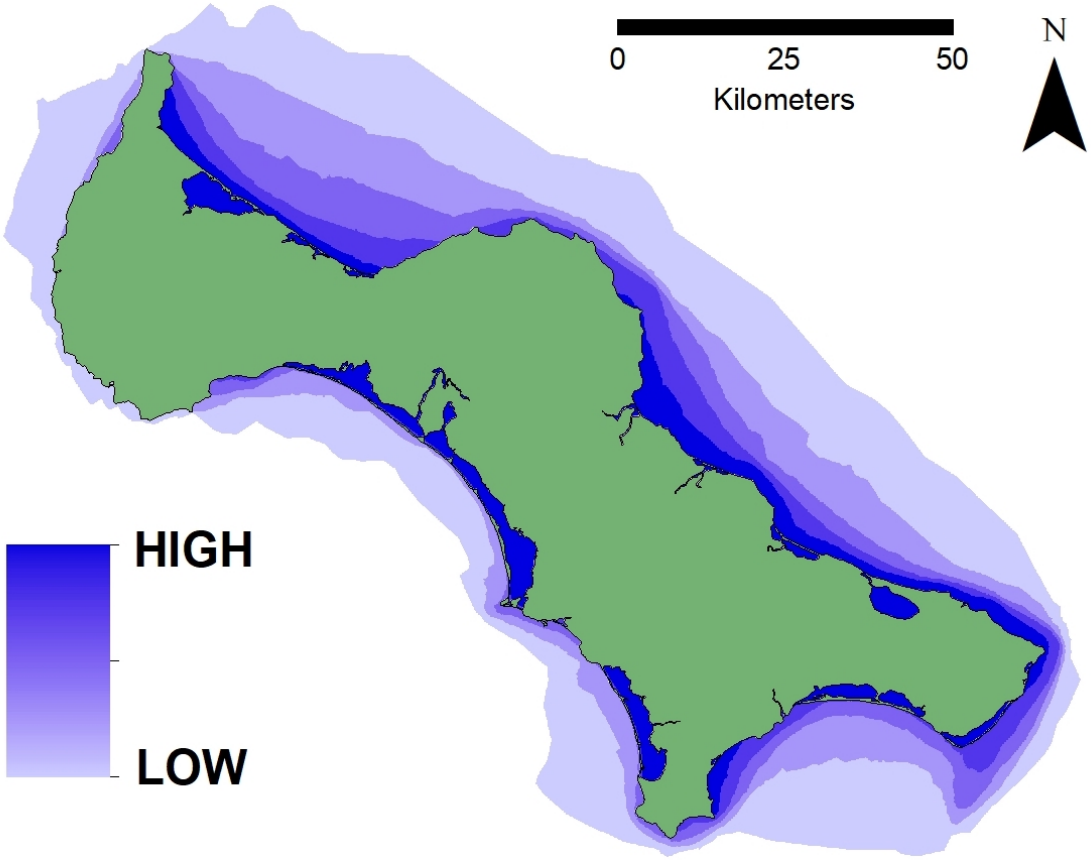

Figure 6: All landfast ice polygons used as inputs for modeling. The shade of blue represents the fraction a given area is occupied by landfast ice polygons. The darkest shade of blue represents areas that are always covered by landfast ice polygons.

Table 1: Model parameters

Parameter	Definition	Data Source	Resolution	Justification
Landfast Ice	Coast-contiguous sea ice that remains stationary for ~20 days.	Created by authors using Synthetic Aperture Radar satellite imagery. Methodology detailed in Mahoney et al. (2004).	1km grid points	Dependent Variable. This data shows where landfast ice is and is not located.
Bathymetry	Measured distance between the ocean floor and surface.	Alaska Regional Bathymetry Digital Elevation Model. Created by Danielson et al. (2008).	100m	Landfast ice is generally confined to shallower water depths that enable the formation of stabilizing features (e.g. grounded pressure ridges) (Mahoney et al. 2007b).
Hydrological Input Distance	Distance from a given grid point to the nearest freshwater input on the coastline	Flow accumulation analysis performed on Alaska 2 Arc-second DEM – USGS National Map 3DEP	2 arc-second (approximately 60m)	Proximity to hydrological inputs can facilitate the break up and melt of landfast ice by lowering albedo via surface flooding (Dean et al. 1994; Weingartner et al. 2017).
Sinuosity	A quantification of the concavity of nearest section of coastline. Divides shortest possible path between the enpoints of a concave section of coastline by the total length of the coastline measured.	Geospatial processing on Alaska Coast Shapefile – Alaska State Geo-spatial Clearinghouse	NA – vector data	Landfast ice forms in sheltered concave regions such as embayments and lagoons (Mahoney et al. 2007a, 2014). Grids proximate to concave coastlines are expected to have a higher occurrence of landfast ice cover.
Fetch Distance	Measurements of unobstructed distance in a given direction from a given gridpoint	Geospatial processing on grid point data – using fetchR package in R Studio 3.5.3	NA – vector data	Fetch distances determine orientation of a grid point relative to prevailing winds transporting pack ice into coastal zones. Pack ice is generally circulated into the Bering Sea through Northeasterly winds (Coachman & Aagaard 1988; Macklin 1983; Salo et al. 1983).
Sea Ice Concentration	Amount of sea ice areal coverage per defined space for the ~20 day period of landfast ice coverage	Summary statistics extracted from rasters to grid points – National Snow and Ice Data Center	25km	Landfast ice forms with the accretion of pack ice against its seaward edge (Mahoney et al. 2007a).
Sea surface temperature	Average temperature per defined space for the ~20 day period of landfast ice coverage	Summary statistics extracted from daily mean sea surface temperature rasters to grid points – National Centers for Environmental Prediction	0.25-degree	Freezing air temperatures facilitate landfast ice formation and continued presence (Barry et al. 1979; Mahoney et al. 2007a).

Table 2.1: Regression Summary for Northwest Region

Model	McFadden's Pseudo R^2	Parameter	Coefficient	Std. Error	Z Value
NW	0.8	Intercept	-16.27	26.51	-0.61
		Water Depth	-4.04	0.41	-9.85
		Concave Sinuosity	10.81	1.88	5.75
		Hydrological Input	-0.01	0.01	-1.00
		SIC (Max)	0.01	0.01	1.00
		SIC (Std. Dev.)	-0.01	0.01	-1.00
		Surface Temp (Max)	-0.21	0.73	-0.29
		Surface Temp (Std. Dev.)	3.55	2.08	1.71
		Surface Temp (Mean)	-2.45	0.72	-3.40
		Surface Temp (Min)	4.46	0.96	4.65
		North Fetch	-0.16	1.7	-0.09
		East Fetch	-0.01	0.01	-1.00
		West Fetch	-0.05	0.01	-5.00
		Northwest Fetch	-0.01	0.01	-1.00

Table 2.2: Regression Summary for Northeast Region

Model	McFadden's Pseudo R^2	Parameter	Coefficient	Std. Error	Z Value
NE	0.81	Intercept	26.01	2.05	12.69
		Water Depth	-1.26	0.29	-4.34
		Concave Sinuosity	1.21	0.5	2.42
		Hydrological Input	-0.01	0.01	-1.00
		SIC (Max)	0.04	0.01	4.00
		SIC (Std. Dev.)	-0.01	0.01	-1.00
		Surface Temp. (Max)	-2.37	0.24	-9.88
		Surface Temp. (Mean)	1.9	0.33	5.76
		Southeast Fetch	0.05	0.01	5.00
		Southwest Fetch	-0.02	0.01	-2.00
		West Fetch	-0.08	0.02	-4.00

Table 2.3: Regression Summary for Southwest Region

Model	McFadden's Pseudo R^2	Parameter	Coefficient	Std. Error	Z Value
SW	0.68	Intercept	11.6	3.19	3.64
		Water Depth	-1.92	0.6	-3.2
		Concave Sinuosity	-6.62	1.15	-5.76
		Hydrological Input	0.01	0.01	1.00
		SIC (Std. Dev.)	-0.02	0.01	-2.00
		SIC (Min)	0.01	0.01	1.00
		Surface Temp. (Max)	0.94	1.12	0.84
		Surface Temp (Std. Dev.)	6.64	2.56	2.59
		Surface Temp (Mean)	-3.59	0.88	-4.08
		Surface Temp (Min)	1.64	0.96	1.71
		Northeast Fetch	-0.06	0.01	-6.00
		East Fetch	-0.26	0.02	-13.00
		South Fetch	-0.01	0.01	-1.00
		Northwest Fetch	-0.02	1	-0.02

Table 2.4: Regression Summary for SoutheastRegion

Model	McFadden's Pseudo R^2	Parameter	Coefficient	Std. Error	Z Value
SE	0.78	Intercept	-16.8	2.65	-6.34
		Water Depth	-5.16	0.28	-18.43
		Concave Sinuosity	11.66	1.09	10.70
		Hydrological Input	-0.01	0.01	-1.00
		SIC (Max)	-0.01	0.01	-1.00
		SIC (Std. Dev.)	0.04	0.01	4.00
		SIC (Min)	0.01	0.02	0.50
		Surface Temp. (Max)	-3.97	0.77	-5.16
		Surface Temp (Std. Dev.)	10.89	2.17	5.02
		Surface Temp (Mean)	-0.16	0.59	-0.27
		Surface Temp (Min)	5.88	0.85	6.92
		North Fetch	-0.01	0.01	-1.00
		Northeast Fetch	0.01	0.01	1.00
		East Fetch	-0.03	0.01	-3.00
		Southwest Fetch	-0.01	0.04	-0.25
		West Fetch	-0.01	0.01	-1.00
		Northwest Fetch	-0.01	0.02	-0.50

Table 3: Classification accuracy at optimal probability thresholds

Zone	Threshold	Accuracy	Omission Error	Commission Error
NW	0.69	82.7%	0.61	0.17
NE	0.68	93.1%	0.86	0.07
SW	0.73	70.1%	0.25	0.3
SE	0.71	88.7%	0.53	0.11